Wnt signaling gradients establish planar cell polarity by inducing Vangl2 phosphorylation through Ror2

Bo Gao[1], Hai Song[1], Kevin Bishop[1], Gene Elliot[1], Lisa Garrett[1], Milton English[1], Philipp Andre[1], James Robinson[1], Raman Sood[1], Yasuhiro Minami[2], Aris N. Economides[3] and Yingzi Yang[1,*]

[1]National Human Genome Research Institute, Bethesda, MD 20892, USA. [2]Department of Physiology and Cell Biology, Faculty of Medical Sciences, Kobe University, 7-5-1 Kusunoki-cho, Chuo-ku, Kobe 650-0017, Japan, [3]Regeneron Pharmaceuticals, Inc., Tarrytown, NY, USA.

[*]Corresponding author:

Yingzi Yang

Genetic Disease Research Branch

National Human Genome Research Institute

49 Convent Drive, MSC 4472

Bethesda, MD 20892

TEL:(301) 402-2034

FAX:(301) 402-2170

e-mail:yingzi@mail.nih.gov

Abstract

It is fundamentally important that signaling gradients provide positional information to govern morphogenesis of multicellular organisms. Morphogen gradients can generate different cell types in specific spatial order at distinct threshold concentrations. However, it is largely unknown whether and how signaling gradients also control cell polarities by acting as global cues. Here we show that Wnt signaling gradient provides directional information to a field of cells. Vangl2, a core component in planar cell polarity, forms Wnt-induced receptor complex with Ror2 to sense Wnt dosages. Wnts dose-dependently induce Vangl2 phosphorylation of Serine/Threonine residues and Vangl2 activities depend on its levels of phosphorylation. In the limb bud, Wnt5a signaling gradient controls limb elongation by establishing PCP in chondrocytes along the proximal-distal axis through regulating Vangl2 phosphorylation. Our studies have provided new insight to Robinow Syndrome, Brachydactyly Type B1 and spinal bifida which are caused by mutations in human ROR2, WNT5A or VANGL.

Introduction

Multicellular organisms control their morphogenesis by forming signaling gradients to coordinate growth and patterning (Lawrence, 2001; Turing, 1952; Wolpert, 1969), during which establishment of polarity in a field of cells is essential. Wnts are a class of secreted ligands that can transduce their signals through several distinct pathways to regulate a diverse array of developmental processes (Angers and Moon, 2009; Logan and Nusse, 2004). A critical function of Wnt signaling in vertebrates is to regulate planar cell polarity (PCP) (Heisenberg et al., 2000; Qian et al., 2007; Rauch et al., 1997). PCP, which originally refers to the polarity of epithelial cells within a plane orthogonal to their apical–basal axis, is well characterized genetically in *Drosophila melanogaster* and is regulated by a group of evolutionarily conserved core PCP components including a four-pass transmembrane protein, Van Gogh (Vang) (McNeill, 2010; Seifert and Mlodzik, 2007; Tree et al., 2002; Wang and Nathans, 2007; Zallen, 2007). Its vertebrate homologues are *Vang like 1 and 2* (*Vangl1 and Vangl2)* (Jessen and Solnica-Krezel, 2004; Kibar et al., 2001; Murdoch et al., 2001; Song et al., 2010; Torban et al., 2007). However, a long-range positional cue that globally coordinates PCP and creates the initial polarity required for asymmetrical cellular behaviors in vertebrate development remains to be identified (Lawrence et al., 2007; Strutt, 2009).

In mammals, PCP has emerged as a fundamental regulatory mechanism controlling many critical developmental processes (Borovina et al., 2010; Guirao et al., 2010; Hashimoto et al., 2010; McNeill, 2010; Song et al., 2010; Torban et al., 2008). For instance in humans, disrupted convergent extension (CE) movement, a process regulated by PCP (Heisenberg et al., 2000; Jessen et al., 2002), results in failure of neural tube

closure, which causes the condition of spina bifida, a common permanently disabling birth defect. Mutations in *VANGL1* have been identified in spina bifida patients (Kibar et al., 2007). In addition, mutations in *VANGL2* led to stillborn fetuses with various neural tube defects (Lei et al., 2010). However, despite the critical roles of PCP and Wnt signaling in vertebrate development, surprisingly little is known about the mechanism underlying PCP regulated by Wnt signaling *in vivo*.

Some Wnts, like Wnt5a, transduce their signals mainly through the β-catenin-independent non-canonical pathways *in vivo* (Topol et al., 2003; Westfall et al., 2003) and *Wnt5a* genetically interact with *Vangl2* (Qian et al., 2007), suggesting that *Wnt5a* may regulate PCP. Wnt5a has also been suggested to signal through Ror2, a single pass transmembrane protein with a tyrosine kinase domain, which binds Wnt5a through its extracellular cysteine-rich Wnt binding domain (CRD) (Oishi et al., 2003). Ror2 mediates Wnt5a signal to inhibit the β-catenin-dependent canonical Wnt signaling activity and activate c-Jun N-terminal kinase (JNK) *in vitro* (Mikels and Nusse, 2006; Oishi et al., 2003). Because mutations in human *ROR2* and *WNT5A* lead to Robinow syndrome and/or BDB1 (Afzal et al., 2000; Person et al., 2010; Schwabe et al., 2000; van Bokhoven et al., 2000) and mouse *Wnt5a* and *Ror2* mutant embryos bear many similar phenotypes (DeChiara et al., 2000; Oishi et al., 2003; Takeuchi et al., 2000; Yamaguchi et al., 1999; Yang et al., 2003), Ror2 may mediate Wnt5a signaling *in vivo*. However, the mechanisms underlying Wnt5a signaling through Ror2 and short limb phenotypes of Robinow syndrome and BDB1 remain elusive.

Here we have found that Ror2 and Vangl2 form a Wnt-induced receptor complex that is essential to establish PCP, hence directional growth, by interpreting Wnt dosage

gradients. Wnts including Wnt5a induced Vangl2 phosphorylation on two clusters of serine (S) and threonine (T) residues in a Wnt5a dose-dependent manner both *in vitro* and *in vivo*. Wnt5a-induced Vangl2 phosphorylation was essential for its function. More highly phosphorylated Vangl2 is more active. Our data suggest that by translating Wnt5a gradients into a Vangl2 activity gradient, chondrocytes are polarized along the proximal-distal (P-D) axis and such polarization is required for P-D limb elongation.

Results

Ror2 and Vangl2 act together to transduce the Wnt5a signal

The mouse *Wnt5a*$^{-/-}$ and *Ror2*$^{-/-}$ exhibited similar phenotypes of shortened anterior-posterior (A-P) body axis to that of the *Lp* (*Vangl2*$^{Lp/+}$) mutants that was caused by a dominant negative allele of *Vangl2* (DeChiara et al., 2000; Kibar et al., 2001; Song et al., 2010; Takeuchi et al., 2000; Yamaguchi et al., 1999), suggesting that Ror2 may act in the Wnt5a pathway to control PCP during CE. In addition, the *Wnt5a*$^{-/-}$, *Ror2*$^{-/-}$ and *Vangl2*$^{Lp/Lp}$ mutants showed shortened limbs along the P-D axis (Fig. 1A). These observations suggested that limb elongation along the P-D axis may be regulated by Wnt5a and Ror2 in a process similar to CE and requiring PCP. To test these hypotheses, we first examined *Ror2* expression patterns in mouse embryos. Using a *LacZ* "knock in" allele of *Ror2* (DeChiara et al., 2000), we found that *Ror2* was broadly expressed and its expression overlapped with that of *Wnt5a* and *Vangl2* temporally and spatially (Yamaguchi et al., 1999)(Fig.S1A). However, the phenotypes of *Ror2*$^{-/-}$ and even *Ror1*$^{-/-}$*; Ror2*$^{-/-}$ mutants (Nomi et al., 2001) were less severe than those of the *Wnt5a*$^{-/-}$ mutants,

but the *Wnt5a*$^{-/-}$*; Ror2*$^{-/-}$ and *Wnt5a*$^{-/-}$ mutants displayed identical phenotypes (Fig. S1B). Thus, the Ror family members only mediate part of Wnt5a signaling *in vivo*.

Since a major driving force of limb elongation along the P-D axis is the directional growth of the long bone cartilage, we tested whether reduced P-D elongation of the limb in the *Wnt5a*$^{-/-}$ and *Ror2*$^{-/-}$ mutants is due to disrupted PCP in chondrocytes of the limb (Fig. 1B). The wild type chondrocytes were flattened and stacked in columns along the P-D axis. Such organization of chondrocytes in the *Wnt5a*$^{-/-}$ and *Ror2*$^{-/-}$ embryos was altered substantially and looked similar to those in the *Vangl2*$^{Lp/Lp}$ limb bud (Fig. 1B, C, S1C, D). Thus, chondrocytes are likely to be polarized along the P-D axis and Vangl2 may mediate Wnt5a signal together with Ror2 in regulating such polarity. This hypothesis predicts that the *Ror2* mutant should genetically interact with the *Vangl2*$^{Lp/+}$ mutant. Indeed, the *Ror2*$^{-/-}$*; Vangl2*$^{Lp/+}$ mice exhibited open neural tube and disrupted hair cell polarity in the sensory epithelium of the cochlea, which are typical PCP defects in mammals that rarely occurred in either *Ror2*$^{-/-}$ or *Vangl2*$^{Lp/+}$ mutants (Fig. 1D and S1E, F) (Qian et al., 2007). Using a *Vangl2*$^{-}$ allele (previously referred to as the *Vangl2*$^{\Delta}$ allele) we have generated (Song et al., 2010), strong genetic interactions of *Ror2* and *Vangl2* were also observed in the developing cartilage of the limb (Fig. S1G). Thus, *Ror2*, like *Wnt5a*, also regulates PCP in mammalian embryonic development including limb elongation. These results led us to hypothesize that Wnt5a signal is transduced by both Ror2 and Vangl2. Indeed, we found that *Wnt5a*$^{-/-}$ and *Ror2*$^{-/-}$*; Vangl2*$^{-/-}$ embryos showed almost identical phenotypes in places like the limb, tail and frontonasal processes (Fig. 1E). In the forelimb, distal digits failed to form (Fig. 1F).

In addition to the morphological defects, we found that expression of *Sox9*, the

earliest known marker for cartilage formation (Bi et al., 1999), was not detected in the *Ror2*$^{-/-}$*; Vangl2*$^{-/-}$ distal limb buds, similar to what was observed in the *Wnt5a*$^{-/-}$ embryos (Topol et al., 2003) (Fig. 2A). As in the distal limb of the *Wnt5a*$^{-/-}$ embryos, anti-chondrogenic Wnt/ß-catenin signaling was also upregulated in the distal limb of the *Ror2*$^{-/-}$*; Vangl2*$^{-/-}$ mutant, but not the *Ror2*$^{-/-}$ or *Vangl2*$^{-/-}$ mutant at E13.5 (Fig. 2B, S2A). Upregulated Wnt/ß-catenin signaling in the wild type limb mesenchyme was observed around the forming joint which expressed *Gdf5* (Fig. 2B, S2B), but in the *Ror2*$^{-/-}$*; Vangl2*$^{-/-}$ mutant limb, there was no ectopic joint formation shown by lack of ectopic *Gdf5* expression in the distal limb (Fig. S2B). Thus, ectopic upregulation of Wnt/ß-catenin signaling in the *Ror2*$^{-/-}$*; Vangl2*$^{-/-}$ mutant was not caused by abnormal cell fate change. Consistent with this, Wnt5a inhibition of the Wnt/ß-catenin signaling was abolished in the *Ror2*$^{-/-}$ mouse embryonic fibroblast (MEF) cells, but in the *Ror2*$^{-/-}$*; Vangl2*$^{-/-}$ MEF cells, Wnt5a further increased Wnt/ß-catenin signaling stimulated by Wnt3a (Fig. 2C). Loss of both *Ror2* and *Vangl2* may have allowed uncovering Wnt5a's activity to signal through the canonical Wnt pathway. Wnt5a-induced cell migration was also more severely impaired in the *Ror2*$^{-/-}$*; Vangl2*$^{-/-}$ MEF cells (Fig. S2C). As previous findings have indicated that non-canonical Wnt signaling regulates JNK and Rho activation (Kikuchi et al., 2009; Yamamoto et al., 2008), we have examined JNK and Rho activation and found that loss of *Ror2* and *Vangl2* led to reduced induction of c-Jun phosphorylation and Rho activation in MEF cells (Fig. S2D, E). Together, these analyses indicate that Ror2 and Vangl2 act together to transduce multiple aspects of non-canonical Wnt signaling in embryonic development.

Wnt5a induces Ror2 and Vangl2 complex formation

We next tested whether Ror2 and Vangl2 form a receptor complex to transduce Wnt signal as Ror2 binds Wnt5A (Oishi et al., 2003). Both Ror2 and Vangl2 were distributed randomly on the cell membrane of limb bud mesenchymal cells before E11.5 and strikingly, when chondrocytes form in an E12.5 distal limb, asymmetrical localization of Vangl2 protein along the P-D axis of the limb was observed in chondrocytes, not in the non-chondrocyte mesenchymal cells in the limb (Fig. 3A, S3A), demonstrating that chondrocytes in the developing cartilage of the limb are indeed polarized and oriented along the P-D axis. Consistent with this, *Ror2* expression is selectively upregulated in the forming cartilage (Fig. S1A and DeChiara et al., 2000). Closer examination of Vangl2 staining showed that it was localized to the proximal side of chondrocytes (Fig. S3B), but it did not colocalize with cilia (Fig. S3C). Ror2 and Vangl2 were found in the same protein complex in the limb bud at E12.5 (Fig. S3D), but no asymmetrical Ror2 protein localization was observed (Fig. 3A).

Importantly, Wnt ligands including Wnt5a strongly induced Ror2 and Vangl2 complex formation (Fig. 3B and Fig. S3E). In the *Wnt5a*$^{-/-}$ limb, Ror2-Vangl2 complex formation was reduced (Fig. S3D). To test whether Ror2 and Vangl2 interact directly in the Wnt5a receptor complex, we performed YFP/CFP Fluorescence Resonance Energy Transfer (FRET) analysis and found that Ror2 and Vangl2 were localized in close proximity on the plasma membrane. Such interaction was significantly more stable in the presence of Wnt5a (Fig. 3C). A *Lp* mutant Vangl2 protein (S464N) that is trapped in the ER (Merte et al., 2010) failed to form a complex with Ror2, even in the presence of Wnt5a (Fig. 3D), suggesting that Ror2-Vangl2 complex formation occurs on the plasma membrane and is required for Wnt5a signal transduction.

To test whether Wnt5a-induced Ror2-Vangl2 complex formation is a prerequisite for asymmetrical Vangl2 localization, a functional readout of PCP, Vangl2 protein localization was examined in different mutants (Fig. 4A, S4A). In the *Wnt5a*$^{-/-}$ mutant or the *Vangl2*$^{Lp/Lp}$ mutant where Vangl2 protein failed to reach the membrane and form a complex with Ror2 in vitro, Vangl2 asymmetrical localization was lost in chondrocytes (Fig. 4A, S4A). In the *Ror2*$^{-/-}$ limb, Vangl2 asymmetrical localization was reduced in chondrocytes of the distal limb (Fig. 4A), but in more mature chondrocytes of the more proximal limb, Vangl2 asymmetrical localization was lost (Fig. S4A). These results suggest that weakened Wnt signaling in the *Ror2*$^{-/-}$ limb chondrocytes failed to establish Vangl2 asymmetrical localization in the proximal limb. Because *Wnt5a* is expressed in a gradient along the P-D axis of the limb (Fig, S4B), we examined whether there was a gradient of Vangl2 asymmetrical localization. We found that the relative number of cells showing Vangl2 asymmetrical localization was reduced progressively along the P-D axis (Fig. 4B), demonstrating that there is a correlation between Wnt5a signaling strength and the level of Vangl2 asymmetrical localization. Indeed in the *Ror2*$^{-/-}$ limb, Vangl2 asymmetrical localization declined rapidly along the P-D axis (Fig. 4B). Considering that all of *Wnt5a*$^{-/-}$, *Ror2*$^{-/-}$ and *Vangl2*$^{Lp/Lp}$ mutants exhibited loss of Vangl2 asymmetrical localization and shorter and broader long bone cartilages (Fig. 1A, S4C), PCP in chondrocytes plays an essential role to control directional cartilage growth in the limb. Failure to transduce the Wnt5a signal together with Ror2 is responsible for the limb phenotypes of the *Vangl2*$^{Lp/Lp}$ mutant. Taken together, these data indicate that Wnt5a modulates the canonical Wnt signaling activity and controls PCP by inducing Ror2-Vangl2 complex formation.

Wnts act through Ror2 to induce Vangl2 phosphorylation

To investigate the molecular mechanism whereby Wnt signal controls PCP through the Ror2-Vangl2 receptor complex, we tested whether Wnts regulate Vangl2 activity by inducing its posttranslational modification. We found that some of the Vangl2 protein showed retarded gel mobility by the SDS-PAGE analysis (Fig. 5A). Since such protein mobility shift was completely abolished by treating the samples with calf intestinal phosphatase (CIP), Vangl2 protein was phosphorylated. Interestingly, Vangl2 phosphorylation was enhanced by overexpression of many *Wnts*, *Ror2* and most strongly by coexpression of *Wnts* and *Ror2* (Fig. 5B). *Wnt5a* has the strongest effects in inducing Vangl2 phosphorylation (Fig. 5B, S5A), consistent with its prominent role in controlling PCP in mammalian development. Thus, we focused on *Wnt5a* in the rest of the study. Vangl2 phosphorylation appears to be an early event of Wnt5a signaling as Wnt5a-induced Vangl2 phosphorylation was detected by 1 hour after Wnt5a treatment (Fig. S5B). Wnt5a has been shown to bind Ror2 and in the *Ror2*$^{-/-}$ MEF cells, Wnt5a-induced Vangl2 phosphorylation was greatly diminished (Fig. 5C), indicating that Wnt5a acts through Ror2 to regulate Vangl2 phosphorylation.

The diffuse pattern of Vangl2 protein mobility shift indicates that there are multiple forms of phosphorylated Vangl2 and Vangl2 can be hyperphosphorylated on many different sites. To identify these Vangl2 phosphorylation sites, we compared protein sequences of Vangl1 and Vangl2 from multiple invertebrate and vertebrate species and found that there are two clusters of highly conserved S and T residues located in the N-terminal cytoplasmic domain (Fig. 5D and S5C). Mutating these S and T residues to alanine (A) individually or in combination reduced basal level and Wnt5a-induced

Vangl2 phosphorylation (Fig. 5E-G and S5D). Interestingly, in both Cluster I and II, the contribution of each S or T to Vangl2 phosphorylation differs depending on its location in the cluster. In Cluster I, when mutated individually, S84A, followed by the S82A, has the strongest impact on reducing basal level Vangl2 phosphorylation. The S84A mutation almost completely abolished Vangl2 basal level phosphorylation. When mutated in combination, S84A and S82A together most severely reduced basal level and Wnt5a-induced Vangl2 phosphorylation (Fig. 5E). The two triple mutation combinations of T76A-T78A-S79A and T71A-T72A-T73A had progressively weaker impact on basal level and Wnt5a-induced Vangl2 phosphorylation and both of these combinations had weaker effect than S84A (Fig. 5E). These results indicate that phosphorylation in Cluster I occurs in a relay fashion starting from the C-terminus and suggest that phosphorylation on the two C-terminal sites (S84 and S82) is required for phosphorylation of the more N-terminal sites in the direction of S79 to T71. However, S82A and S84A mutations did not completely abolish Wnt5a-induced Vangl2 phosphorylation (Fig. 5E), suggesting that Wnt5a also induces Vangl2 phosphorylation outside of Cluster I. Indeed, mutating the S residues in Cluster II led to significantly reduced basal level and Wnt5a-induced Vangl2 phosphorylation, too (Fig. 5F). Furthermore, mutating S sites closer to the N-terminus of cluster II resulted in progressively more severe reduction of Wn5a-induced Vangl2 phosphorylation (Fig. 5F), indicating that phosphorylation in cluster II also occurs in a relay fashion, but starting from the N-terminus and suggest that phosphorylating the N-terminal site (S5A) is required to phosphorylate the more C-terminal sites in the direction from S5 to S20.

To further test the effects of S84, S82 and S5 as founder sites for Vangl2 phosphorylation, we mutated S5~17 and all of the Cluster I S/T sites and found this resulted in similarly reduced Vangl2 phosphorylation when only S5 and Cluster I sites were mutated, indicating S5 is indeed a founder site for Cluster II phosphorylation (Fig. 5G). Similarly, mutating S5~17 and only S82, S84 had similar effects as mutating S5~17 and all Cluster I sites (Fig. 5G). Furthermore, mutating all of the three founder sites, but not any two of them (S84+S5, S82+S5 or S82+S84) completely abolished basal level and Wnt5a-induced Vangl2 phosphorylation just like mutating all Cluster I and II sites (Fig. 5G and S5D). Thus, phosphorylation of S84, S82 and S5 is required for phosphorylating other sites in Cluster I and Cluster II, respectively. S84 and S82 act together as founder sites for cluster I phosphorylation. These results further demonstrate that Wnt5a-induced Vangl2 phosphorylation mostly occurred on the S and T residues of Cluster I and II. Indeed, basal level or Wnt5a-induced Vangl2 tyrosine (Tyr) phosphorylation was not detected and a kinase-dead Ror2 mutant (Hikasa et al., 2002) still retained the ability to enhance Wnt5a-induced Vangl2 phosphorylation (Fig. S5E-G, 6B).

As a first attempt to further understand the regulation of Vangl2 phosphorylation, we set out to identify the kinase(s) that phosphorylates Vangl2. In *Drosophila*, Casein Kinase 1 (CKI) (Klein et al., 2006; Strutt et al., 2006) has been shown to be a mandatory factor in the PCP pathway. We tested whether CKI is also involved in regulating Vangl2 phosphorylation. In CHO cells, overexpression of CKIδ, but not CKIε promoted Vangl2 phosphorylation. Conversely, treatment by D4476, a pharmacological inhibitor of CKI (Rena et al., 2004), inhibited Vangl2 phosphorylation by Wnt5a and Ror2 (Fig. 5H), suggesting that CKIδ is required to phosphorylate Vangl2 in response to Wnt5a.

Vangl2 activities are regulated by its phosphorylation

To test the functional significance of Vangl2 phosphorylation, we noticed that one of human VANGL1 mutation S83L identified in spinal dysraphisms is equivalent to the mouse Vangl2 S79 (Kibar et al., 2009) which is in Vangl2 phosphorylation cluster I. In addition, a mutation of a phosphorylation founder site in cluster I of human VANGL2, S84F, has been found in stillborn fetuses (Lei et al., 2010), suggesting that Vangl2 phosphorylation is required for its function in vivo. In agreement with this, we found that the WNT5A mutations (C83S and C182R) associated with the dominant form of Robinow Syndrome (Person et al., 2010) had weakened ability to induce Vangl2 phosphorylation (Fig. 6A). Furthermore, we found that *Ror2* mutations identified in the recessive form of Robinow syndrome or BDB1 (Kani et al., 2004) exhibited reduced activity in promoting Vangl2 phosphorylation compared to the wild type *Ror2* in *Ror2*$^{-/-}$ cells, whereas the kinase dead mutant of *Ror2* showed similar activity as the wild type control (Fig. 6B). These results suggest that reduction of VANGL2 phosphorylation impairs its function and reduced VANGL2 activity due to abnormal WNT5A/ROR2 signaling is an important mechanism underlying Robinow Syndrome and BDB1.

The functional significance of Vangl2 phosphorylation was also supported by the two *Lp* mutations (D255E and S464N) which caused Vangl2 protein to be trapped in the ER and fail to form complex with Ror2. Both basal level and Wnt5a-induced Vangl2 phosphorylation was completely abolished by the *Lp* mutations, but not the S464A mutation (Fig. 6C). Furthermore, we raised antibodies recognizing phospho-Vangl2 to detect Vangl2 phosphorylation *in vivo* (Fig. S6A-C). The Vangl2 protein levels and phosphorylation were both drastically reduced in an *Lp* mutant mouse strain (S464N)

(Fig. 6D), supporting that Vangl2 phosphorylation is regulated by Wnt5a/Ror2 signaling at the plasma membrane. Interestingly, when coexpressed with the S464N mutant, phosphorylation of wild type Vangl2 was also reduced (Fig. 6E), providing molecular evidence that the *Lp* mutation is dominant negative. These results suggest that loss of Vangl2 phosphorylation due to Vangl2 ER trapping underlies the developmental abnormalities of the *Vangl2*$^{Lp/+}$ and *Vangl2*$^{Lp/Lp}$ embryos as Wnt/PCP signaling is severely impaired in the mutants.

To directly test whether Vangl2 phosphorylation is required for its function, we first examined activation of c-Jun N-terminal kinases (JNK) and Rho by Vangl2 (Fig. S6D). The Vangl2 mutant that could not be phosphorylated exhibited diminished activity in activating JNK or Rho. Furthermore, we took advantage of the zebrafish *trilobite* (*tri*) mutant caused by a null mutation of *Vangl2* (*tri*$^{m209/m209}$)(Jessen et al., 2002) and tested the function of *Vangl2* variants by comparing their rescuing efficiency (Fig. 6F). While injecting the control GFP mRNA did not perturb the phenotypes (Fig. S6Ea), injecting the wild type mouse *Vangl2* mRNA to the wild type or heterozygous (*tri*$^{m209/+}$) fish led to CE defects as PCP signaling is dose sensitive and both loss and gain of function PCP mutants show similar phenotypes (Fig. 6Ga, d, S6Eb). Therefore, different doses of wild type and mutant *Vangl2* mRNA were injected (Fig. 6G, S6E). Importantly, 60pg wild type mouse *Vangl2* mRNA rescued the CE defects in about 95% of the injected *tri*$^{m209/m209}$ fish embryos (Fig. 6Ga). Higher or lower dosages of wild type mouse *Vangl2* mRNA both reduced its recuing efficiency (Fig. 6Gd, S6Eb). However, while the mouse S84A *Vangl2* mRNA was more potent in causing CE defects in the wild type and *tri*$^{m209/+}$ embryos, it was much less efficient in rescuing the CE defects of the *tri*$^{m209/m209}$ fish at all

doses tested (Fig. 6Gb, e, S6Ec). Furthermore, the most severe *Vangl2* phospho-mutant (S5~17A::S76~84A) almost completely lost its ability to rescue the *tri*$^{m209/m209}$ embryo at all doses tested (Fig. 6Gc, f, S6Ed). We have also generated phospho-mimicking mutant of Vangl2 by mutating S5, 82 and 84 to glutamate (E). The phospho-mimicking mutant of *Vangl2* exhibited higher rescuing efficiency at a lower dosage compared to the wild type control (Fig. 6Gg vs. a, d) and slightly increasing the dose of phospho-mimicking mutant of *Vangl2* quickly reduces its rescuing efficiency (Fig. S6Ee), indicating that the phospho-mimicking mutant of *Vangl2* is an activated form of Vangl2. We then tested whether differential rescuing abilities of the *Vangl2* mutants are caused by the difference in protein stability or membrane localization. We examined the protein made from the injected *Vangl2* mRNAs. The stability of the all phospho-mutant S5~17A::S76~84A was reduced, but the stability of the S84A mutant was normal although it had reduced activity. In addition, the phospho-mimicking mutant S5,82,84E had increased activity, which did not correlate with increased protein stability. Furthermore, the S84A mutant showed comparable membrane localization to the wild type Vangl2 protein and the all phospho-mutant was also found on the membrane, although less efficiently (Fig. S6F). These results demonstrate that Vangl2 phosphorylation is required for its function and higher levels of phosphorylation result in more active Vangl2.

Wnt5a gradient establishes PCP by inducing distinct levels of Vangl2 phosphorylation

As Wnt5a forms a dosage gradient in many places in the mouse embryo including the limb (Fig. S4B) and Wnt5a is required for PCP (Fig. 1, 4), we tested whether Wnt5a dosage gradient acts as a global cue to establish PCP by controlling Vangl2 activity

through phosphorylation. We first examined Vangl2 phosphorylation in the developing embryo and found that Vangl2 protein from the brain and limb was hyperphosphorylated (Fig. S6B). We then tested whether Wnt5a dosage gradient is sensed in responding cells by inducing distinct levels of Vangl2 phosphorylation. We divided the E11.5 limb bud into three zones along the P-D axis and a gradient of Vangl2 phosphorylation was found (Fig. 7A). The distal cells were most highly phosphorylated. When the frontonasal processes were divided into distal (high *Wnt5a* expression) and proximal parts (lower *Wnt5a* expression), we also found that Vangl2 was hyperphosphorylated in the distal parts (Fig. S7A). In the *Ror2*$^{-/-}$ and *Wnt5a*$^{-/-}$ distal limb bud, hyperphosphorylated Vangl2 was reduced (Fig. 7B). In the *Wnt5a*$^{-/-}$ mutant, Vangl2 phosphorylation levels in the distal limb were reduced to those similar to the proximal limb bud (Fig. S7B), indicating that Vangl2 phosphorylation gradient in the limb bud is regulated by Wnt5a through Ror2. However, when phosphorylation at the S84 and S82 sites were examined by phospho-specific antibodies, there was no difference between wild type control and the *Wnt5a* or *Ror2* mutants (Fig. 7B), suggesting that priming at the S84 and S82 may not require Wnt5a signaling. To further test that different levels of Vangl2 phosphorylation are induced by distinct dosages of Wnt5a, we cocultured cells expressing *Vangl2* and *Ror2* with various numbers of *Wnt5a*-expressing cells or increasing concentrations of Wnt5a recombinant protein (Fig. 7C, D). Indeed, increasing Wnt5a dosages led to progressively more extensive Vangl2 phosphorylation. We then tested whether changing the Wnt5a gradient would alter Vangl2 asymmetrical localization. We grafted chick embryonic fibroblast (CEF) cell pellets that have been infected with the RCAS-Wnt5a virus to the chick limb bud (Fig. S7C). Because the RCAS-Wnt5a virus produced in the CEF cell

pellets can infect neighboring tissues, 3 days after grafting, most of the limb had already been infected by the virus, hence expressed *Wnt5a* (Fig. 7C). As a result of this wide-spread expression of *Wnt5a*, unidirectional and asymmetrical Vangl2 localization was disrupted (Fig. S7C). Taken together, these data indicate that Wnt5a forms a signaling gradient that controls PCP and embryonic morphogenesis by inducing distinct levels of Vangl2 phosphorylation.

Discussion

Although fundamental in development, the molecular mechanism by which directional cellular and tissue behaviors are controlled is still poorly understood. For instance, it is an outstanding question in limb development what controls directional limb outgrowth along the P-D axis. Here we show by Vangl2 asymmetrical localization that chondrocytes of the developing mouse limb are indeed polarized along the P-D axis and such polarization is required for the P-D elongation of the long bone cartilage. A key controlling event in establishing PCP is a global directional cue that orients a field of cells. However, the nature and identity of this global cue in vertebrates are not clear. In *Drosophila*, Wnts have not been found to control PCP. Here in the mouse developing limb, our *in vivo* and *in vitro* studies indicate that a Wnt5a signaling gradient provides directional cues to a field of cells by controlling distinct levels of Vangl2 phosphorylation, hence Vangl2 activities, in these cells (Fig. 7E, F).

Secreted signaling molecules like Wnts are fundamentally important in development by acting as morphogens in a field of initially homogeneous cells to produce specific cellular responses determined by morphogen concentration. The nature of the cellular

response and the molecular mechanisms underlying dosage sensing and interpretation in responding cells lie at the center of our understanding of morphogen function. Despite the important roles Wnts play in many developmental processes, it was not clear until now that Wnt gradients also regulate morphogenesis by controlling cell polarity. In this regard, Wnts may act as a unique class of morphogens to control PCP in a field of cells by inducing distinct levels of Vangl2 phosphorylation at varying dosages through Ror2 (Fig. 7E, F). It is conceivable that Wnt morphogen gradients not just regulate cell fate specification, they also coordinate cell proliferation and differentiation with cell polarity establishment. Here we show that a Wnt protein gradient in a field of cells is translated into a Vangl2 activity gradient, which in turn establishes unidirectional PCP (Fig. 7F). When establishing PCP, a cell senses an initial small difference in Vangl2 activity in its immediate neighbors located on its two opposite sides. This difference is then amplified by cell-cell interactions and positive feedback loops such that Wnt induces Vangl2 protein aggregation only on the proximal side of the limb bud cell, laying the ground for further asymmetric cellular behavior. This is consistent with regulation of PCP in the *Drosophila* wing in which a $Vang^{-/-}$ clone reorients Vang protein localization in the surrounding wild type cells to the side closer to the $Vang^{-/-}$ clone through cell-cell interaction (Taylor et al., 1998; Fig. 1 of Bastock et al., 2003). Because the Wnt5a signaling gradient determines that Vangl2 activity in the limb bud is the highest in the distal and lowest in the proximal end, by analogy to the *Drosophila* wing, the result of cell-cell interaction will cause Vangl2 protein to be localized to the proximal side of chondrocytes. It is interesting to note that there is a P-D gradient of Vangl2 asymmetrical localization (Fig. 4B), suggesting that distal chondrocytes are more polarized. Because

Wnt5a also signals through Ror2 and Vangl2 to inhibit the antichondrogenic Wnt/β-catenin signaling, Wnt5a signaling is required for distal limb chondrogenesis and cartilage elongation by coordinating chondrocyte cell fate determination and cell polarity. It is likely that in other places such as the frontonasal processes, a Wnt5a protein gradient also defines a unidirectional polarity. In support of this, *Wnt5a* is expressed in a graded fashion in the limb, branchial arches and tail bud and *Wnt5a*$^{-/-}$, *Ror2*$^{-/-}$ and *Vangl2*$^{Lp/Lp}$ mutants showed similar defects in cartilage elongation, craniofacial morphogenesis and CE movement (DeChiara et al., 2000; Oishi et al., 2003; Yamaguchi et al., 1999). In addition, a recent series of studies have shown that while there are stage-specific variations, the theme underlying different stages of limb bud initiation and elongation is that mesoderm and cartilage cells in the limb bud have a distinct polarity that drives oriented cell behaviours and that noncanonical Wnt signalling, driven at least in part by the ligand Wnt5a, is important to all stages of limb bud outgrowth (Boehm et al., 2010; Wyngaarden et al., 2010; Gros et al., 2010). It is likely that Wnt5a regulation of PCP is also important prior to cartilage formation in the limb. As stabilization of PCP requires close cell-cell contact, which is not possible or much weaker in the loose limb mesenchymal cells before mesenchymal condensation to form cartilage, asymmetrical Vangl2 localization was only observed upon chondrocyte differentiation. Thus, defects in craniofacial morphogenesis and cartilage elongation in Robinow syndrome and BDB1 can be attributed to defects in PCP. *Wnt5a* has also been found to be expressed in discrete patterns in the developing cartilage and bone (Yang et al., 2003), it will be interesting to further determine the function of PCP regulated by Wnt5a in the later developing skeletal system. As many different Wnts can act through Ror2 to induce Vangl2 phosphorylation,

controlling PCP is another fundamental role of vertebrate Wnts in development. Lack of open neural tube and inner ear hair cell polarity defects in the *Wnt5a*$^{-/-}$ embryos suggests that *Wnt5a*'s function has been compensated by other *Wnt*s. For instance, Wnt11 can act as a directional cue to organize the elongation of early muscle fibers through the PCP pathway (Gros et al., 2009). In the limb, the non-redundant role of Wnt5a in controlling PCP is likely due to the fact that *Wnt5a* expression is much stronger than other *Wnt*s and is the only *Wnt* that is expressed in a gradient in the limb mesenchyme along the P-D axis (Gavin et al., 1990; Parr et al., 1993; Yamaguchi et al., 1999 and Fig. S4B).

Interestingly, a recent study found that the ground polarity in *C. elegans* is established by instructive Wnt/EGL-20 activity via the Ror receptor tyrosine kinase CAM-1 and the planar cell polarity component Van Gogh (Green et al., 2008), suggesting that this pathway is evolutionarily conserved. In this regard, it will be important to test whether the *Drosophila Ror2* orthologue also plays a regulatory role in PCP. In addition, because CKI is required to regulate Vangl2 phosphorylation and CKI is essential in controlling PCP in *Drosophila*, it is likely that Vangl2 is a functionally significant substrate of CKI.

We noticed that the phenotypes of *Ror2*$^{-/-}$ and *Vangl2*$^{-/-}$ are not identical and the more severe *Ror2*$^{-/-}$;*Vangl2*$^{-/-}$ double mutants phenocopied *Wnt5a*$^{-/-}$ in the limb. *Ror2* and *Vangl2* must have roles independent of each other. It is also possible that Frizzleds are other Wnt binding proteins in the Ror2/Vangl2 complex and the function of Ror2 might be to enhance or stabilize Wnt binding to this complex. While Wnt5a has been shown to play a permissive role in directional melanoma cell movement by inducing the formation of a Frizzled-containing receptor-actin-myosin intracellular structure (Witze et al., 2008), our data argue strongly that *in vivo* Wnt5a plays an instructive role to control cell polarity

by inducing Vangl2 phosphorylation in a dose-dependent manner. Understanding non-canonical Wnt signal transduction has been hampered in the past by lacking a robust and reliable immediate signaling readout. Identification of Ror2 and Vangl2 as essential Wnt receptor components for PCP and Wnt-induced Vangl2 phosphorylation have laid the foundations for further understanding of Wnt/PCP signal transduction.

Acknowledgment

We thank the Yang lab for stimulating discussion, Drs. Jeff Rubin and Alan Kimmel for critical reading of the manuscript and Stephen Wincovitch for confocal microscopic analysis. We are grateful to Dr. Jeff Rubin for CKI cDNA constructs, Dr. Mathew Kelley for the Vangl2 antibodies and Dr. Roel Nusse for Ror2 antibodies. This study is supported by the intramural research program of National Human Genome Research Institute.

Experimental procedures

Mouse lines and genotyping. *Ror2*, *Wnt5a*, *Topgal* and *Vangl2* mouse strains and their genotyping methods have been described previously (DeChiara et al., 2000; Takeuchi et al., 2000; Yamaguchi et al., 1999; Song et al., 2010; Topol et al., 2003; Kibar et al., 2001).

Plasmids and Antibodies. Flag, Myc or HA tag was added to C-terminal end of Ror2 or N-terminal end of Vangl2 protein. YFP peptide was fused to N-terminus of Vangl2 protein and CFP peptide was fused to C-terminus of Ror2 protein. All Vangl2 S or T to A mutations, *Loop tail* mutations (D255E, S464N), kinase dead Ror2 mutations (K507R,

K510R, K512R) or Wnt5a mutations (C83S, C182R) were introduced by site-directed mutagenesis. Phospho-specific Vangl2 antibodies (pS84, pS82/84 and pS82+pS84) were generated by immunizing rabbits with respective phospho-peptide corresponding to amino acids 76~94, and affinity purified sequentially through columns covalently coupled with phospho-peptides and un-phospho-peptides. Other antibodies used in this study are described in the Extended Experimental Procedures.

Immunostaining and confocal microscopy. Embryos were fixed in 4%PFA for 30 minutes and subject to standard protocols of cryosection and fluorescent immunohistochemistry. Wheat germ agglutinin staining was performed following manufacture's protocol (Invitrogen). Confocal images were acquired by a Zeiss LSM 510 NLO Meta system. Projected Z-stack images were acquired at 0.2μm intervals for 4μm~8μm and projected by Zeiss LSM 510 software.

Luciferase assay. Mouse embryonic fibroblasts (MEFs) were transfected with Super-TOPFLASH (gift from Randy Moon) and Renilla Luciferase plasmids (Promega) by Lipofectamine 2000 (Invitrogen). 0.5% FCS-contained control medium, Wnt3a or Wnt5a conditioned medium from L Cells were added to the cells 24 hours after transfection and incubated for 24 hrs. Luciferase activity was measured on Lumat LB9507 Luminometer (EG&G Berthold) according to the Dual Luciferase Reporter Assay System Manual (Promega). The Super-TOPFLASH luciferase activity was normalized to Renilla luciferase activity.

Immunoprecipitation and Immunoblotting. In Co-IP experiment, transfected cells were lysed in lysis buffer (20 mM Tris-HCl, pH 7.4, 150 mM NaCl, 0.5% Nonidet P-40) with protease inhibitors cocktail (Roche) and phosphatase inhibitors (10mM NaF, 20mM

β-glycerophosphate, 1mM Na_3VO_4) and incubated with the indicated antibodies for overnight at 4 °C followed by 2 hours incubation of Protein-G Plus (Santa Cruz) at 4°C. Immunoprecipitates were washed three times in lysis buffer, dissolved in NuPAGE LDS sample buffer (Invitrogen), and subjected to standard Western immunoblot analysis.

Vangl2 phosphorylation assay. CHO cells ($1x10^5$) were seeded in 12-well plate for 24 hours before the cells were transfected with *Vangl2*, *Ror2* or *Wnt* expression plasmids by using Lipofectamine 2000 (Invitrogen). After 48 hours, cells were lysed in the above lysis buffer containing protease and phosphoatase inhibitors and proteins in the lysates were separated by 10% Bis-Tris Gel for 4 hours at 130V. Vangl2 protein was examined by standard immunoblot analysis. In coculture experiments, *Vangl2*-expressing and *Wnt5a*-expressing cells were trypsinized and mixed in various ratios 16 hours after transfection and cultured for 32 hours before harvesting. Wnt5a recombinant protein at indicated concentration was added into the medium of *Vangl2 and Ror2* -expressing cells 16 hours after transfection and the cells were incubated for 2 hours before harvesting.

FRET assay. YFP-Vangl2 or/and Ror2-CFP transfected MDCK cells growing on chambered coverglass were examined under Zeiss LSM 510 NLO Meta system. CFP, YFP, and FRET Images were obtained from three channels, respectively, using Zeiss AIM software. Sensitized Emission crosstalk coefficients were determined using control cells that expressed only YFP-Vangl2 or Ror2-CFP. Multiple cells and regions were chosen, processed and calculated by LSM FRET Tool Version 3.0. FRET efficiency was shown as N-FRET with intensities converted from the FRET index calculated for each pixel using the Xia method.

Zebrafish assay. mRNAs encoding wild type or mutant mouse *Vangl2* were synthesized using the Ambion mMessage mMachine Kit following its instructions. Different doses of mRNA were injected into offspring of $tri^{m209/+}$ zebrafish mating at 1 cell stage. After 48 hours, all injected zebrafish were classified into four groups according to phenotypes prior to genotyping. Genotyping method is described in the Extended Experimental Procedures. For western blot analysis, mRNAs were injected into wild type zebrafish embryos at 1 cell stage. The embryos were harvested and lysed after 24 hours.

References

Afzal, A.R., Rajab, A., Fenske, C.D., Oldridge, M., Elanko, N., Ternes-Pereira, E., Tuysuz, B., Murday, V.A., Patton, M.A., Wilkie, A.O., *et al.* (2000). Recessive Robinow syndrome, allelic to dominant brachydactyly type B, is caused by mutation of ROR2. Nat Genet *25*, 419-422.

Angers, S., and Moon, R.T. (2009). Proximal events in Wnt signal transduction. Nat Rev Mol Cell Biol *10*, 468-477.

Bastock, R., Strutt, H., and Strutt, D. (2003). Strabismus is asymmetrically localised and binds to Prickle and Dishevelled during Drosophila planar polarity patterning. Development *130*, 3007-3014.

Bi, W., Deng, J.M., Zhang, Z., Behringer, R.R., and de Crombrugghe, B. (1999). Sox9 is required for cartilage formation. Nat Genet *22*, 85-89.

Boehm, B., Westerberg, H., Lesnicar-Pucko, G., Raja, S., Rautschka, M., Cotterell, J., Swoger, J., and Sharpe, J. (2010). The role of spatially controlled cell proliferation in limb bud morphogenesis. PLoS Biol *8*, e1000420.

Borovina, A., Superina, S., Voskas, D., and Ciruna, B. (2010). Vangl2 directs the posterior tilting and asymmetric localization of motile primary cilia. Nat Cell Biol *12*, 407-412.

DeChiara, T.M., Kimble, R.B., Poueymirou, W.T., Rojas, J., Masiakowski, P., Valenzuela, D.M., and Yancopoulos, G.D. (2000). Ror2, encoding a receptor-like tyrosine kinase, is required for cartilage and growth plate development. Nat Genet *24*, 271-274.

Gavin, B.J., McMahon, J.A., and McMahon, A.P. (1990). Expression of multiple novel Wnt-1/int-1-related genes during fetal and adult mouse development. Genes Dev *4*, 2319-2332.

Green, J.L., Inoue, T., and Sternberg, P.W. (2008). Opposing Wnt pathways orient cell polarity during organogenesis. Cell *134*, 646-656.

Gros, J., Serralbo, O., and Marcelle, C. (2009). WNT11 acts as a directional cue to organize the elongation of early muscle fibres. Nature *457*, 589-593.

Gros, J., Hu, J.K., Vinegoni, C., Feruglio, P.F., Weissleder, R., and Tabin, C.J. (2010). WNT5A/JNK and FGF/MAPK pathways regulate the cellular events shaping the vertebrate limb bud. Curr Biol *20*, 1993-2002.

Guirao, B., Meunier, A., Mortaud, S., Aguilar, A., Corsi, J.M., Strehl, L., Hirota, Y., Desoeuvre, A., Boutin, C., Han, Y.G., *et al.* (2010). Coupling between hydrodynamic forces and planar cell polarity orients mammalian motile cilia. Nat Cell Biol *12*, 341-350.

Hashimoto, M., Shinohara, K., Wang, J., Ikeuchi, S., Yoshiba, S., Meno, C., Nonaka, S., Takada, S., Hatta, K., Wynshaw-Boris, A., *et al.* (2010). Planar polarization of node cells determines the rotational axis of node cilia. Nat Cell Biol *12*, 170-176.

Heisenberg, C.P., Tada, M., Rauch, G.J., Saude, L., Concha, M.L., Geisler, R., Stemple, D.L., Smith, J.C., and Wilson, S.W. (2000). Silberblick/Wnt11 mediates convergent extension movements during zebrafish gastrulation. Nature *405*, 76-81.

Hikasa, H., Shibata, M., Hiratani, I., and Taira, M. (2002). The Xenopus receptor tyrosine kinase Xror2 modulates morphogenetic movements of the axial mesoderm and neuroectoderm via Wnt signaling. Development *129*, 5227-5239.

Jessen, J.R., and Solnica-Krezel, L. (2004). Identification and developmental expression pattern of van gogh-like 1, a second zebrafish strabismus homologue. Gene Expr Patterns *4*, 339-344.

Jessen, J.R., Topczewski, J., Bingham, S., Sepich, D.S., Marlow, F., Chandrasekhar, A., and Solnica-Krezel, L. (2002). Zebrafish trilobite identifies new roles for Strabismus in gastrulation and neuronal movements. Nat Cell Biol *4*, 610-615.

Kani, S., Oishi, I., Yamamoto, H., Yoda, A., Suzuki, H., Nomachi, A., Iozumi, K., Nishita, M., Kikuchi, A., Takumi, T., *et al.* (2004). The receptor tyrosine kinase Ror2 associates with and is activated by casein kinase Iepsilon. J Biol Chem *279*, 50102-50109.

Kibar, Z., Bosoi, C.M., Kooistra, M., Salem, S., Finnell, R.H., De Marco, P., Merello, E., Bassuk, A.G., Capra, V., and Gros, P. (2009). Novel mutations in VANGL1 in neural tube defects. Hum Mutat *30*, E706-715.

Kibar, Z., Torban, E., McDearmid, J.R., Reynolds, A., Berghout, J., Mathieu, M., Kirillova, I., De Marco, P., Merello, E., Hayes, J.M., *et al.* (2007). Mutations in VANGL1 associated with neural-tube defects. N Engl J Med *356*, 1432-1437.

Kibar, Z., Vogan, K.J., Groulx, N., Justice, M.J., Underhill, D.A., and Gros, P. (2001). Ltap, a mammalian homolog of Drosophila Strabismus/Van Gogh, is altered in the mouse neural tube mutant Loop-tail. Nat Genet *28*, 251-255.

Kikuchi, A., Yamamoto, H., and Sato, A. (2009). Selective activation mechanisms of Wnt signaling pathways. Trends Cell Biol *19*, 119-129.

Klein, T.J., Jenny, A., Djiane, A., and Mlodzik, M. (2006). CKIepsilon/discs overgrown promotes both Wnt-Fz/beta-catenin and Fz/PCP signaling in Drosophila. Curr Biol *16*, 1337-1343.

Lawrence, P.A. (2001). Morphogens: how big is the big picture? Nat Cell Biol *3*, E151-154.

Lawrence, P.A., Struhl, G., and Casal, J. (2007). Planar cell polarity: one or two pathways? Nat Rev Genet *8*, 555-563.

Lei, Y.P., Zhang, T., Li, H., Wu, B.L., Jin, L., and Wang, H.Y. (2010). VANGL2 mutations in human cranial neural-tube defects. N Engl J Med *362*, 2232-2235.

Logan, C.Y., and Nusse, R. (2004). The wnt signaling pathway in development and disease. Annu Rev Cell Dev Biol *20*, 781-810.

McNeill, H. (2010). Planar cell polarity: keeping hairs straight is not so simple. Cold Spring Harb Perspect Biol *2*, a003376.

Merte, J., Jensen, D., Wright, K., Sarsfield, S., Wang, Y., Schekman, R., and Ginty, D.D. (2010). Sec24b selectively sorts Vangl2 to regulate planar cell polarity during neural tube closure. Nat Cell Biol *12*, 41-46; sup pp 41-48.

Mikels, A.J., and Nusse, R. (2006). Purified Wnt5a protein activates or inhibits beta-catenin-TCF signaling depending on receptor context. PLoS Biol *4*, e115.

Murdoch, J.N., Doudney, K., Paternotte, C., Copp, A.J., and Stanier, P. (2001). Severe neural tube defects in the loop-tail mouse result from mutation of Lpp1, a novel gene involved in floor plate specification. Hum Mol Genet *10*, 2593-2601.

Nomi, M., Oishi, I., Kani, S., Suzuki, H., Matsuda, T., Yoda, A., Kitamura, M., Itoh, K., Takeuchi, S., Takeda, K., *et al.* (2001). Loss of mRor1 enhances the heart and skeletal

abnormalities in mRor2-deficient mice: redundant and pleiotropic functions of mRor1 and mRor2 receptor tyrosine kinases. Mol Cell Biol *21*, 8329-8335.

Oishi, I., Suzuki, H., Onishi, N., Takada, R., Kani, S., Ohkawara, B., Koshida, I., Suzuki, K., Yamada, G., Schwabe, G.C., *et al.* (2003). The receptor tyrosine kinase Ror2 is involved in non-canonical Wnt5a/JNK signalling pathway. Genes Cells *8*, 645-654.

Parr, B.A., Shea, M.J., Vassileva, G., and McMahon, A.P. (1993). Mouse Wnt genes exhibit discrete domains of expression in the early embryonic CNS and limb buds. Development *119*, 247-261.

Person, A.D., Beiraghi, S., Sieben, C.M., Hermanson, S., Neumann, A.N., Robu, M.E., Schleiffarth, J.R., Billington, C.J., Jr., van Bokhoven, H., Hoogeboom, J.M., *et al.* (2010). WNT5A mutations in patients with autosomal dominant Robinow syndrome. Dev Dyn *239*, 327-337.

Qian, D., Jones, C., Rzadzinska, A., Mark, S., Zhang, X., Steel, K.P., Dai, X., and Chen, P. (2007). Wnt5a functions in planar cell polarity regulation in mice. Dev Biol *306*, 121-133.

Rauch, G.J., Hammerschmidt, M., Blader, P., Schauerte, H.E., Strahle, U., Ingham, P.W., McMahon, A.P., and Haffter, P. (1997). Wnt5 is required for tail formation in the zebrafish embryo. Cold Spring Harb Symp Quant Biol *62*, 227-234.

Rena, G., Bain, J., Elliott, M., and Cohen, P. (2004). D4476, a cell-permeant inhibitor of CK1, suppresses the site-specific phosphorylation and nuclear exclusion of FOXO1a. EMBO Rep *5*, 60-65.

Schwabe, G.C., Tinschert, S., Buschow, C., Meinecke, P., Wolff, G., Gillessen-Kaesbach, G., Oldridge, M., Wilkie, A.O., Komec, R., and Mundlos, S. (2000). Distinct

mutations in the receptor tyrosine kinase gene ROR2 cause brachydactyly type B. Am J Hum Genet *67*, 822-831.

Seifert, J.R., and Mlodzik, M. (2007). Frizzled/PCP signalling: a conserved mechanism regulating cell polarity and directed motility. Nat Rev Genet *8*, 126-138.

Song, H., Hu, J., Chen, W., Elliott, G., Andre, P., Gao, B., and Yang, Y. (2010). Planar cell polarity breaks the bilateral symmetry by controlling ciliary positioning. Nature *In press*.

Strutt, D. (2009). Gradients and the specification of planar polarity in the insect cuticle. Cold Spring Harb Perspect Biol *1*, a000489.

Strutt, H., Price, M.A., and Strutt, D. (2006). Planar polarity is positively regulated by casein kinase Iepsilon in Drosophila. Curr Biol *16*, 1329-1336.

Takeuchi, S., Takeda, K., Oishi, I., Nomi, M., Ikeya, M., Itoh, K., Tamura, S., Ueda, T., Hatta, T., Otani, H., *et al.* (2000). Mouse Ror2 receptor tyrosine kinase is required for the heart development and limb formation. Genes Cells *5*, 71-78.

Taylor, J., Abramova, N., Charlton, J., and Adler, P.N. (1998). Van Gogh: a new Drosophila tissue polarity gene. Genetics *150*, 199-210.

Topol, L., Jiang, X., Choi, H., Garrett-Beal, L., Carolan, P.J., and Yang, Y. (2003). Wnt-5a inhibits the canonical Wnt pathway by promoting GSK-3-independent {beta}-catenin degradation. J Cell Biol *162*, 899-908.

Torban, E., Patenaude, A.M., Leclerc, S., Rakowiecki, S., Gauthier, S., Andelfinger, G., Epstein, D.J., and Gros, P. (2008). Genetic interaction between members of the Vangl family causes neural tube defects in mice. Proc Natl Acad Sci U S A *105*, 3449-3454.

Torban, E., Wang, H.J., Patenaude, A.M., Riccomagno, M., Daniels, E., Epstein, D., and Gros, P. (2007). Tissue, cellular and sub-cellular localization of the Vangl2 protein during embryonic development: effect of the Lp mutation. Gene Expr Patterns *7*, 346-354.

Tree, D.R., Ma, D., and Axelrod, J.D. (2002). A three-tiered mechanism for regulation of planar cell polarity. Semin Cell Dev Biol *13*, 217-224.

Turing, A.M. (1952). The chemical basis of morphogenesis,. Philosophical Transactions of the Royal Society of London B *237*, 37-72.

van Bokhoven, H., Celli, J., Kayserili, H., van Beusekom, E., Balci, S., Brussel, W., Skovby, F., Kerr, B., Percin, E.F., Akarsu, N., *et al.* (2000). Mutation of the gene encoding the ROR2 tyrosine kinase causes autosomal recessive Robinow syndrome. Nat Genet *25*, 423-426.

Wang, Y., and Nathans, J. (2007). Tissue/planar cell polarity in vertebrates: new insights and new questions. Development *134*, 647-658.

Westfall, T.A., Brimeyer, R., Twedt, J., Gladon, J., Olberding, A., Furutani-Seiki, M., and Slusarski, D.C. (2003). Wnt-5/pipetail functions in vertebrate axis formation as a negative regulator of Wnt/{beta}-catenin activity. J Cell Biol *162*, 889-898.

Witze, E.S., Litman, E.S., Argast, G.M., Moon, R.T., and Ahn, N.G. (2008). Wnt5a control of cell polarity and directional movement by polarized redistribution of adhesion receptors. Science *320*, 365-369.

Wolpert, L. (1969). Positional information and the spatial pattern of cellular differentiation. J Theor Biol *25*, 1-47.

Wyngaarden, L.A., Vogeli, K.M., Ciruna, B.G., Wells, M., Hadjantonakis, A.K., and Hopyan, S. (2010). Oriented cell motility and division underlie early limb bud morphogenesis. Development *137*, 2551-2558.

Yamaguchi, T.P., Bradley, A., McMahon, A.P., and Jones, S. (1999). A Wnt5a pathway underlies outgrowth of multiple structures in the vertebrate embryo. Development *126*, 1211-1223.

Yamamoto, S., Nishimura, O., Misaki, K., Nishita, M., Minami, Y., Yonemura, S., Tarui, H., and Sasaki, H. (2008). Cthrc1 selectively activates the planar cell polarity pathway of Wnt signaling by stabilizing the Wnt-receptor complex. Dev Cell *15*, 23-36.

Yang, Y., Topol, L., Lee, H., and Wu, J. (2003). Wnt5a and Wnt5b exhibit distinct activities in coordinating chondrocyte proliferation and differentiation. Development *130*, 1003-1015.

Zallen, J.A. (2007). Planar polarity and tissue morphogenesis. Cell *129*, 1051-1063.

Figure legend

Figure 1. Ror2 and Vangl2 mediate Wnt5a signaling in embryonic development. (A) The limb length from the elbow to the distal tip is indicated by a line and quantified in the right column (two-tail *t*-test, all **p* values <0.01). Error bars are ± SD, n=3 (B) Sections of distal limbs showing chondrocyte organization in the newly formed cartilage (schematized in the right panel). Wheat germ agglutinin (red) stains chondrocyte extracellular matrix; DAPI (blue) stains the nucleus. (C) Statistical analysis of length-to-width ratio of chondrocytes shown in Figure 1B (two-tail *t*-test, all **p* values <0.01). Error bars are ± SD, n>100. L, length; W, width. (D) Neural tube was open (red arrows) in >50% of the *Ror2*$^{-/-}$; *Vangl2*$^{Lp/+}$ embryo. (E) The *Ror2*$^{-/-}$*; Vangl2*$^{-/-}$ and the *Wnt5a*$^{-/-}$ embryos exhibited identical phenotypes of loss of distal digits (circles), shortened frontonasal processes (arrows) and tails (arrowheads). The limb was enlarged in the lower panel. (F) Skeletal preparations stained by alcian blue and alizarin red of forelimbs. See also Figure S1.

Figure 2. Ror2 and Vangl2 together mediate Wnt5a inhibition of the Wnt/β-catenin signaling. (A) *Sox9* expression detected by whole mount *in situ* hybridization. Arrows indicate lack of chondrocyte differentiation in the distal limb mesenchymal cells of the *Ror2*$^{-/-}$; *Vangl2*$^{-/-}$ and *Wnt5a*$^{-/-}$ embryos. (B) X-gal staining of limb buds showed endogenous staining in the joint (black arrows) and ectopic staining in the distal limb of the *Ror2*$^{-/-}$; *Vangl2*$^{-/-}$; *TopGal* embryo (red arrows). (C) The Wnt/β-catenin signaling activity was measured by the TOPFLASH luciferase assay in MEF cells. The ability of Wnt5a to inhibit Wnt3a-induced Wnt/β-catenin activity in wild type MEFs (two-tail *t* test

*p=0.0013) is impaired in the *Ror2*$^{-/-}$ and *Ror2*$^{-/-}$; *Vangl2*$^{-/-}$ MEFs (two-tail *t* test, *p=0.0015). Error bars are ± SD, n=3. The control and Wnt3a conditioned medium was mixed with that of Wnt5a at a 1:1 ratio. See also Figure S2.

Figure 3. Wnt5a induces Ror2 and Vangl2 complex formation. (A) Fluorescent immunohistochemistry of Ror2 (red) and Vangl2 (green) (viewed by projected Z-stack) showing asymmetrical Vangl2 localization at E12.5, not E11.5 (arrows). Selected limb fields are schematized in the right panel. (B) Co-IP of Ror2 and Vangl2 in HEK293T cells. Wnt5a strongly increased their interaction. (C) MDCK cells expressing YFP-Vangl2 and Ror2-CFP were assayed for fluorescence resonance energy transfer efficiency (N-FRET) with (0.13 s.d. ± 0.02) or without Wnt5a (0.11 s.d. ± 0.05), Kolmogorov-Smirnov two-sample test (two-tail): p=0.029. (D) A *Loop-tail* mutant Vangl2^{Lp} (S464N) protein failed to form complex with Ror2 in HEK293T cells, even in the presence of Wnt5a. See also Figure S3.

Figure 4. Wnt5a is required for Vangl2 asymmetrical localization. (A) Digit chondrocytes of E12.5 embryos is shown by Sox9 expression (red) (upper panel). The selected regions (boxed) are enlarged and shown with Vangl2 (green) and β-catenin (red) co-staining (projected Z-stacks) (middle panel). The boxed regions are shown in lower panel with separate staining of Vangl2 and β-catenin. Vangl2 asymmetrical localization (arrow) is completely lost in the *Wnt5a*$^{-/-}$ limb. In the *Ror2*$^{-/-}$ mutant limb, Vangl2 asymmetrical localization was lost in the more mature cartilage (see Fig. S4A), but still detectable in the distal limb bud with reduced intensity (arrow). Vangl2 is still localized

to the cell membrane in *Wnt5a*$^{-/-}$ mutants (arrowhead). D, distal; P, proximal. (B) Projected Z-stack pictures of Vangl2 staining (green) from distal (D), middle (M) or proximal (P) parts of E12.5 wild type or *Ror2*$^{-/-}$ embryonic distal limbs (schematized in left panel). The number of cells with Vangl2 asymmetrical localization is progressively reduced from distal to proximal parts and much reduced in the *Ror2*$^{-/-}$ mutant. Quantified results were shown in lower panel. Error bars are ± SD, n=2. See also Figure S4.

Figure 5. Wnts act through Ror2 to induce Vangl2 phosphorylation. (A) Mobility shift of Vangl2 expressed in CHO cells on SDS-PAGE gel was enhanced by Wnt5a, but abolished after treatment with calf intestine phosphatase (CIP). (B) CHO cells were transfected to express different mouse *Wnts*, *Ror2* and *Vangl2* in the indicated combination. Vangl2 phosphorylation was analyzed by immunoblot. Arrows indicate hyperphosphorylated (upper), hypophosphorylated (middle) and unphosphorylated (lower) Vangl2 forms. (C) MEF cells were treated with recombinant Wnt5a protein for 2 hours and Vangl2 phosphorylation was analyzed. (D) Mouse Vangl2 with two phosphorylation clusters. Founder sites of Cluster I and II are underlined and shown in bold. Mutant Vangl2 with various serine/threonine (S/T) to alanine (A) variants are shown. (E) S84 and S82 are founder sites for Cluster I phosphorylation. Phosphorylation of Cluster II sites still occurred when all Cluster I sites were mutated. (F) S sites in Cluster II of *Vangl2* were individually mutated to A. Wnt5a-induced Vangl2 phosphorylation was progressively more reduced from S20A to S5A. (G) Mutating all three founder sites, S5, 82, 84, is sufficient to completely abolish both basal level and Wnt5a-induced phosphorylation in CHO cells. (H) Vangl2 phosphorylation is induced by

CK1δ not CK1ε and partially blocked by CKI inhibitor D4476 (100uM) in CHO cells. See also Figure S5.

Figure 6. Wnt-induced Vangl2 phosphorylation is required for its function. (A) CHO cells expressing wild type or the indicated mutant *Wnt5a* were cocultured with *Vangl2*- and *Ror2*- expressing CHO cells at a ratio of 4:1. (B) Ror2-BDB (W749X) and Ror2-RS (Q502X) mutants failed to enhance Wnt5a-induced Vangl2 phosphorylation in $Ror2^{-/-}$ MEFs. The kinase-dead Ror2 (Ror2-KD) showed similar activity as the wild type Ror2. (C) Effects of *Vangl2 Lp* mutations (D255E and S464N) and the control S464A mutation on Vangl2 phosphorylation were analyzed by immunoblot in CHO cells. (D) Analysis of endogenous Vangl2 protein levels and phosphorylation by immunoblot in the brain of the $Vangl2^{Lp/Lp}$ embryo. (E) Analysis of wild type Vangl2 phosphorylation in CHO cells when co-expressed with the D255E or S464N *Lp* mutant *Vangl2*. (F) Wild type, S84A, S5~17A::S76~84A (all phospho-mutant) or S5,82,84E (phospho-mimicking) mouse *Vangl2* mRNA was injected to offsprings from the zebrafish $tri^{m209/+}$ x $tri^{m209/+}$ matings at different doses. The phenotypes of injected zebrafish embryos were classified into four groups (group A, B, C and D) as shown by the representative pictures. (G) Statistical analysis of results of wild type (a, d), S84A (b, e), S5~17A::S76~84A (c, f) and S5,82,84E (g) mouse *Vangl2* mRNA injection. Numbers of injected zebrafish embryos of the indicated genotypes are indicated above the bars. The percentage of rescued $tri^{m209/m209}$ emrbyos (Group A and B) was shown on the right of each panel. (H) Analysis of Vangl2 proteins in the injected fish embryos. HA-tagged wild type and mutant Vangl2 proteins synthesized from different amounts of injected mRNA in wild type embryos

were shown in left panel. Quantified results by densitometer were shown in the right panel. Error bars are ± SD, n=3. See also Figure S6.

Figure 7. Wnt5a gradient controls pattern formation by regulating Vangl2 phosphorylation in a dose-dependent manner. (A) The E11.5 mouse limb bud was separated into distal, middle and proximal parts (schematics) for immunoblot analysis of Vangl2 phosphorylation. (B) Distal limb bud tissues of E11.5 wild type, *Ror2*$^{-/-}$ and *Wnt5a*$^{-/-}$ embryos, as shown by the schematic diagram, were subject to immunoblot analysis using Vangl2 or phospho-specific (pS82/84) Vangl2 antibodies. The Vangl2 in the *Ror2*$^{-/-}$ and *Wnt5a*$^{-/-}$ mutant limb was shifted to hypophosphorylated forms (lower arrows) without altering S84 and S82 phosphorylation. (C) *Wnt5a*-expressing CHO cells were cocultured with CHO cells expressing *Vangl2+Ror2* at increasing ratio. The last boxed lane was extracts from *Wnt5a*, *Ror2* and *Vangl2* co-transfected CHO cells that showed the most robust induction of Vangl2 phosphorylation. (D) Recombinant Wnt5a proteins induced Vangl2 phosphorylation in a dose-dependent manner in CHO cells after 2-hour treatment. Vangl2 phosphorylation was saturated by 500ng/ml of Wnt5a. (E, F) A model of a Wnt5a gradient controlling P-D limb elongation by providing a global directional cue. (E) Wnt5a induces Ror2 and Vangl2 complex formation and as a result, different numbers of S and T residues of Vangl2 in the two clusters were phosphorylated depending on the Wnt5a dosages. (F) Wnt5a is expressed in a gradient (orange) in the developing limb bud and this Wnt5a gradient is translated into an activity gradient of Vangl2 by inducing different levels of Vangl2 phosphorylation (blue). The Vangl2 activity gradient then induces asymmetrical Vangl2 localization (blue) and downstream

polarized events. See also Figure S7.

Figure 1

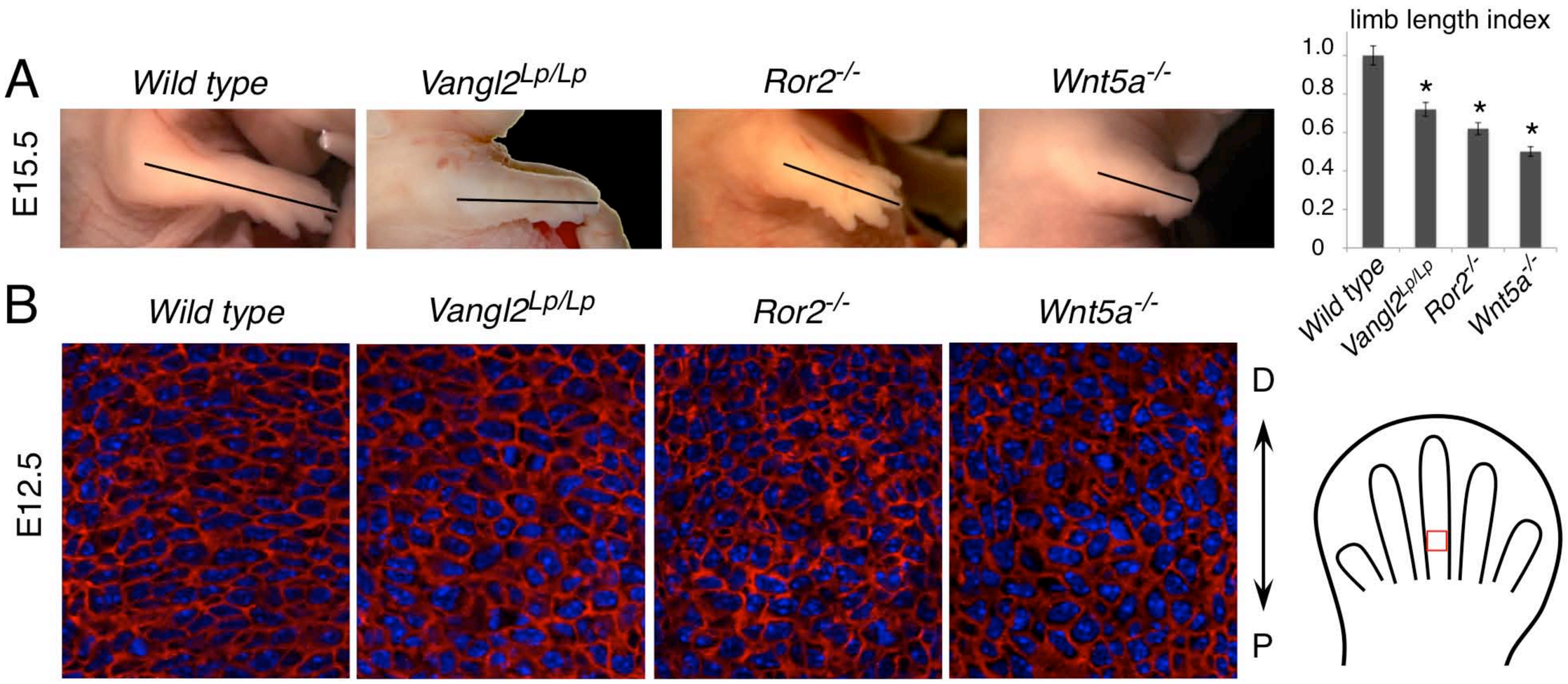
A
Wild type
Vangl2Lp/Lp
Ror2-/-
Wnt5a-/-
E15.5
limb length index
1.0
0.8
0.6
0.4
0.2
0
Wild type
Vangl2Lp/Lp
Ror2-/-
Wnt5a-/-
B
Wild type
Vangl2Lp/Lp
Ror2-/-
Wnt5a-/-
E12.5
D
P

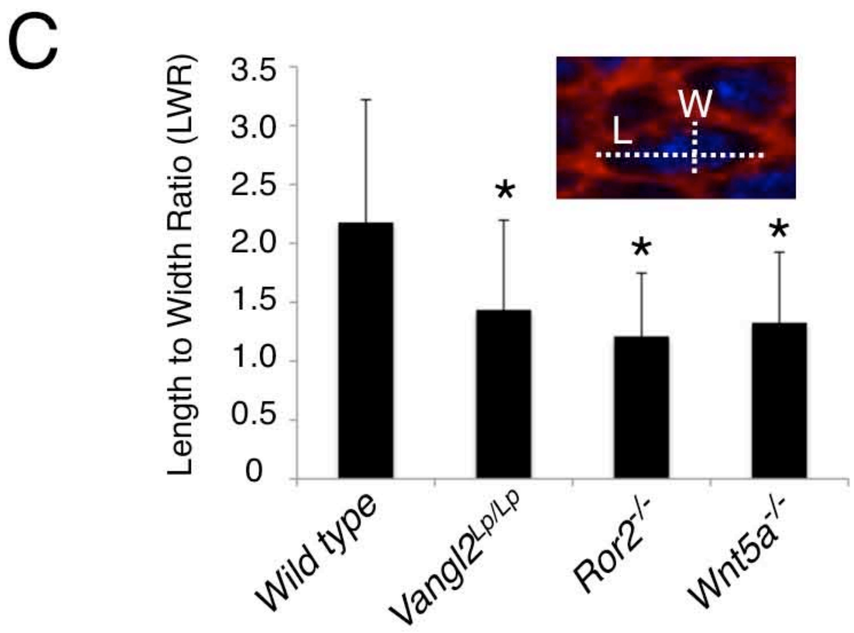
C
Length to Width Ratio (LWR)
3.5
3.0
2.5
2.0
1.5
1.0
0.5
0
L
W
Wild type
Vangl2Lp/Lp
Ror2-/-
Wnt5a-/-

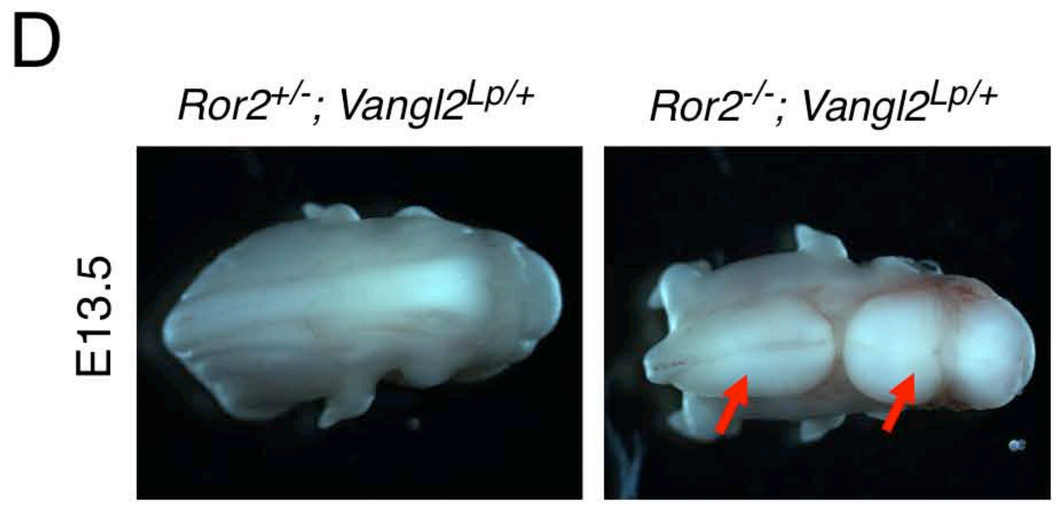
D
Ror2+/-; Vangl2Lp/+
Ror2-/-; Vangl2Lp/+
E13.5

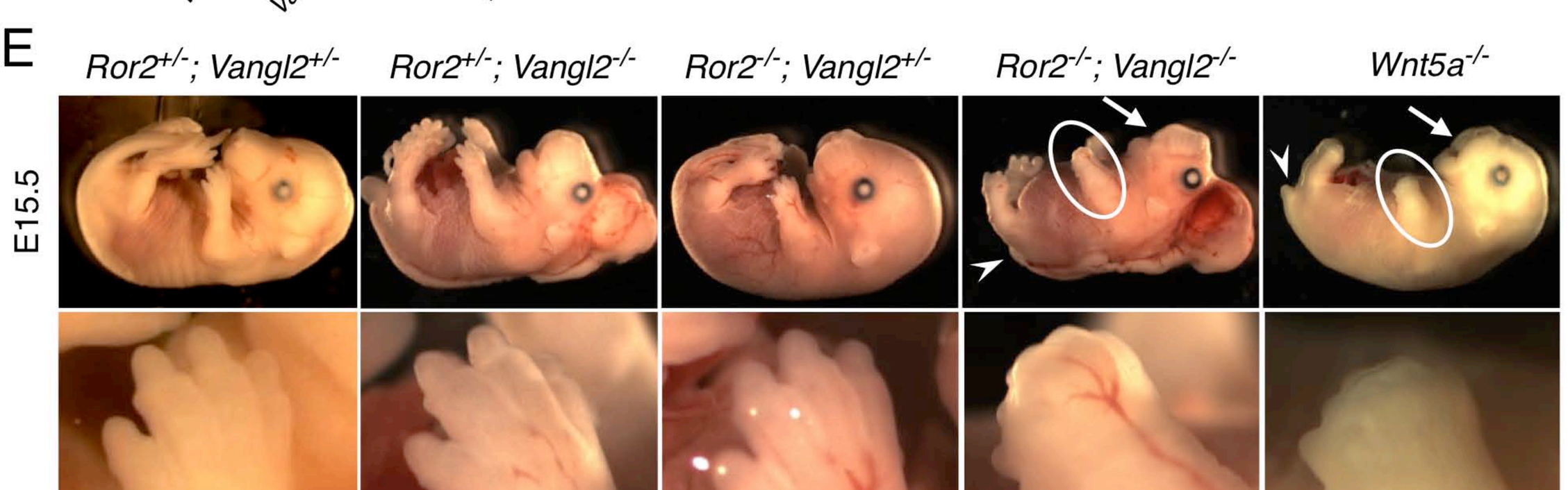
E
Ror2+/-; Vangl2+/-
Ror2+/-; Vangl2-/-
Ror2-/-; Vangl2+/-
Ror2-/-; Vangl2-/-
Wnt5a-/-
E15.5

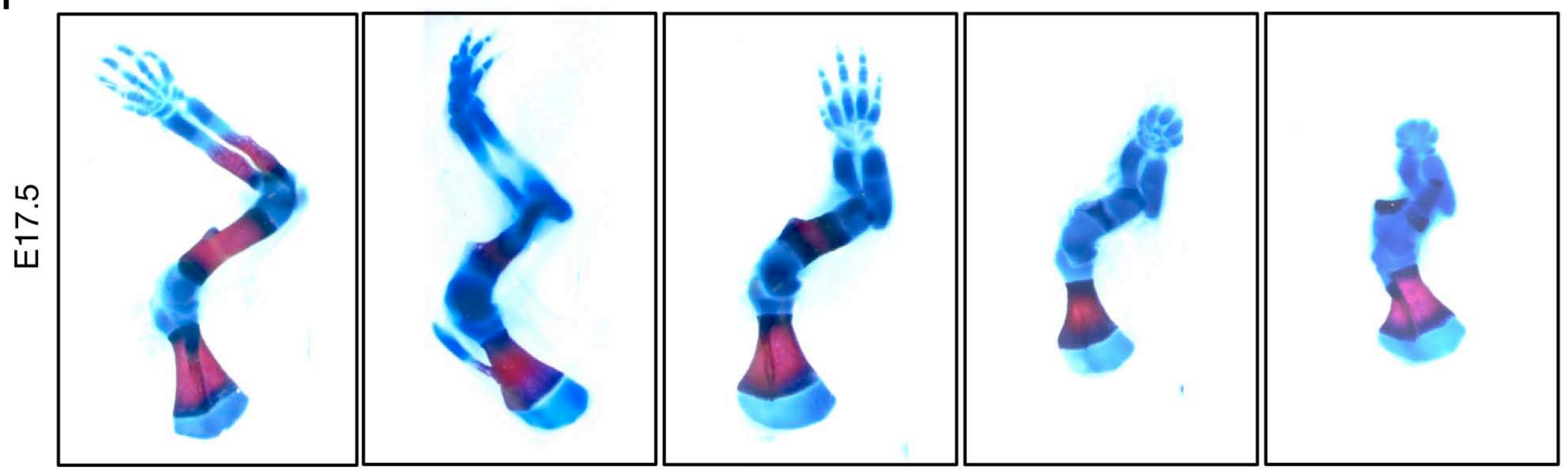
F
E17.5

Figure 2

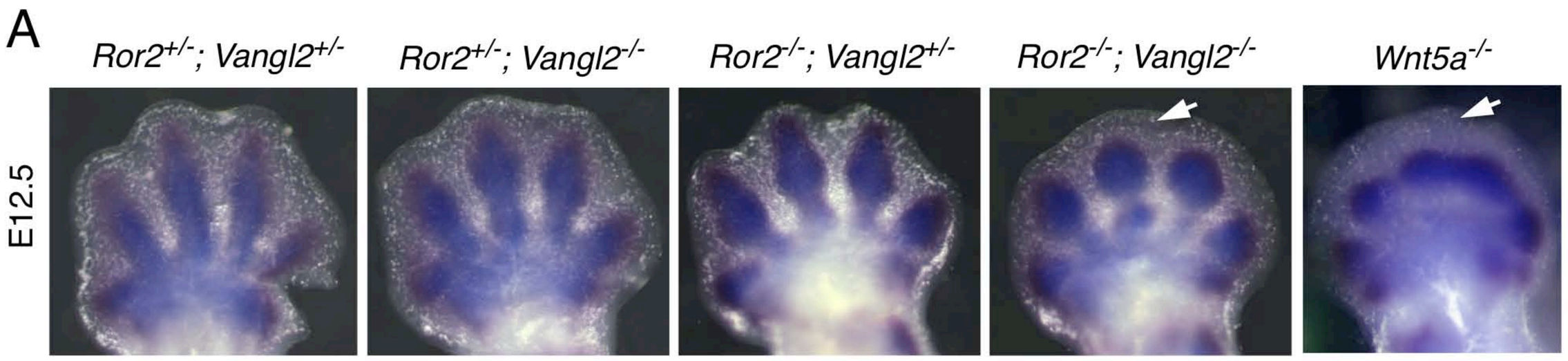
A
Ror2+/-; Vangl2+/-
Ror2+/-; Vangl2-/-
Ror2-/-; Vangl2+/-
Ror2-/-; Vangl2-/-
Wnt5a-/-
E12.5
B
Ror2+/-; Vangl2+/-; TopGal
Ror2-/-; Vangl2-/-; TopGal
E13.5
C
Luciferase activity
60
50
40
30
20
10
0
Wild type
Ror2-/-
Vangl2-/-
Ror2-/-; Vangl2-/-
*
*
Ctrl
Ctrl / Wnt5a
Ctrl / Wnt3a
Wnt3a / Wnt5a

Figure 3

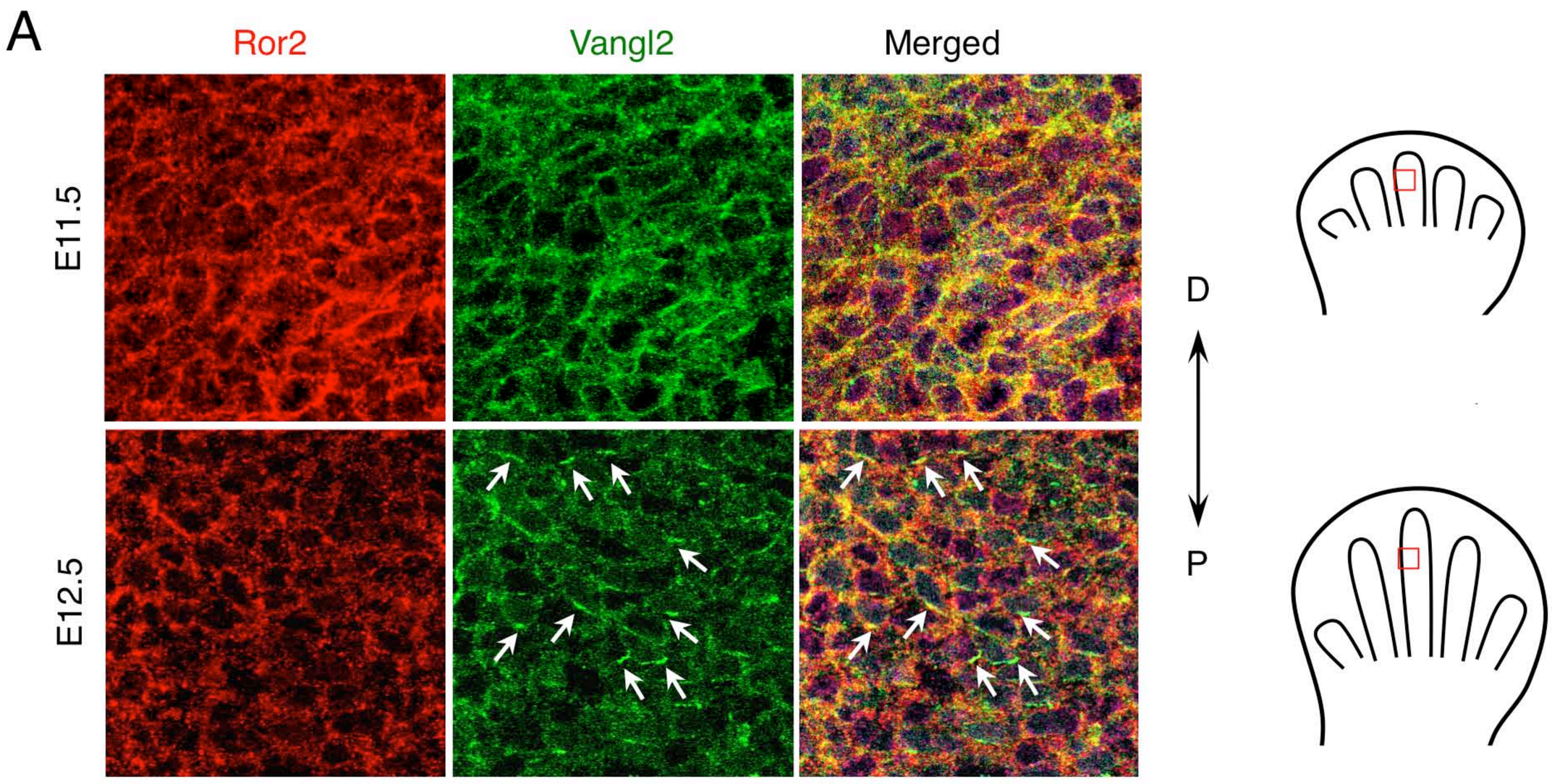
A
Ror2
Vangl2
Merged
E11.5
E12.5
D
P

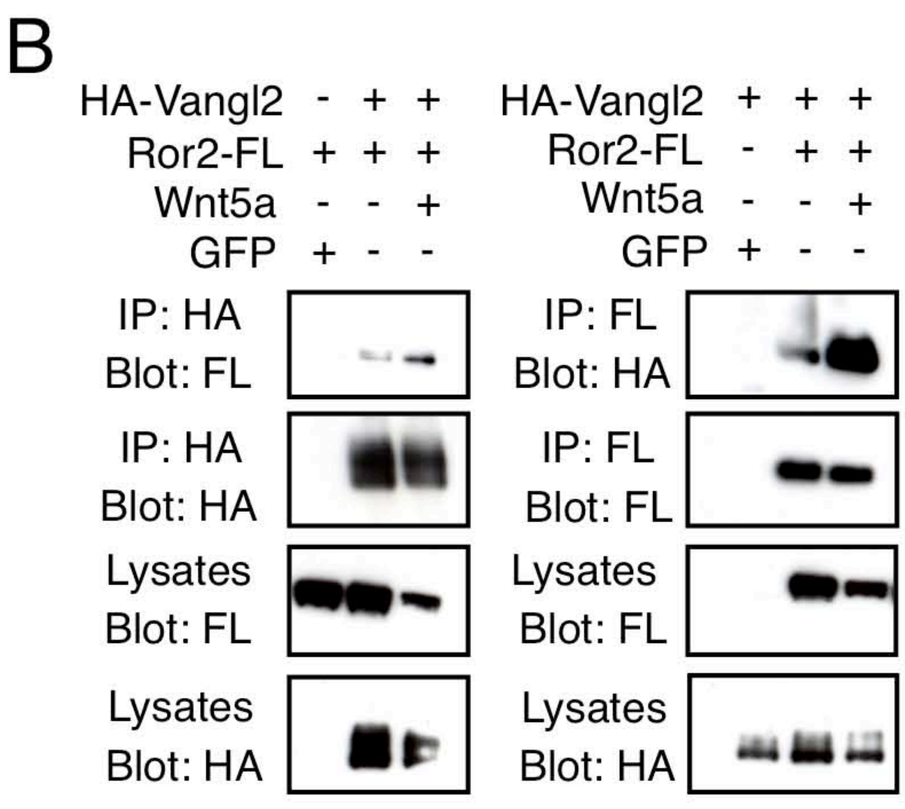
B
HA-Vangl2 - + +
Ror2-FL + + +
Wnt5a - - +
GFP + - -
IP: HA
Blot: FL
IP: HA
Blot: HA
Lysates
Blot: FL
Lysates
Blot: HA
HA-Vangl2 + + +
Ror2-FL - + +
Wnt5a - - +
GFP + - -
IP: FL
Blot: HA
IP: FL
Blot: FL
Lysates
Blot: FL
Lysates
Blot: HA

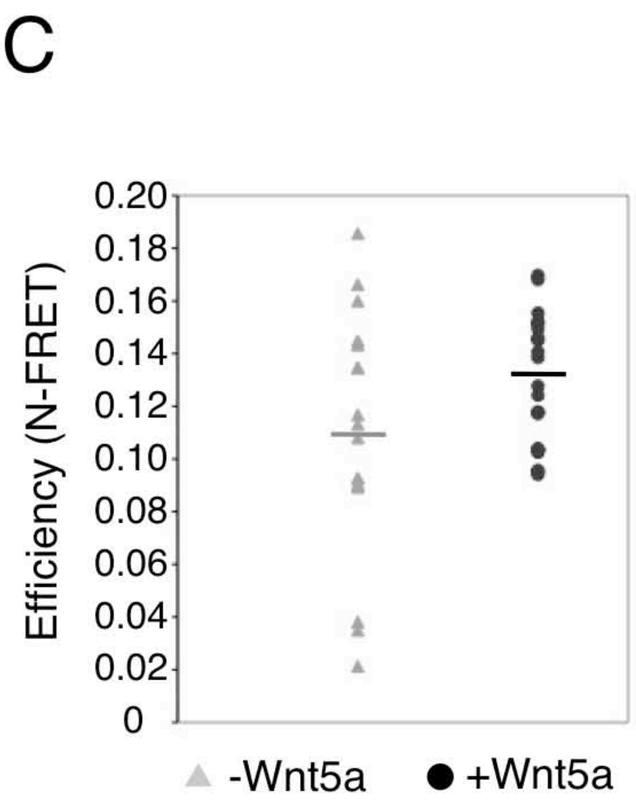
C
Efficiency (N-FRET)
0.20
0.18
0.16
0.14
0.12
0.10
0.08
0.06
0.04
0.02
0
-Wnt5a
+Wnt5a

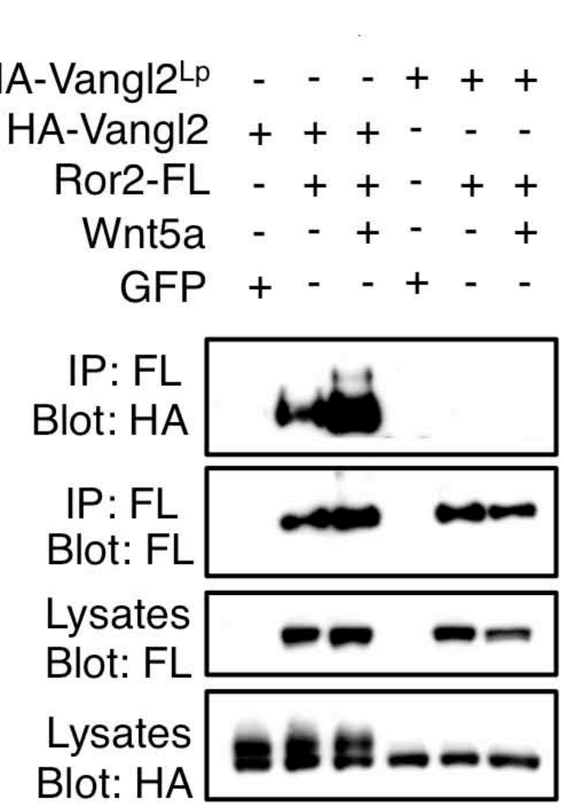
D
HA-Vangl2Lp - - - + + +
HA-Vangl2 + + + - - -
Ror2-FL - + + - + +
Wnt5a - - + - - +
GFP + - - + - -
IP: FL
Blot: HA
IP: FL
Blot: FL
Lysates
Blot: FL
Lysates
Blot: HA

Figure 4

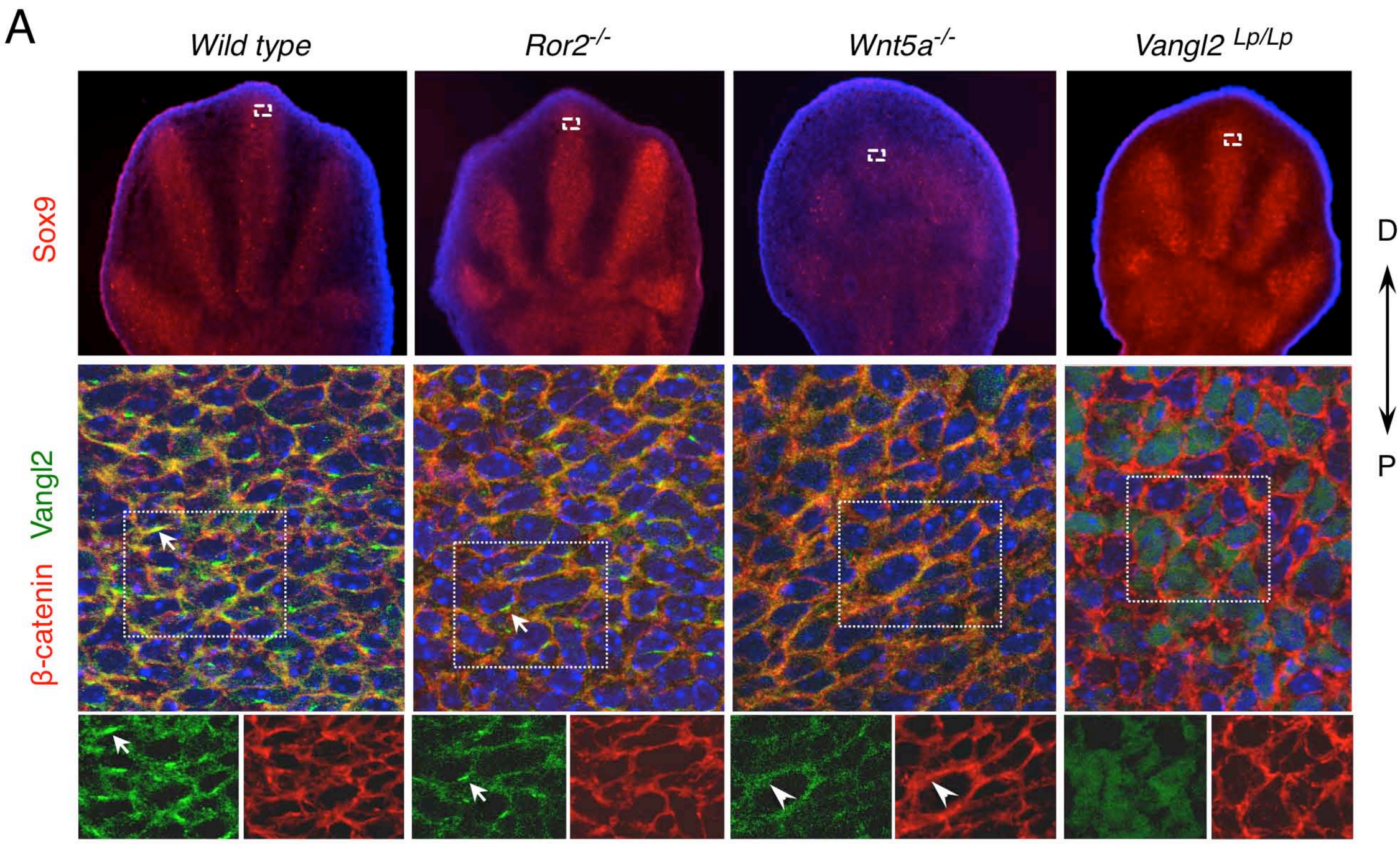
A
Wild type
Ror2-/-
Wnt5a-/-
Vangl2 Lp/Lp
Sox9
β-catenin Vangl2
D
P
B
Distal
Middle
Proximal
Wild type
Vangl2
D
M
P
Ror2-/-
Vangl2
D
P
Percentage of cells with asymmetrically localized Vangl2
50%
40%
30%
20%
10%
0
Wild type
Ror2-/-
Distal
Middle
Proximal

Figure 5

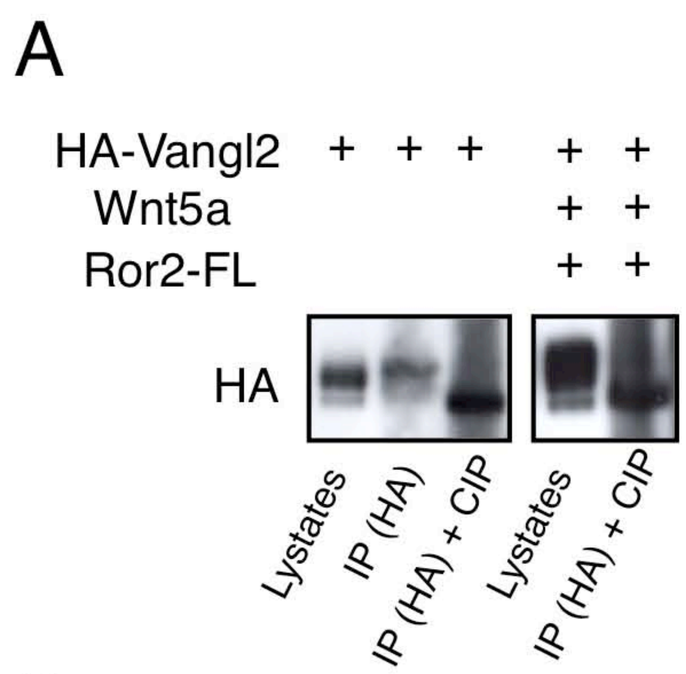
A
HA-Vangl2 + + + + +
Wnt5a + +
Ror2-FL + +
HA
Lystates
IP (HA)
IP (HA) + CIP
Lystates
IP (HA) + CIP

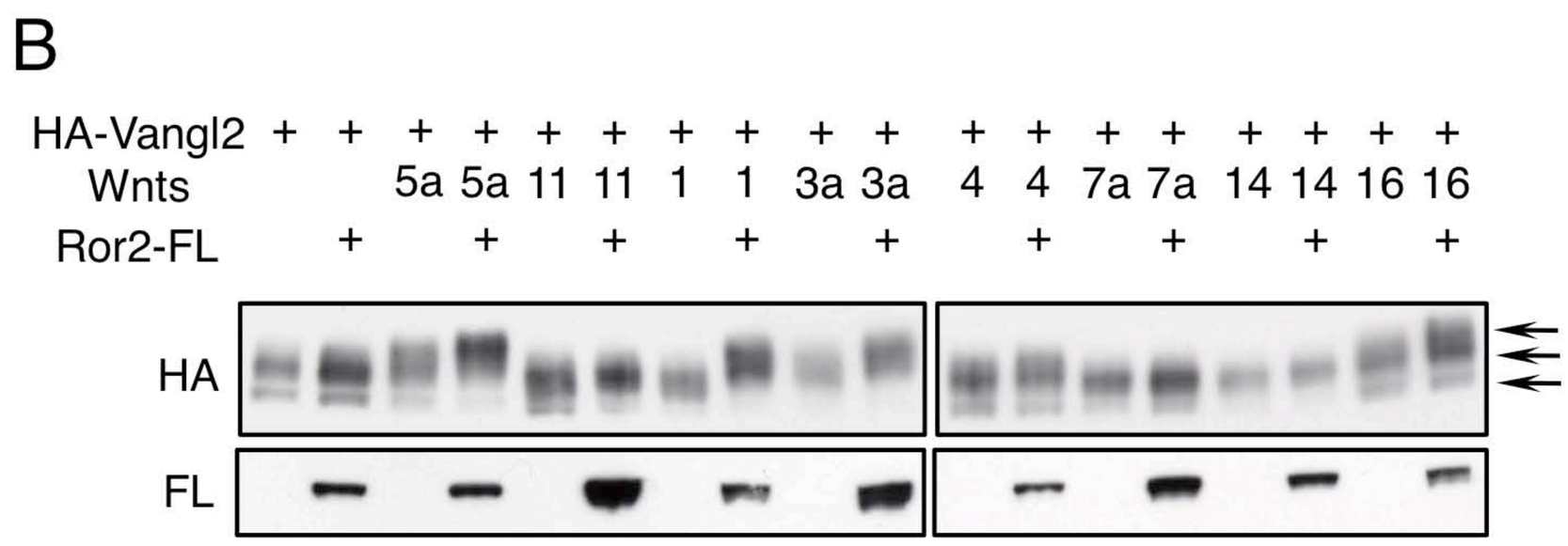
B
HA-Vangl2 + + + + + + + + + + + + + + + +
Wnts 5a 5a 11 11 1 1 3a 3a 4 4 7a 7a 14 14 16 16
Ror2-FL + + + + + + + +
HA
FL

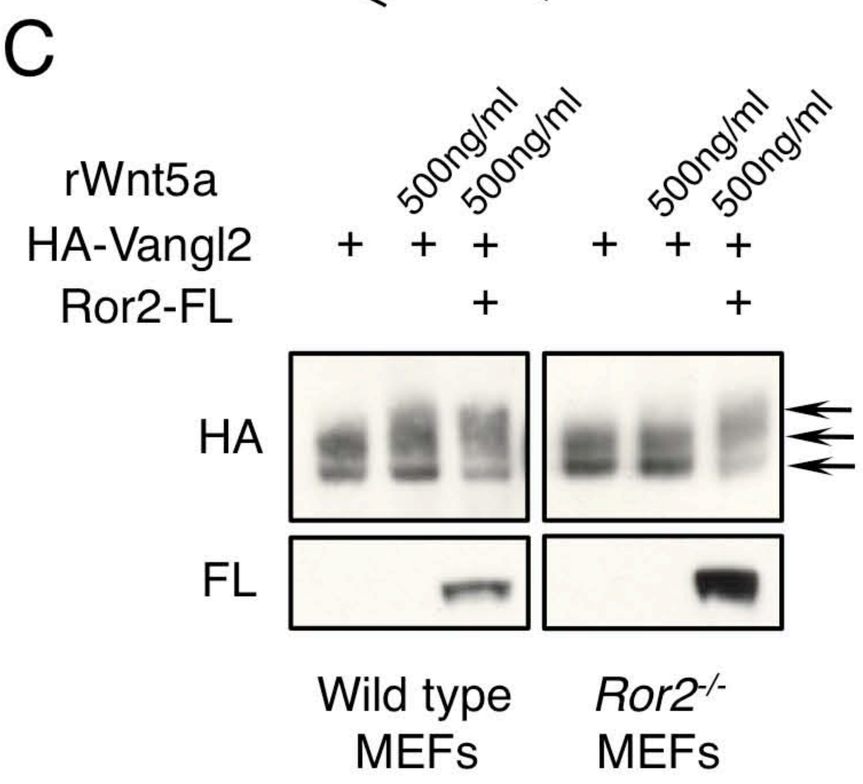
C
rWnt5a 500ng/ml 500ng/ml 500ng/ml 500ng/ml
HA-Vangl2 + + + + + +
Ror2-FL + +
HA
FL
Wild type MEFs
Ror2-/- MEFs

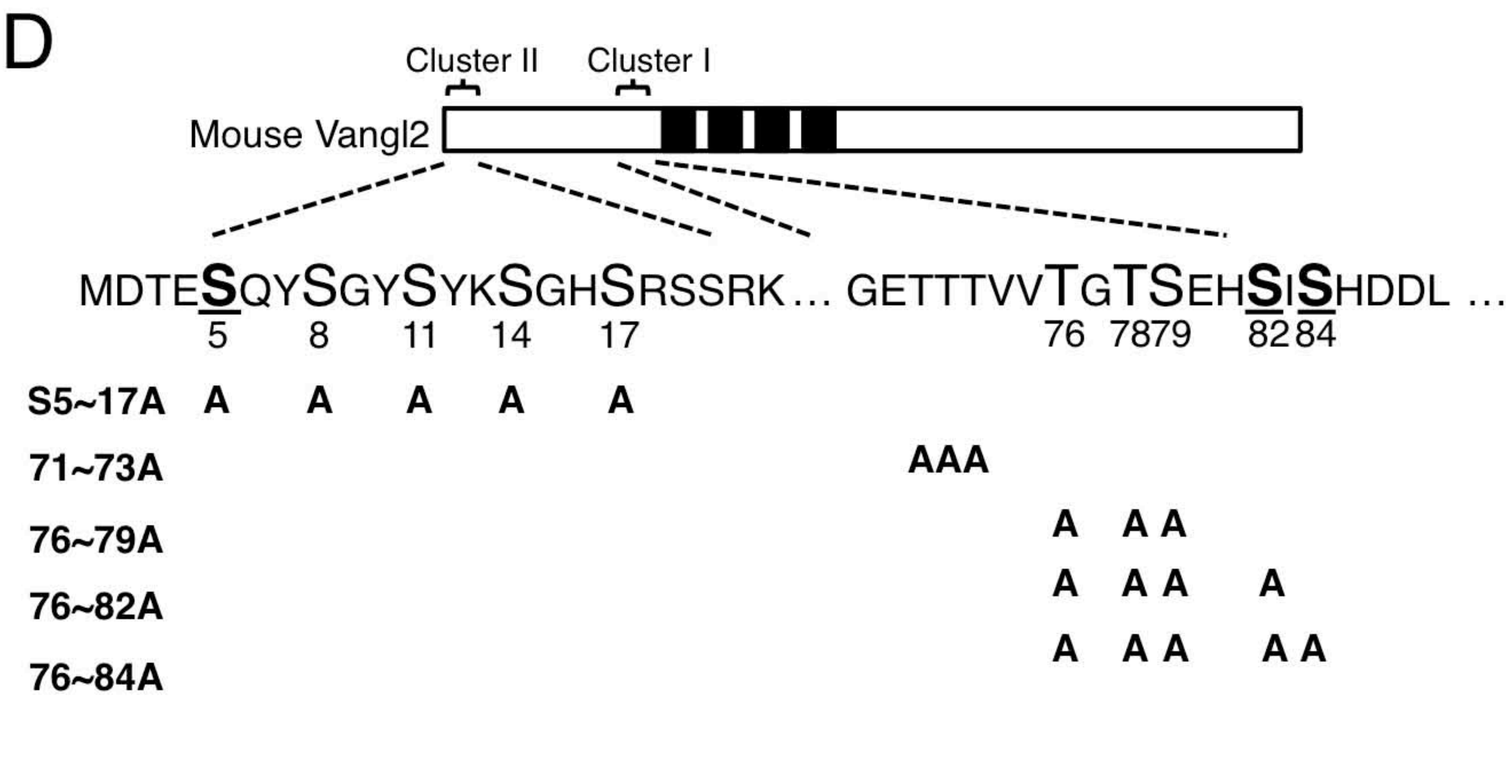
D
Cluster II
Cluster I
Mouse Vangl2
MDTESQYSGYSYKSGHSRSSRK… GETTTVVTGTSEHSISHDDL …
5 8 11 14 17 76 7879 8284
S5~17A A A A A A
71~73A AAA
76~79A A A A
76~82A A A A A
76~84A A A A A A

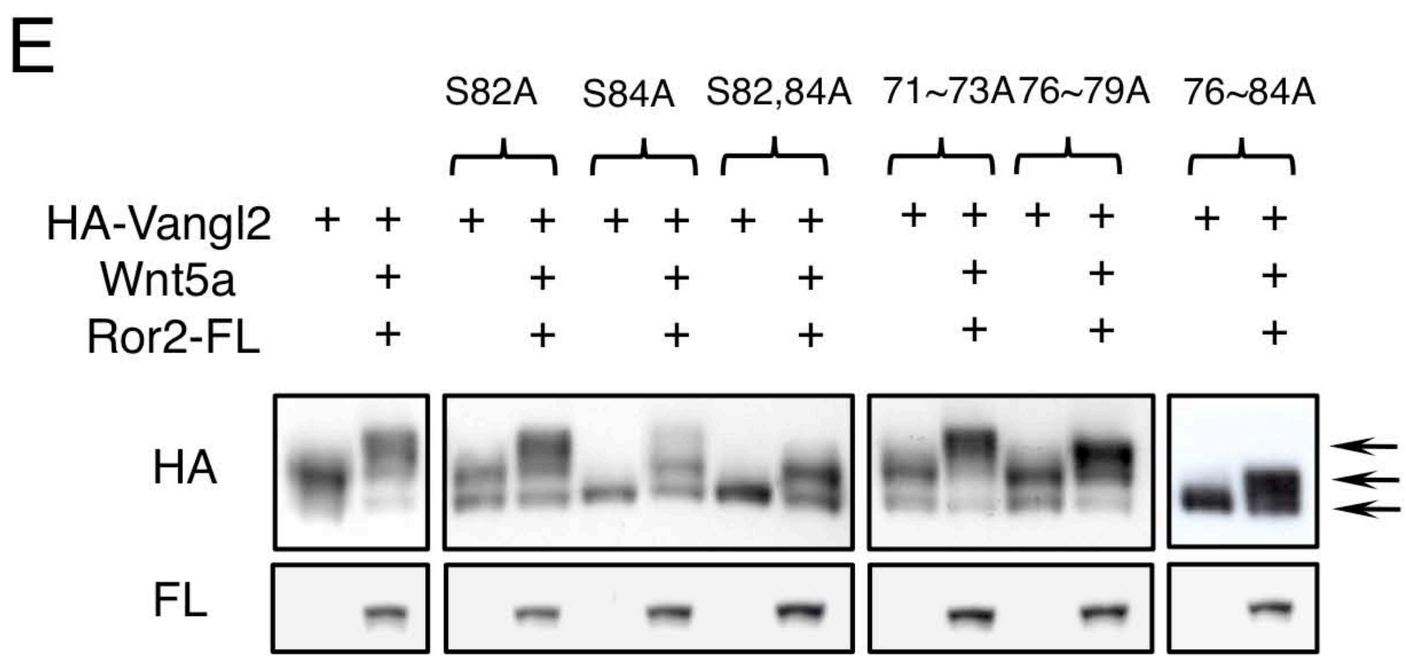
E
S82A S84A S82,84A 71~73A 76~79A 76~84A
HA-Vangl2 + + + + + + + + + + + + + +
Wnt5a + + + + + + + +
Ror2-FL + + + + + + + +
HA
FL

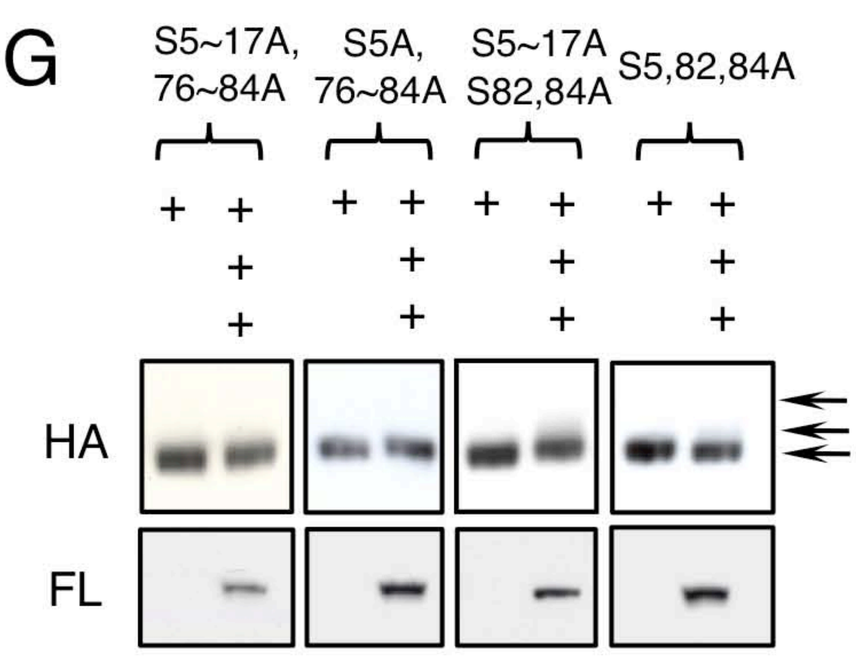
G
S5~17A, 76~84A
S5A, 76~84A
S5~17A S82,84A
S5,82,84A
HA
FL

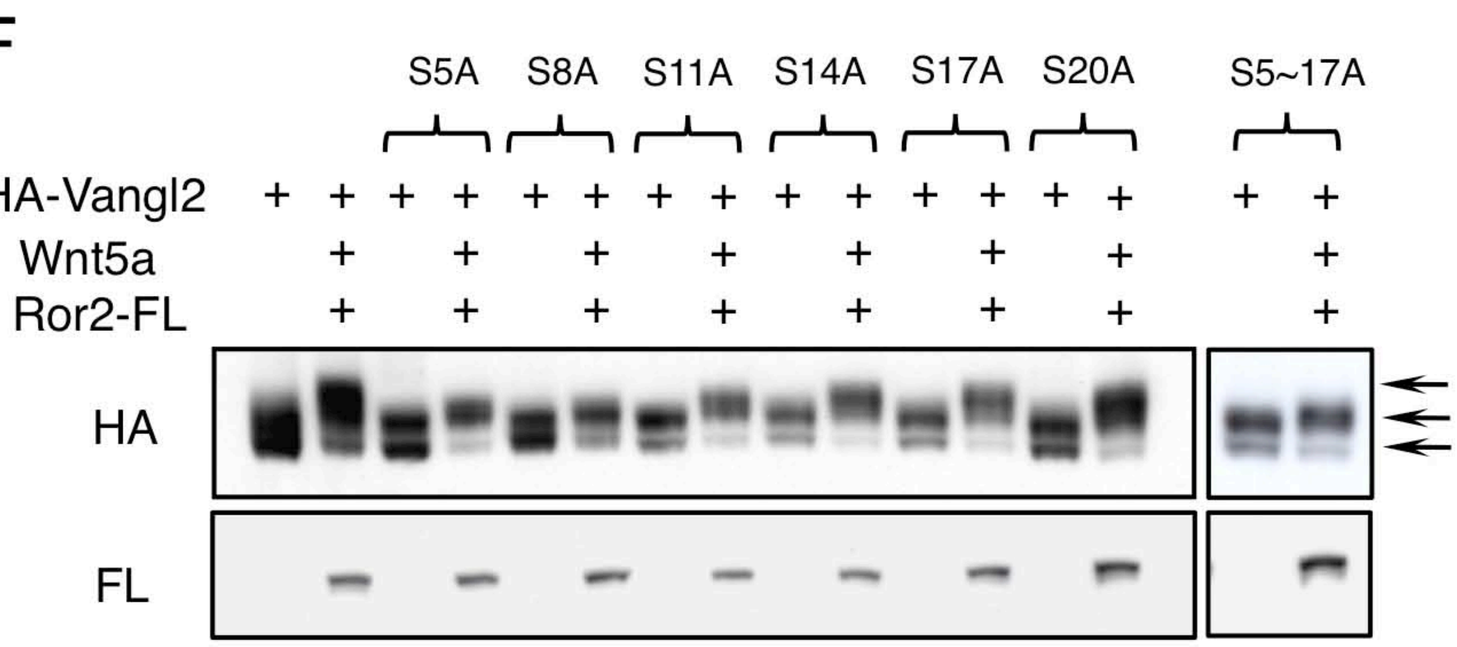
F
S5A S8A S11A S14A S17A S20A S5~17A
HA-Vangl2 + + + + + + + + + + + + + + + +
Wnt5a + + + + + + + +
Ror2-FL + + + + + + + +
HA
FL

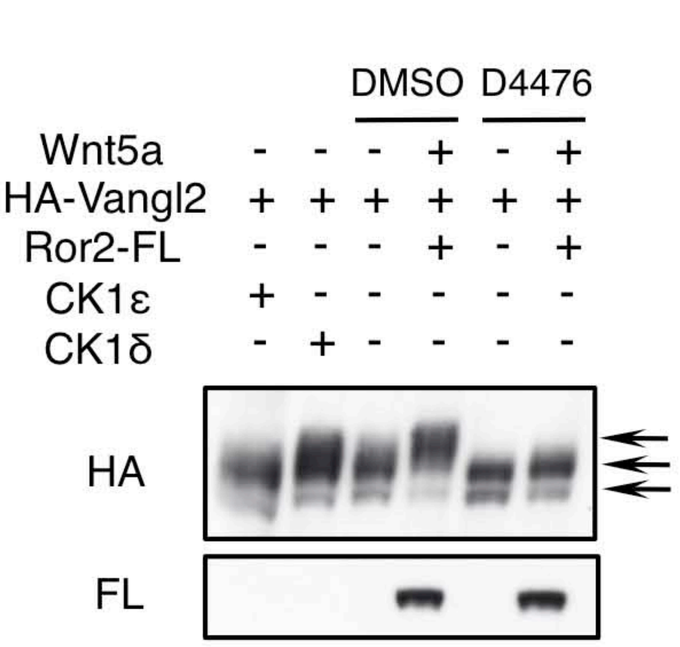
H
DMSO D4476
Wnt5a - - - + - +
HA-Vangl2 + + + + + +
Ror2-FL - - - + - +
CK1ε + - - - - -
CK1δ - + - - - -
HA
FL

Figure 6

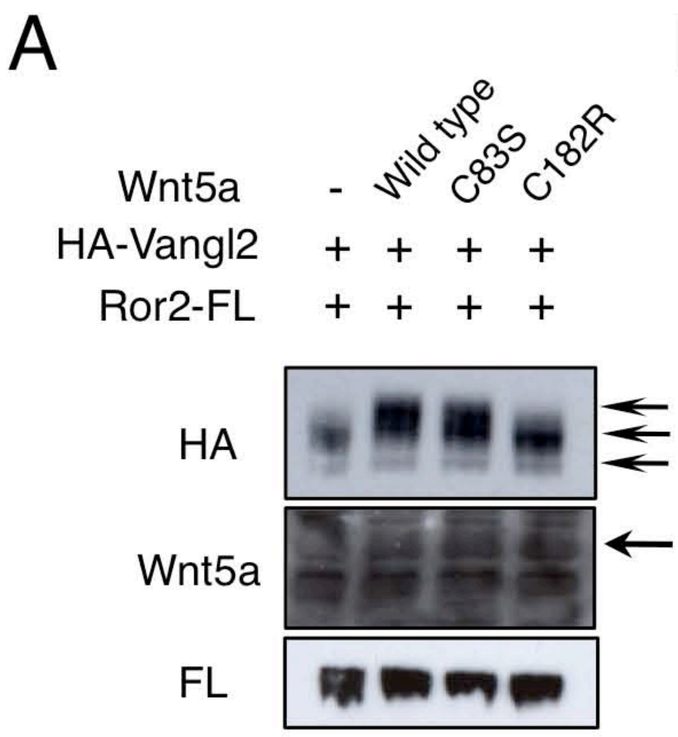
A
Wnt5a
HA-Vangl2
Ror2-FL
-
Wild type
C83S
C182R
HA
Wnt5a
FL

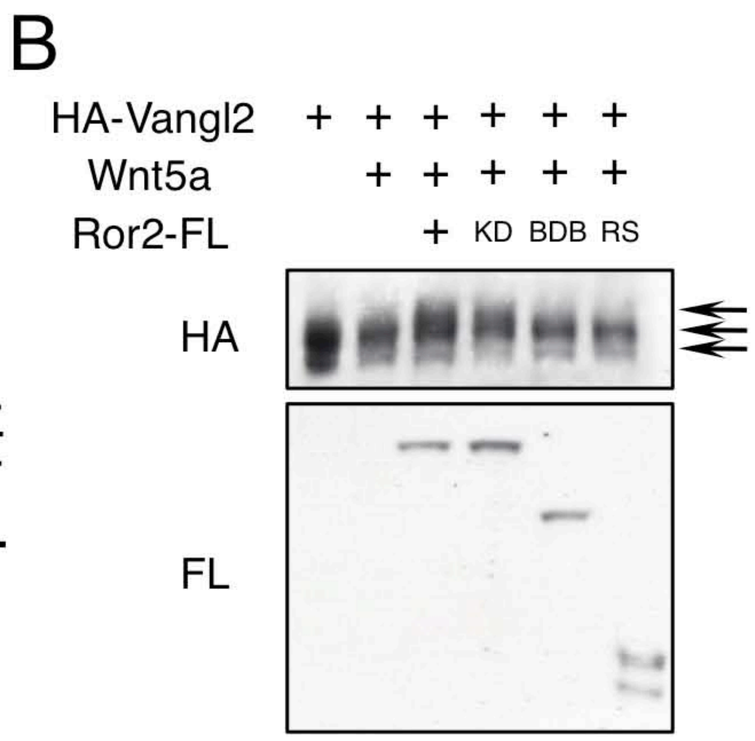
B
HA-Vangl2
Wnt5a
Ror2-FL
KD
BDB
RS
HA
FL

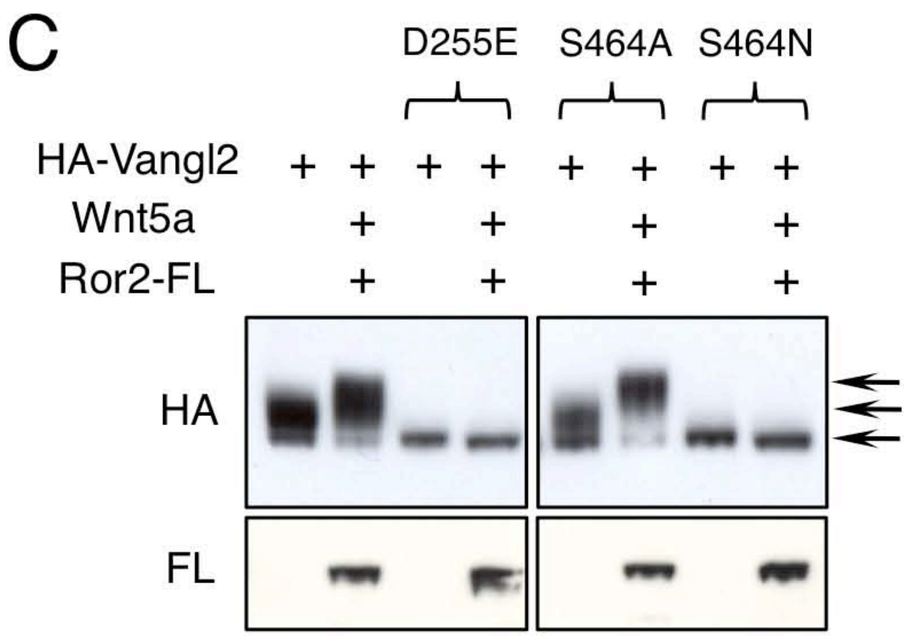
C
D255E
S464A
S464N
HA-Vangl2
Wnt5a
Ror2-FL
HA
FL

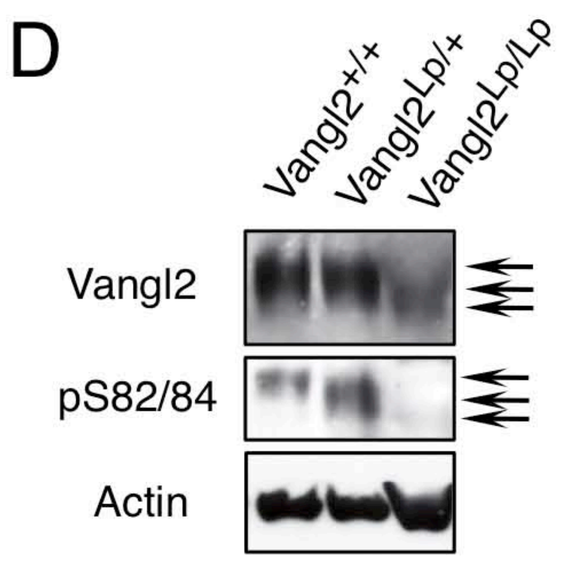
D
Vangl2+/+
Vangl2Lp/+
Vangl2Lp/Lp
Vangl2
pS82/84
Actin

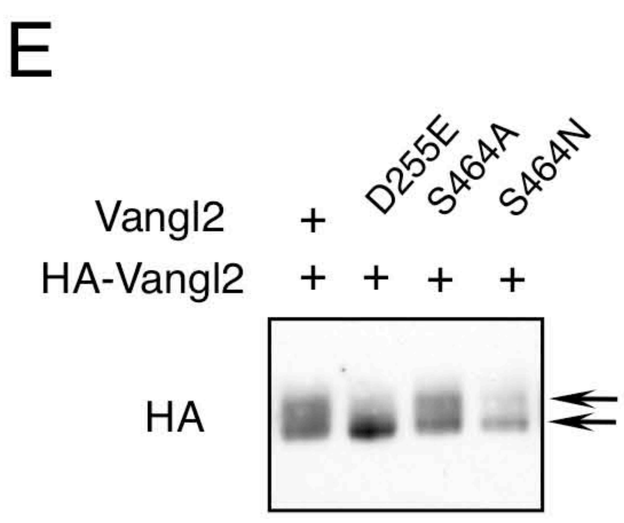
E
Vangl2
D255E
S464A
S464N
HA-Vangl2
HA

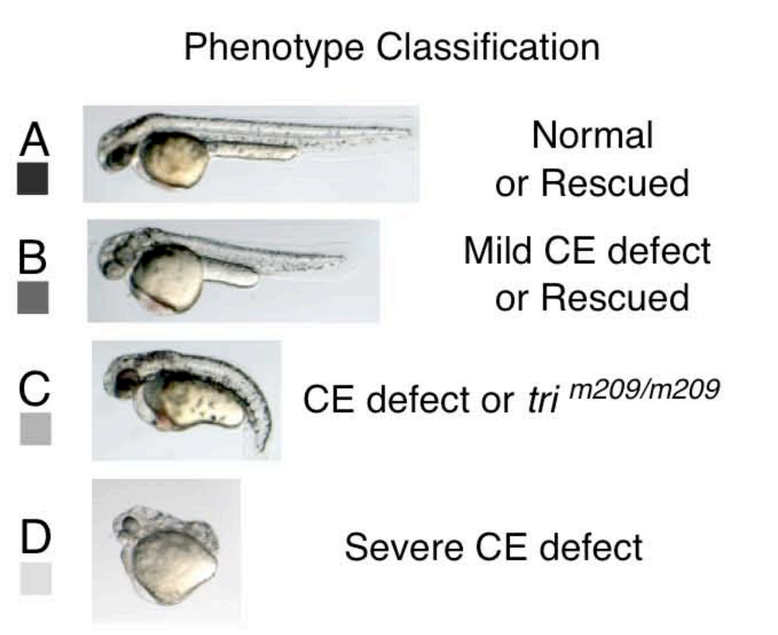
F
Phenotype Classification
A
Normal
or Rescued
B
Mild CE defect
or Rescued
C
CE defect or tri m209/m209
D
Severe CE defect

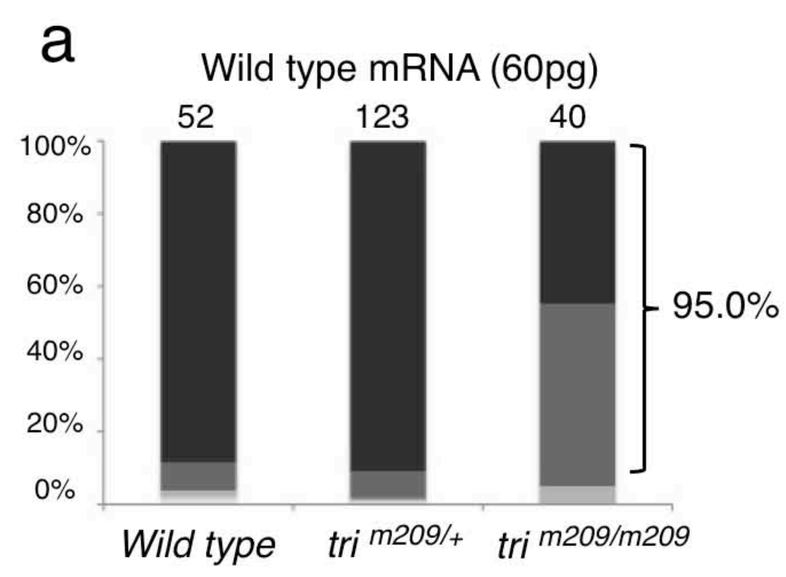
G
a
Wild type mRNA (60pg)
52
123
40
95.0%
Wild type
tri m209/+
tri m209/m209

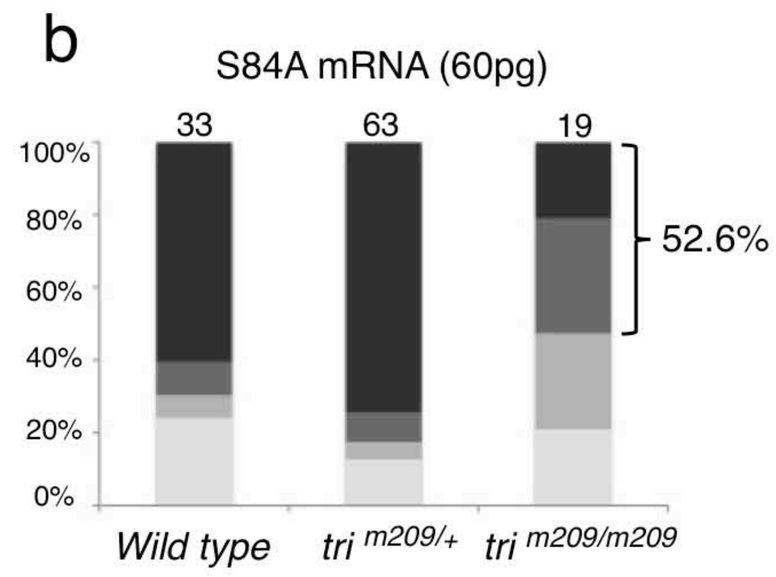
b
S84A mRNA (60pg)
33
63
19
52.6%
Wild type
tri m209/+
tri m209/m209

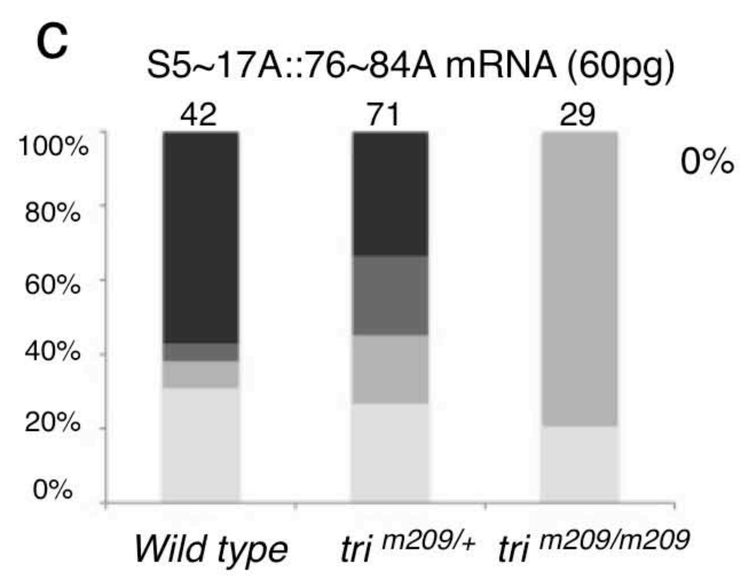
c
S5~17A::76~84A mRNA (60pg)
42
71
29
0%
Wild type
tri m209/+
tri m209/m209

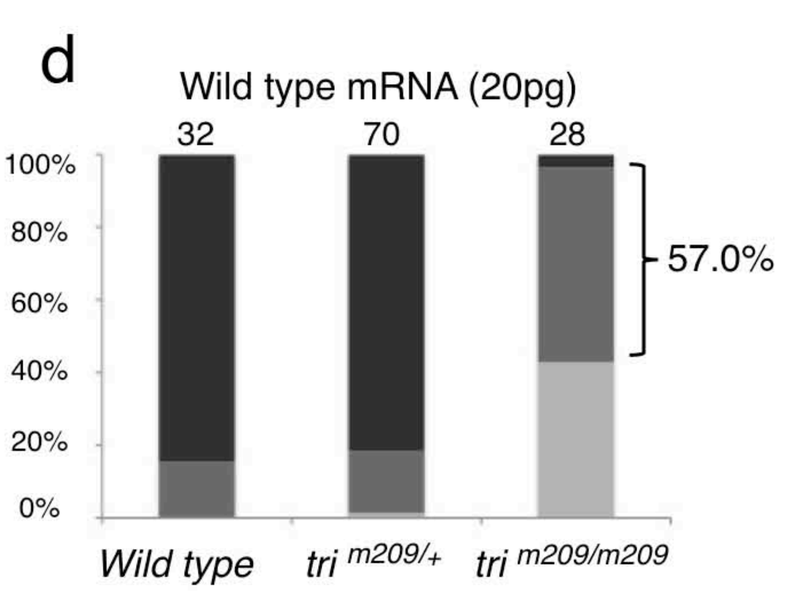
d
Wild type mRNA (20pg)
32
70
28
57.0%
Wild type
tri m209/+
tri m209/m209

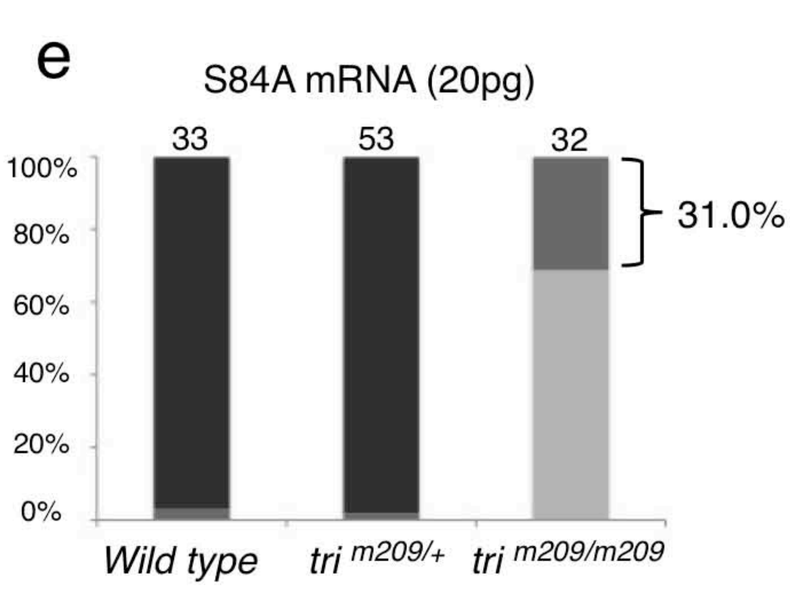
e
S84A mRNA (20pg)
33
53
32
31.0%
Wild type
tri m209/+
tri m209/m209

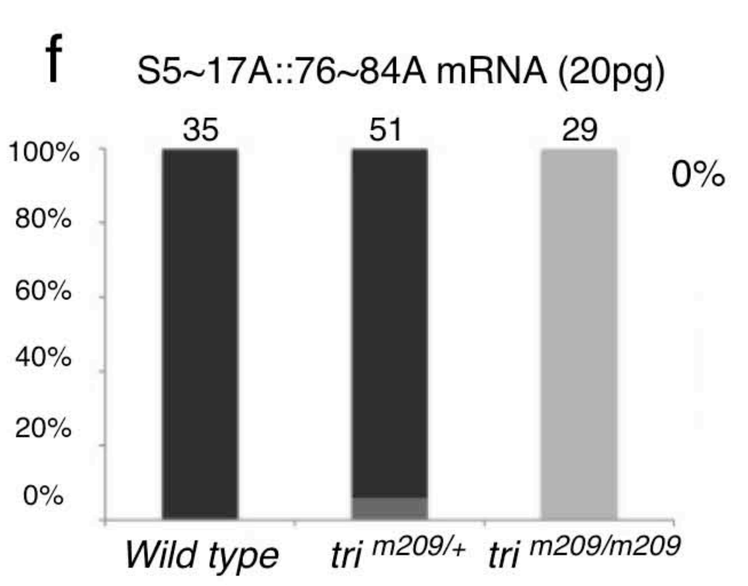
f
S5~17A::76~84A mRNA (20pg)
35
51
29
0%
Wild type
tri m209/+
tri m209/m209

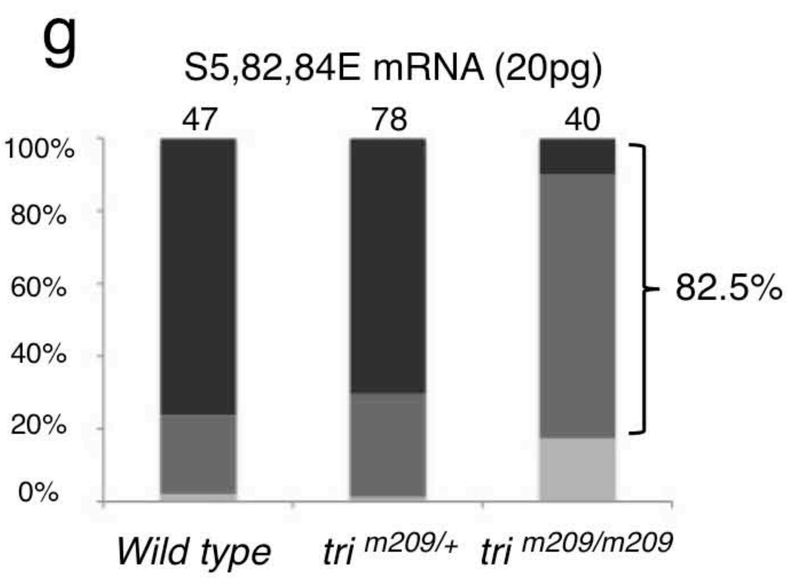
g
S5,82,84E mRNA (20pg)
47
78
40
82.5%
Wild type
tri m209/+
tri m209/m209

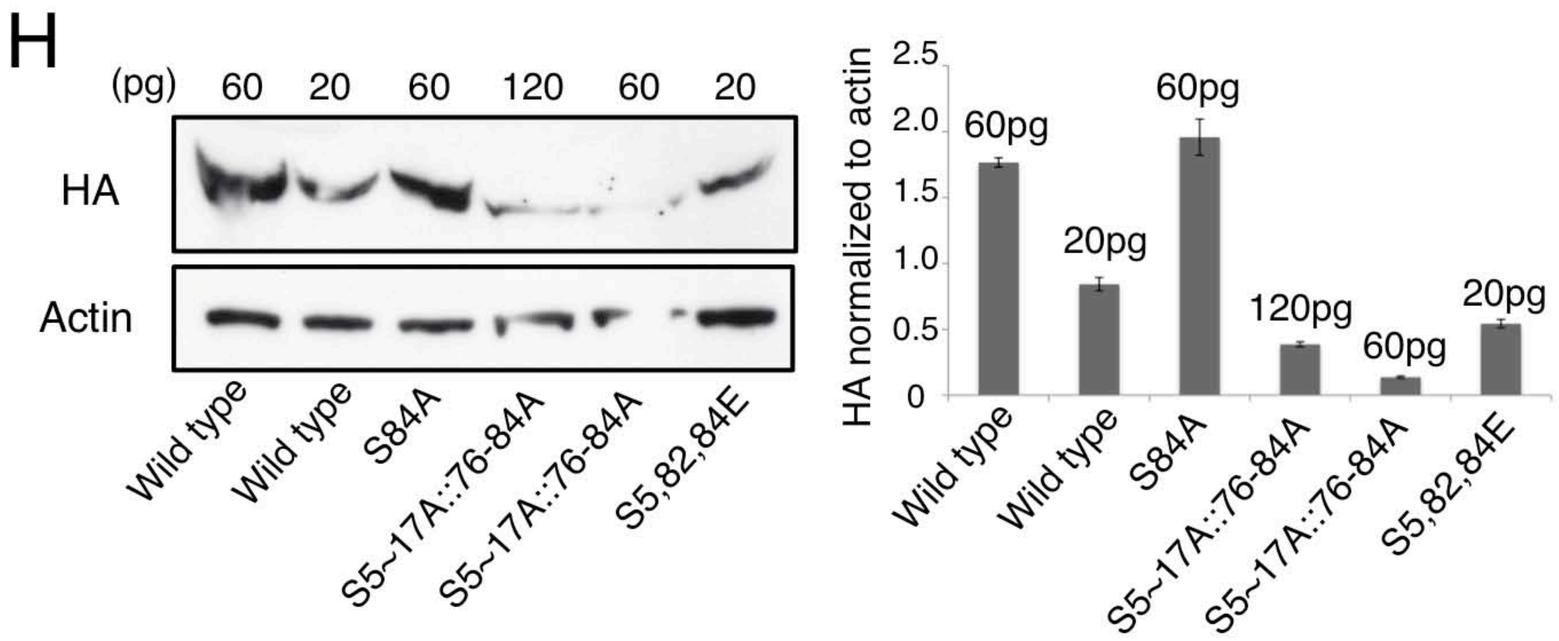
H
(pg)
60
20
60
120
60
20
HA
Actin
Wild type
Wild type
S84A
S5~17A::76-84A
S5~17A::76-84A
S5,82,84E
HA normalized to actin
60pg
20pg
60pg
120pg
60pg
20pg

Figure 7

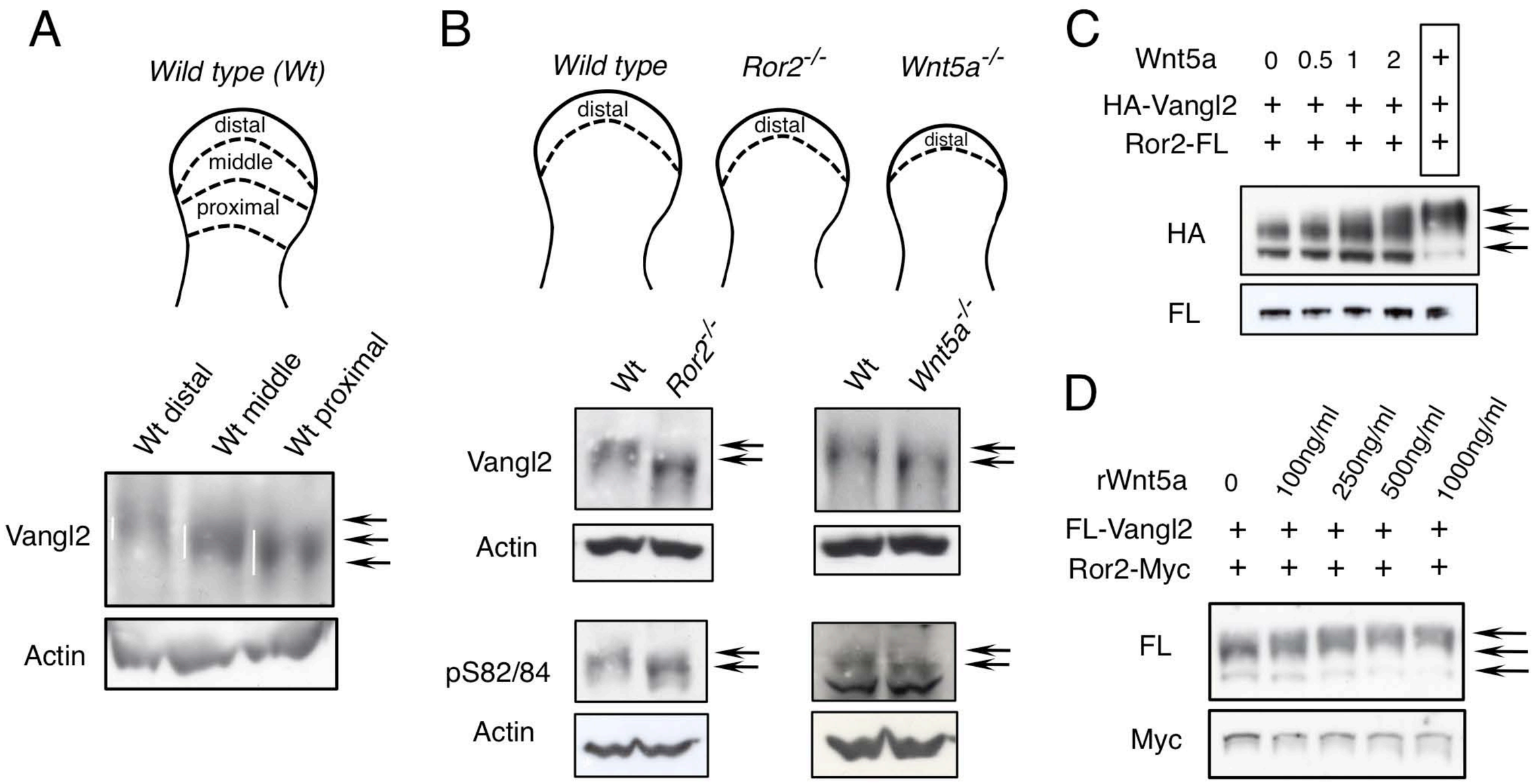
A
Wild type (Wt)
distal
middle
proximal
Wt distal
Wt middle
Wt proximal
Vangl2
Actin
B
Wild type
Ror2-/-
Wnt5a-/-
distal
distal
distal
Wt
Ror2-/-
Wt
Wnt5a-/-
Vangl2
Actin
pS82/84
Actin
C
Wnt5a
0
0.5
1
2
+
HA-Vangl2
+ + + + +
Ror2-FL
+ + + + +
HA
FL
D
rWnt5a
0
100ng/ml
250ng/ml
500ng/ml
1000ng/ml
FL-Vangl2
+ + + + +
Ror2-Myc
+ + + + +
FL
Myc

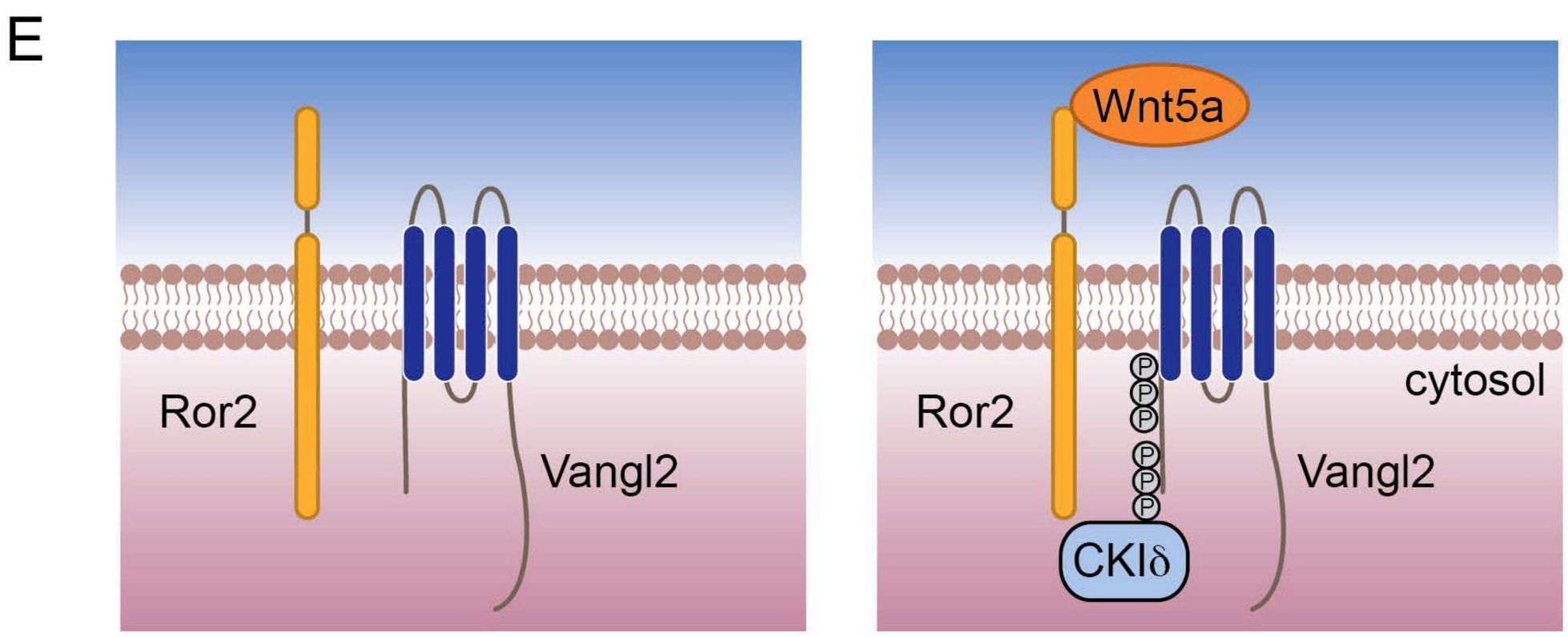
E
Ror2
Vangl2
Wnt5a
cytosol
Ror2
Vangl2
P
CKIδ

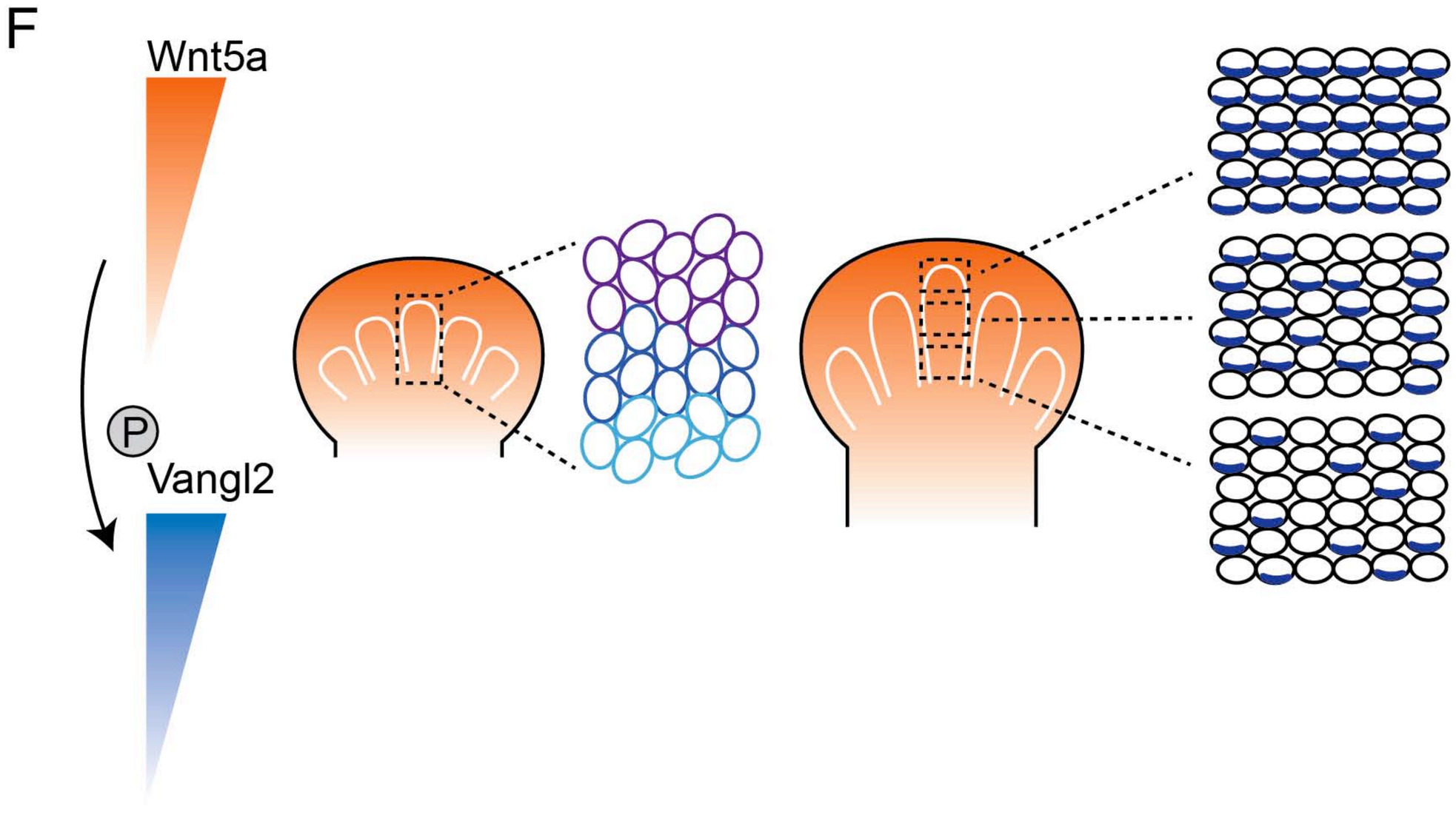
F
Wnt5a
P
Vangl2

Figure S1

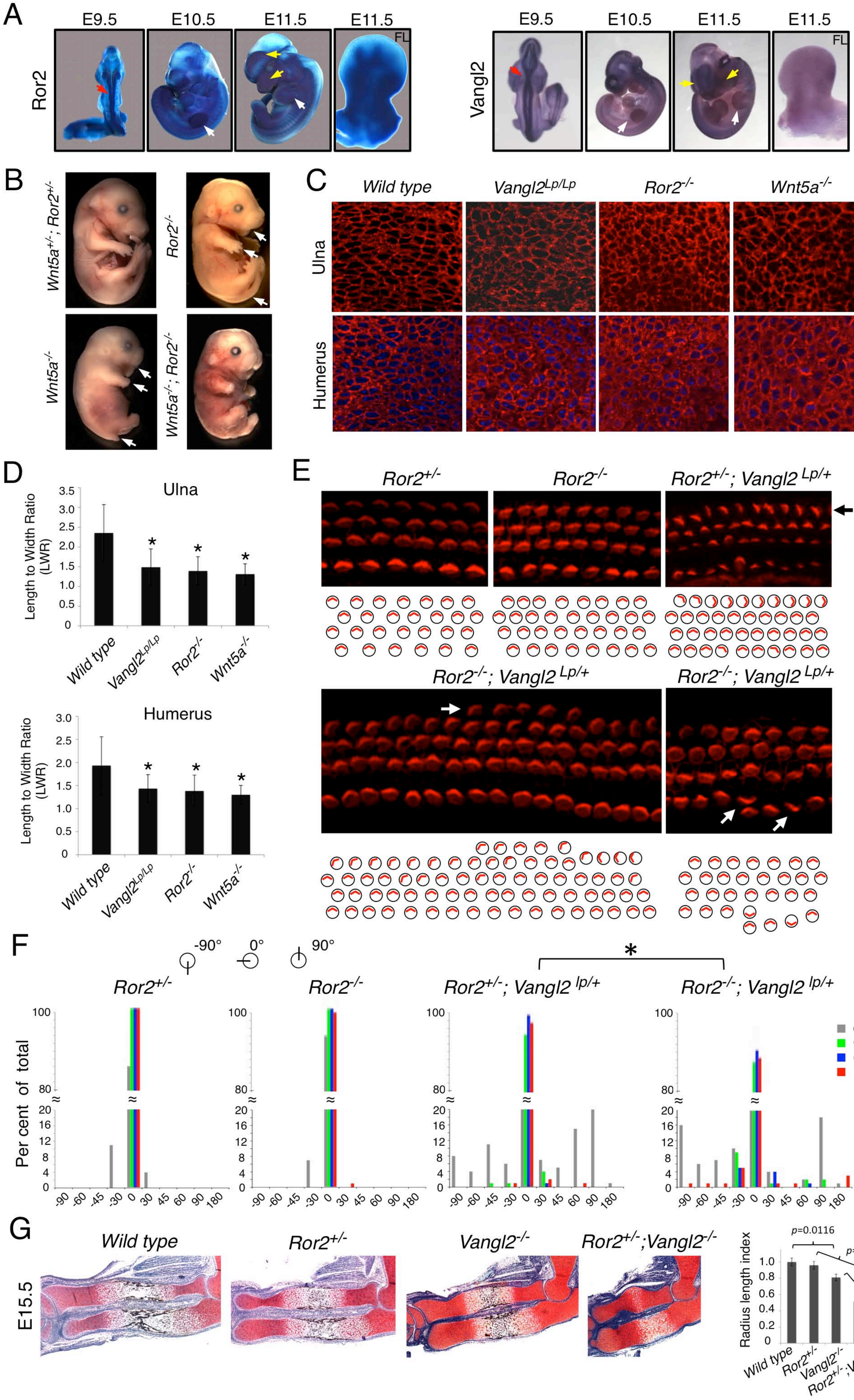
A
E9.5
E10.5
E11.5
E11.5
FL
Ror2
Vangl2
B
Wnt5a+/-; Ror2+/-
Ror2-/-
Wnt5a-/-
Wnt5a-/-; Ror2-/-
C
Wild type
Vangl2Lp/Lp
Ror2-/-
Wnt5a-/-
Ulna
Humerus
D
P
D
Ulna
Length to Width Ratio (LWR)
Wild type
Vangl2Lp/Lp
Ror2-/-
Wnt5a-/-
Humerus
E
Ror2+/-
Ror2-/-
Ror2+/-; Vangl2 Lp/+
Ror2-/-; Vangl2 Lp/+
OHC
IHC
F
-90°
0°
90°
Ror2+/-
Ror2-/-
Ror2+/-; Vangl2 lp/+
Ror2-/-; Vangl2 lp/+
Per cent of total
OHC1
OHC2
OHC3
IHC
G
Wild type
Ror2+/-
Vangl2-/-
Ror2+/-;Vangl2-/-
E15.5
p=0.0116
p=0.0002
p=0.0009
Radius length index

Figure S2

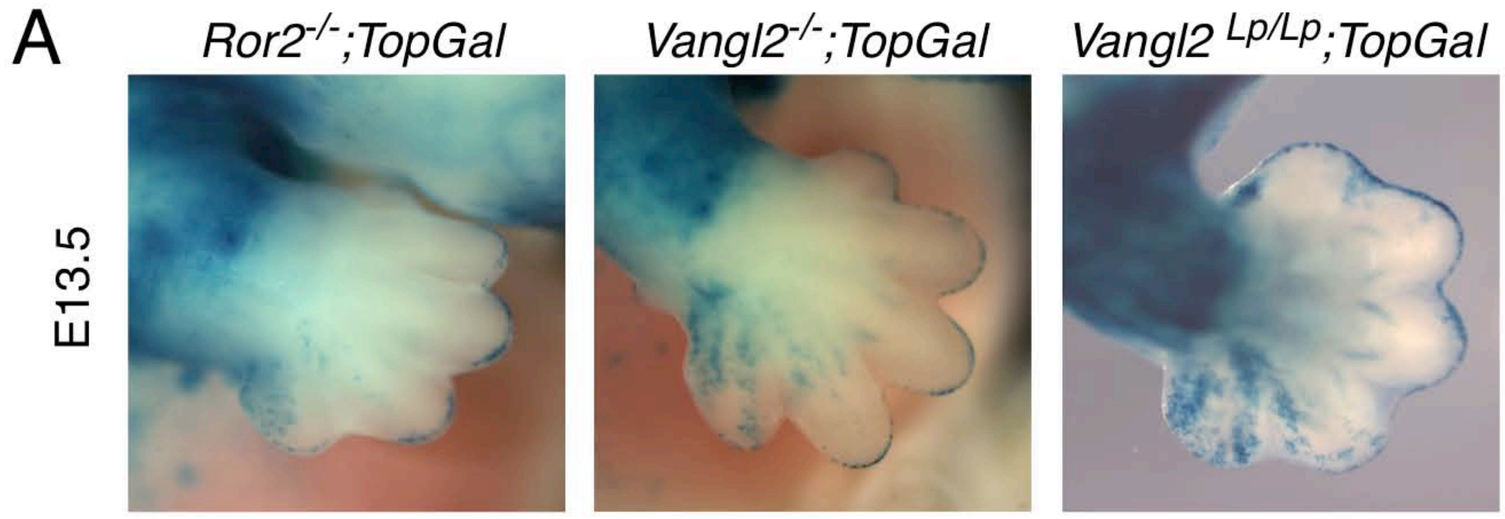
A
Ror2-/-;TopGal
Vangl2-/-;TopGal
Vangl2 Lp/Lp;TopGal
E13.5

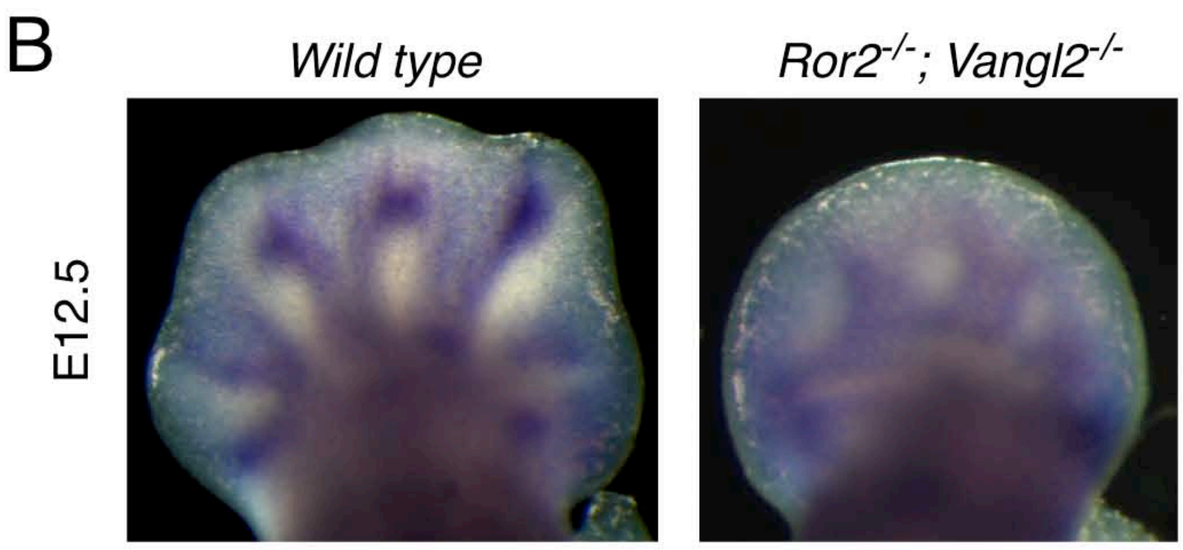
B
Wild type
Ror2-/-; Vangl2-/-
E12.5

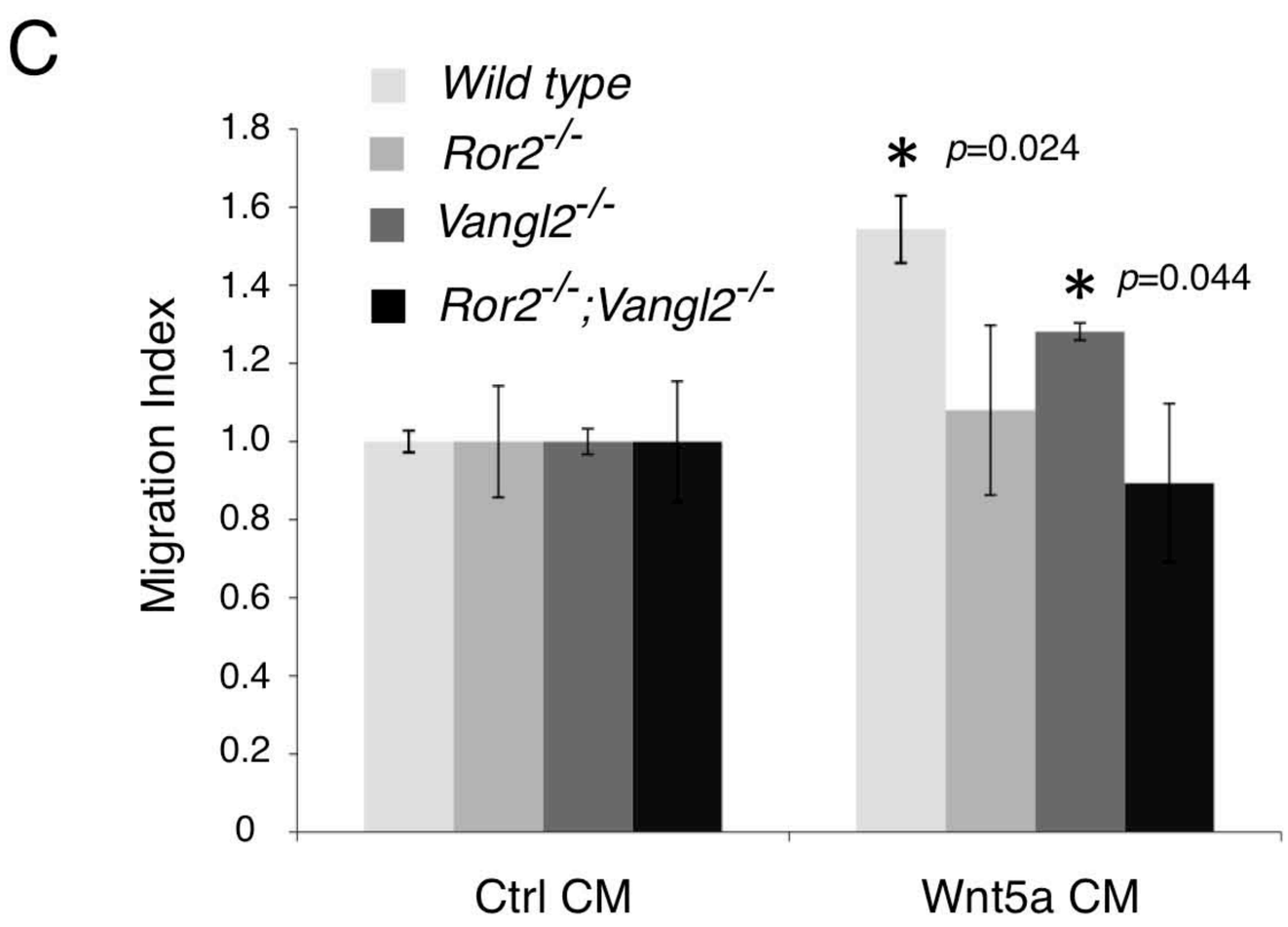
C
Wild type
Ror2-/-
Vangl2-/-
Ror2-/-;Vangl2-/-
Migration Index
1.8
1.6
1.4
1.2
1.0
0.8
0.6
0.4
0.2
0
* p=0.024
* p=0.044
Ctrl CM
Wnt5a CM

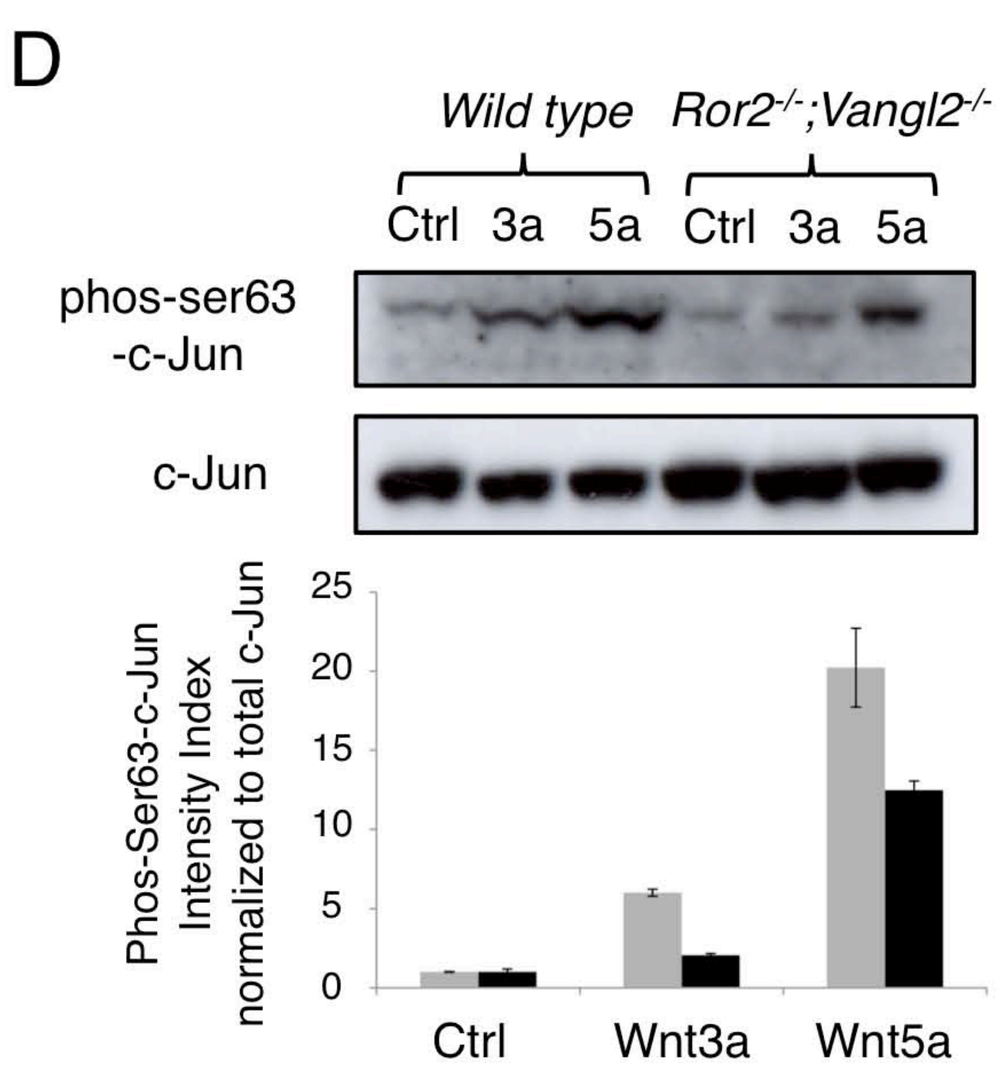
D
Wild type
Ror2-/-;Vangl2-/-
Ctrl 3a 5a Ctrl 3a 5a
phos-ser63
-c-Jun
c-Jun
Phos-Ser63-c-Jun
Intensity Index
normalized to total c-Jun
25
20
15
10
5
0
Ctrl
Wnt3a
Wnt5a

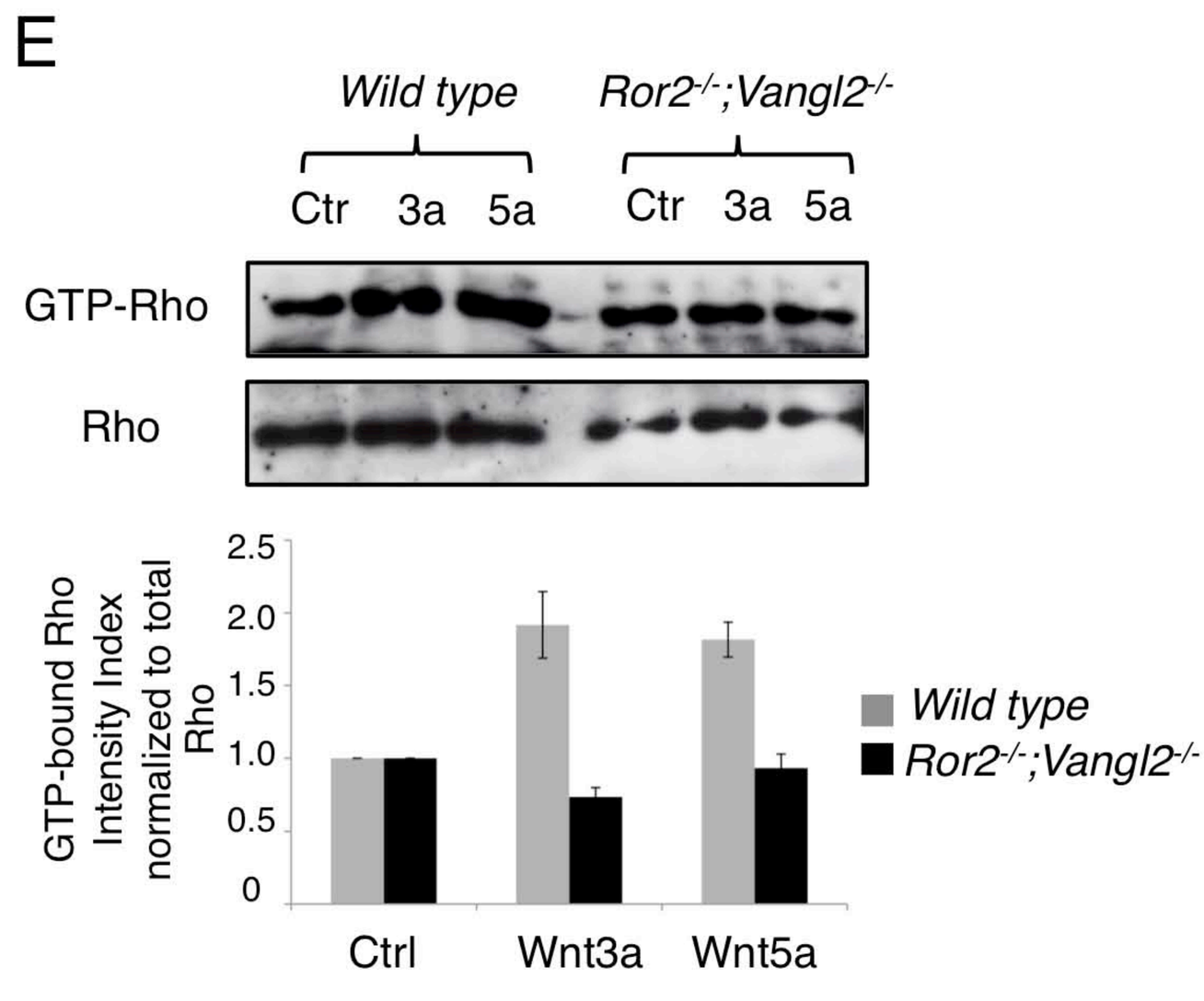
E
Wild type
Ror2-/-;Vangl2-/-
Ctr 3a 5a
Ctr 3a 5a
GTP-Rho
Rho
GTP-bound Rho
Intensity Index
normalized to total
Rho
2.5
2.0
1.5
1.0
0.5
0
Ctrl
Wnt3a
Wnt5a
Wild type
Ror2-/-;Vangl2-/-

Figure S3

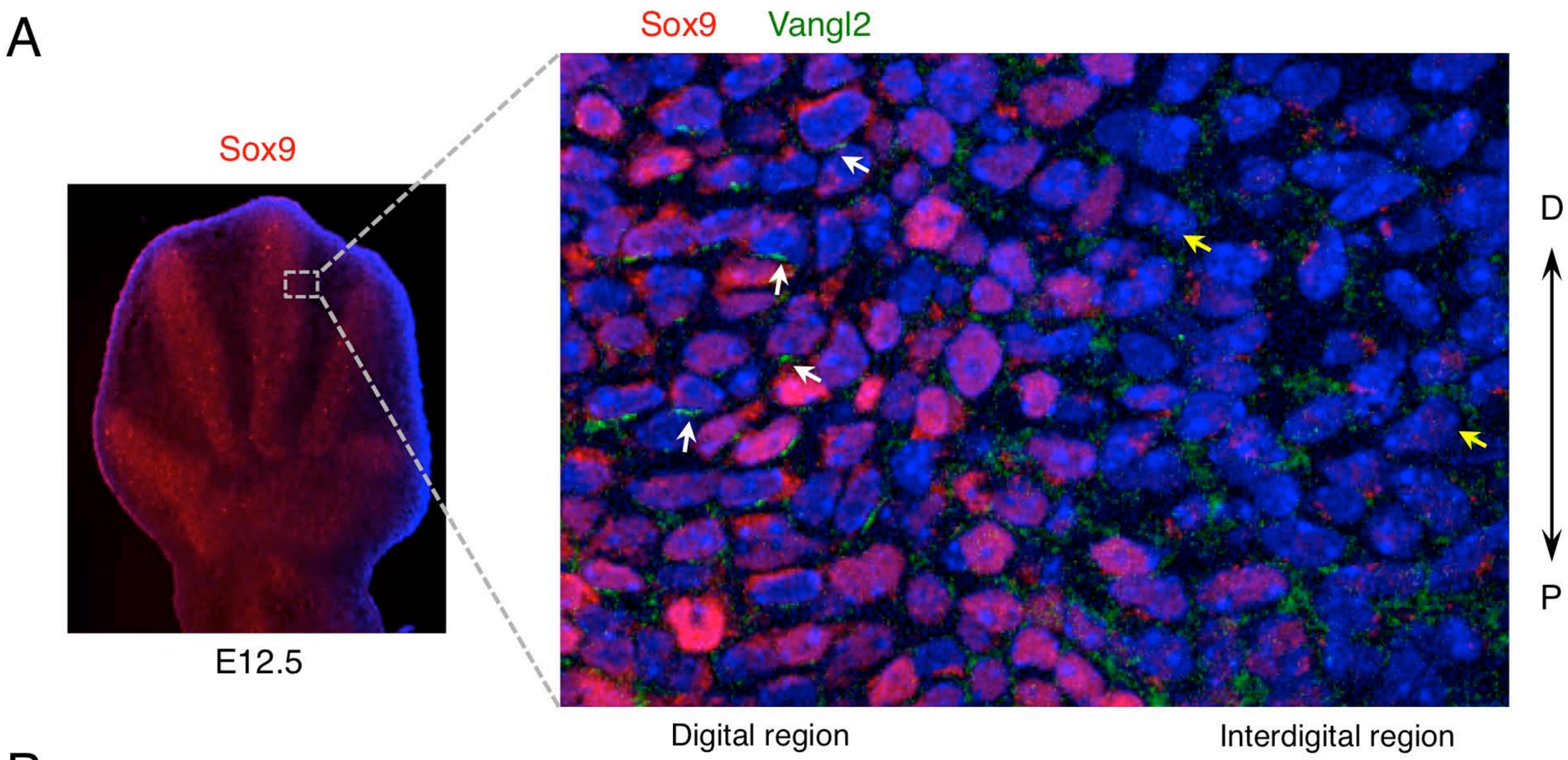
A
Sox9
Sox9
Vangl2
E12.5
D
P
Digital region
Interdigital region

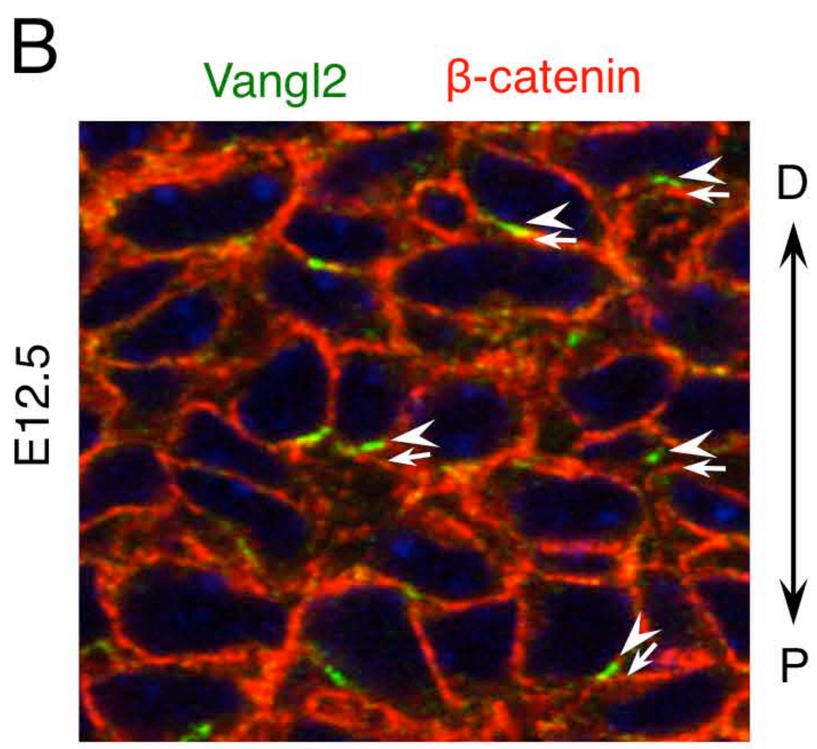
B
Vangl2
β-catenin
E12.5
D
P

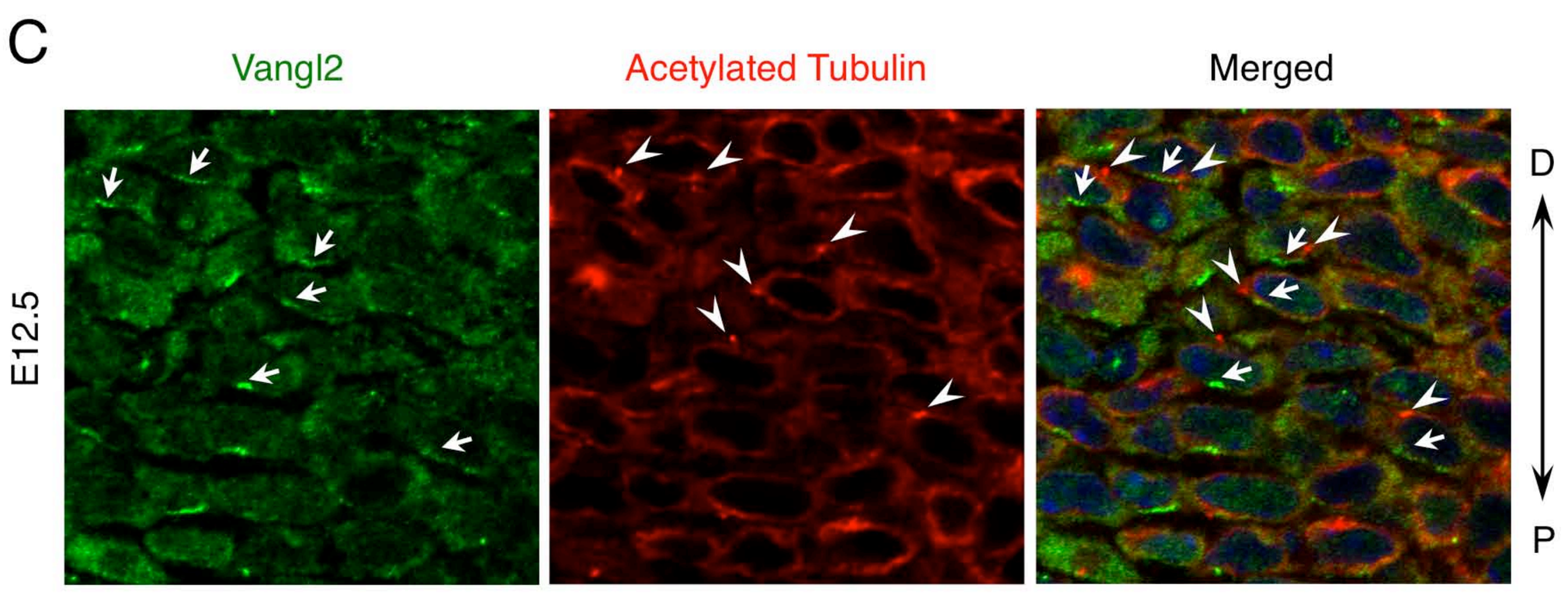
C
Vangl2
Acetylated Tubulin
Merged
E12.5
D
P

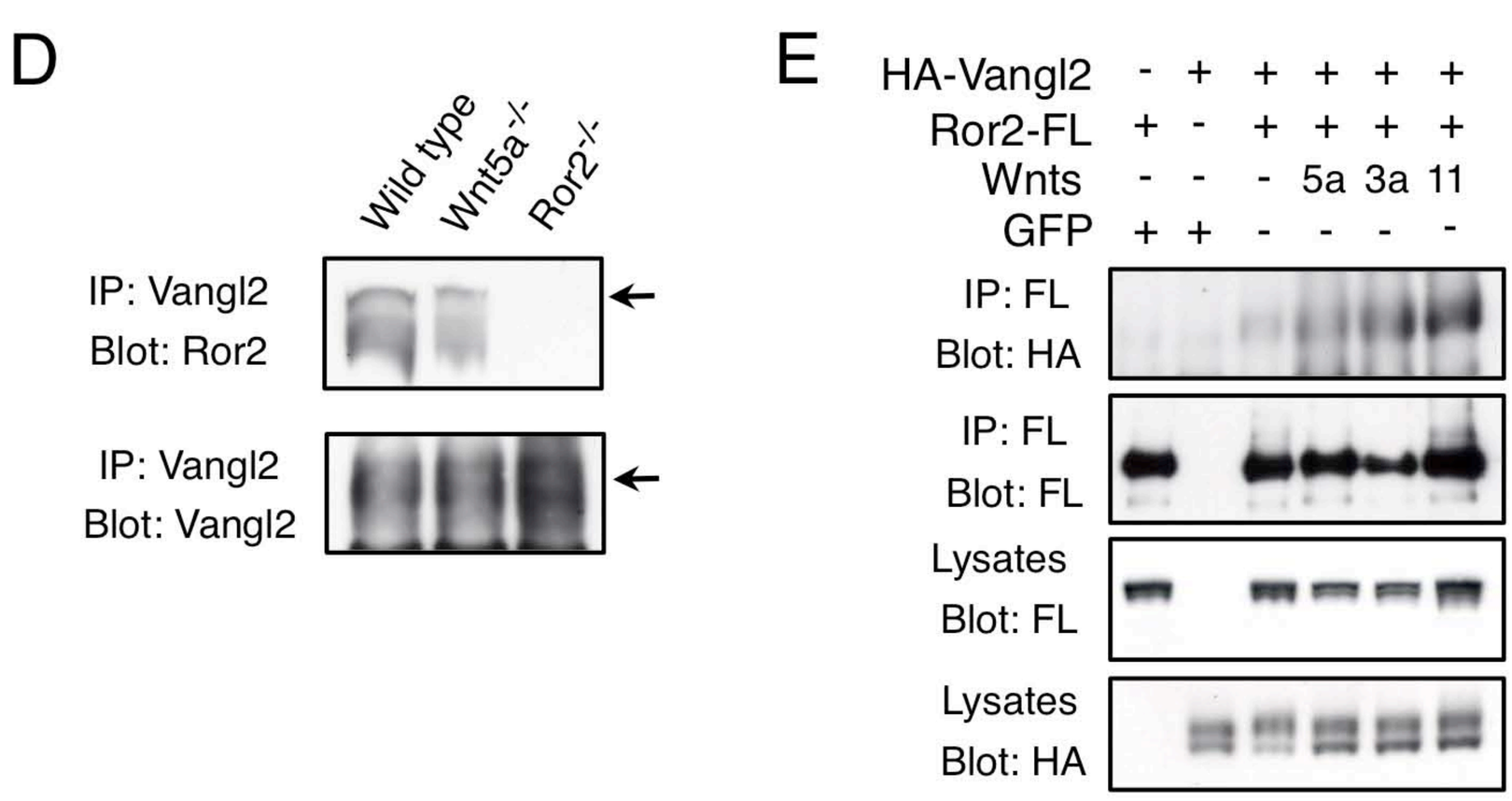
D
Wild type
Wnt5a-/-
Ror2-/-
IP: Vangl2
Blot: Ror2
IP: Vangl2
Blot: Vangl2
E
HA-Vangl2 - + + + + +
Ror2-FL + - + + + +
Wnts - - - 5a 3a 11
GFP + + - - - -
IP: FL
Blot: HA
IP: FL
Blot: FL
Lysates
Blot: FL
Lysates
Blot: HA

Figure S4

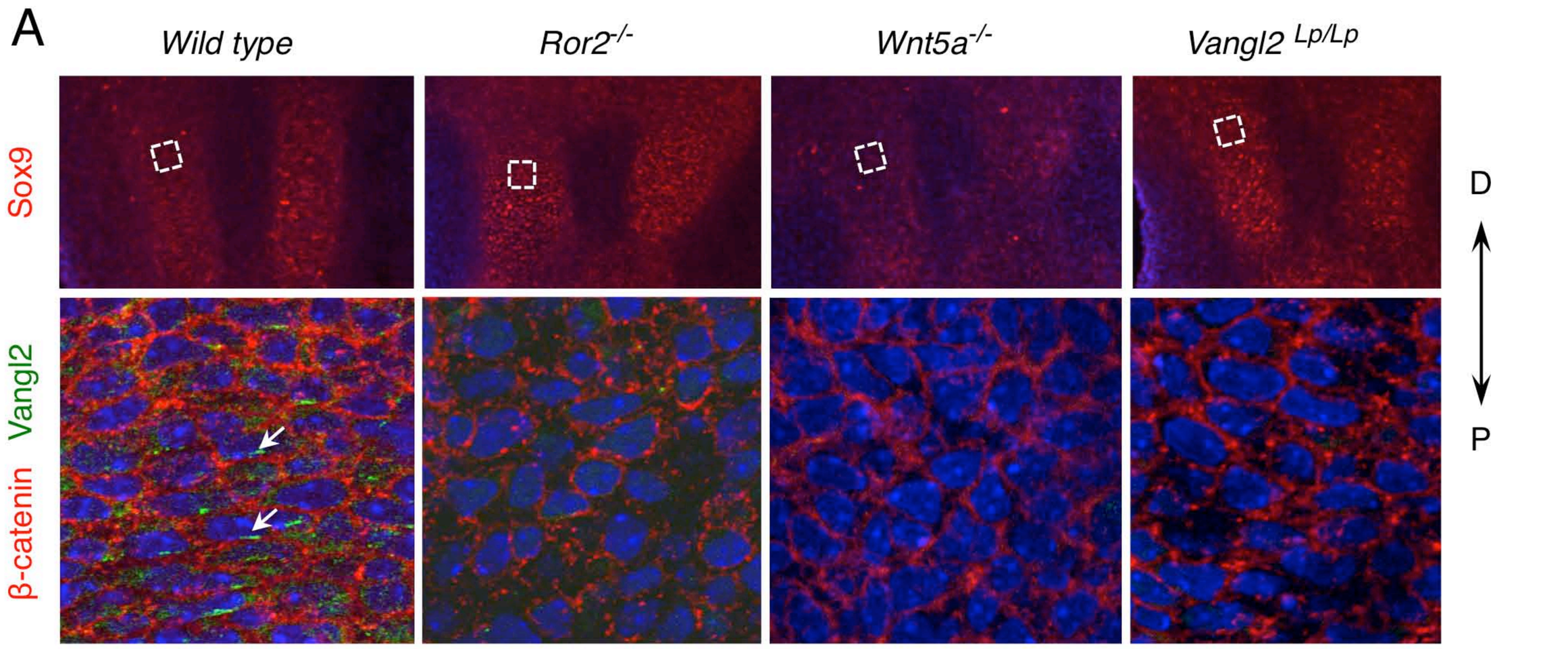
A
Wild type
Ror2-/-
Wnt5a-/-
Vangl2 Lp/Lp
Sox9
Vangl2
β-catenin
D
P

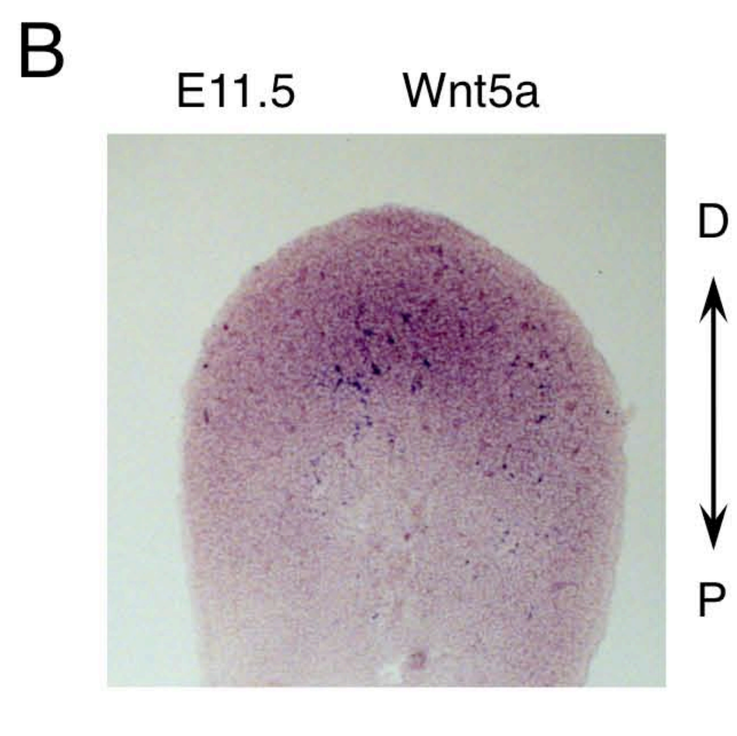
B
E11.5
Wnt5a
D
P

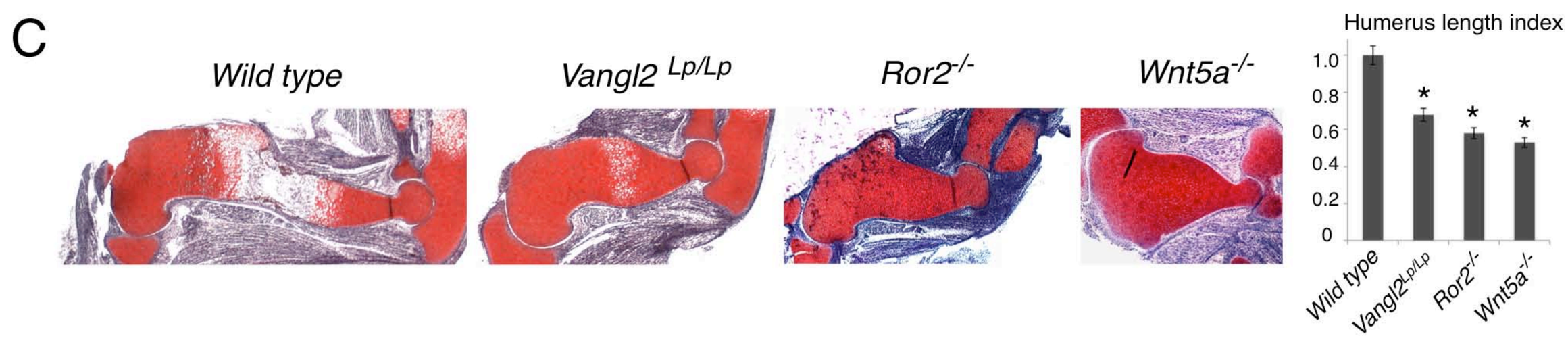
C
Wild type
Vangl2 Lp/Lp
Ror2-/-
Wnt5a-/-
Humerus length index
1.0
0.8
0.6
0.4
0.2
0
*
*
*
Wild type
Vangl2Lp/Lp
Ror2-/-
Wnt5a-/-

Figure S5

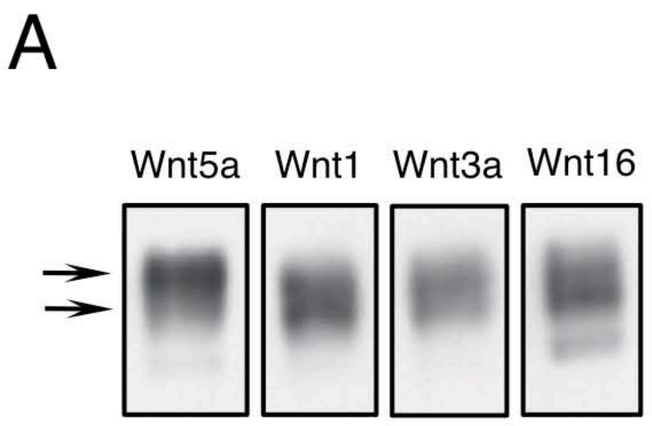
A
Wnt5a
Wnt1
Wnt3a
Wnt16

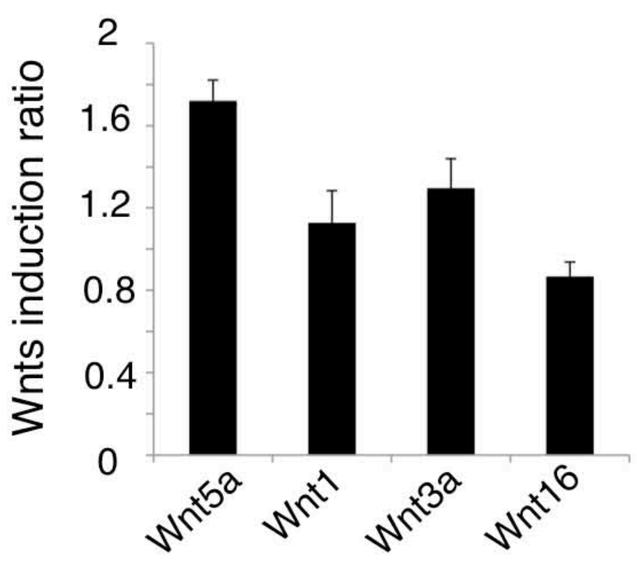
Wnts induction ratio
2
1.6
1.2
0.8
0.4
0
Wnt5a
Wnt1
Wnt3a
Wnt16

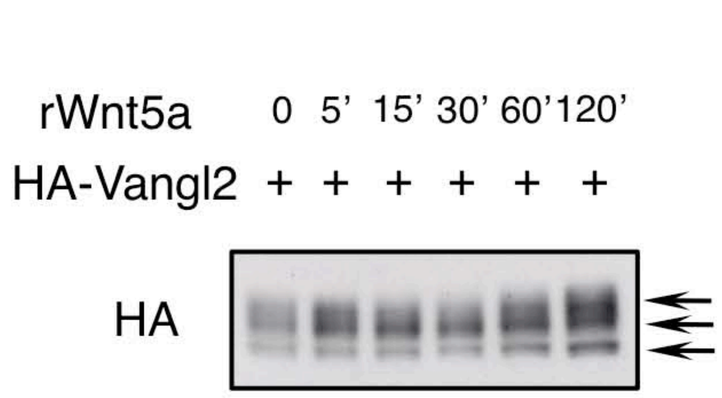
B
rWnt5a 0 5' 15' 30' 60' 120'
HA-Vangl2 + + + + + +
HA


C
Cluster II
MouseVangl2 MDTESQYSGYSYKSGHSRSSRK----------HRDR-------RDRHRSK 33
HumanVangl2 MDTESQYSGYSYKSGHSRSSRK----------HRDR-------RDRHRSK 33
XenopusVangl2 MDNDSQYSGYSYKSGHSRSSRK----------HRDR-------RERHRSK 33
ZebrafishVangl2 MDNESQYSGYSYKSSHSRSSRK----------HRDR-------RDRHRSK 33
MouseVangl1 MDTESTYSGYSYYSSHSKKSHR----------QGERT------RERHKSP 34
HumanVangl1 MDTESTYSGYSYYSSHSKKSHR----------QGERT------RERHKSP 34
ZebrafishVangl1 MDTDSIHSGYSHHSNRSRGSNK----------QSERSS-----RDRHKPH 35
DrosophiliaVangl1 MENESVKSEHSGRSRRSRNHNNNGGGGGGGGGGGGSVNNGYHRERDRSRHSHRSTHSSK 60
Cluster I
MouseVangl2 SRDGS-RGDKS--VTIQAP-GEPLLDNESTRG---DERDDNWGETTTVVTG-TSEHSISH 85
HumanVangl2 SRDGG-RGDKS--VTIQAP-GEPLLDNESTRG---DERDDNWGETTTVVTG-TSEHSISH 85
XenopusVangl2 SREGS-RGDKS--VTIQAP-GEPLLDNESTRG---EDRDDNWGETTTVVTG-TSEHSISH 85
ZebrafishVangl2 SRDSSSRGDKS--VTIQAP-GEPLLDAESTRG---DDRDDNWGETTTVVTG-TSEHSVSN 86
MouseVangl1 RNKDGRGSEKS--VTIQAPAGEPLLANDSARTGAEEVQDDNWGETTTAITG-TSEHSISQ 91
HumanVangl1 RNKDGRGSEKS--VTIQPPTGEPLLGNDSTRT--EEVQDDNWGETTTAITG-TSEHSISQ 89
ZebrafishVangl1 SRDSSSRSDKN--VTISATSVQPQQPDQSSAP--TDAQDDNWGETTTAVTG-TSDHSLSQ 90
DrosophiliaVangl1 SAKGFQRGDMAPYQTSVNMTGDGSHDGQEVIEVQILPQDENWGENTTAVTGNTSEQSISM 120

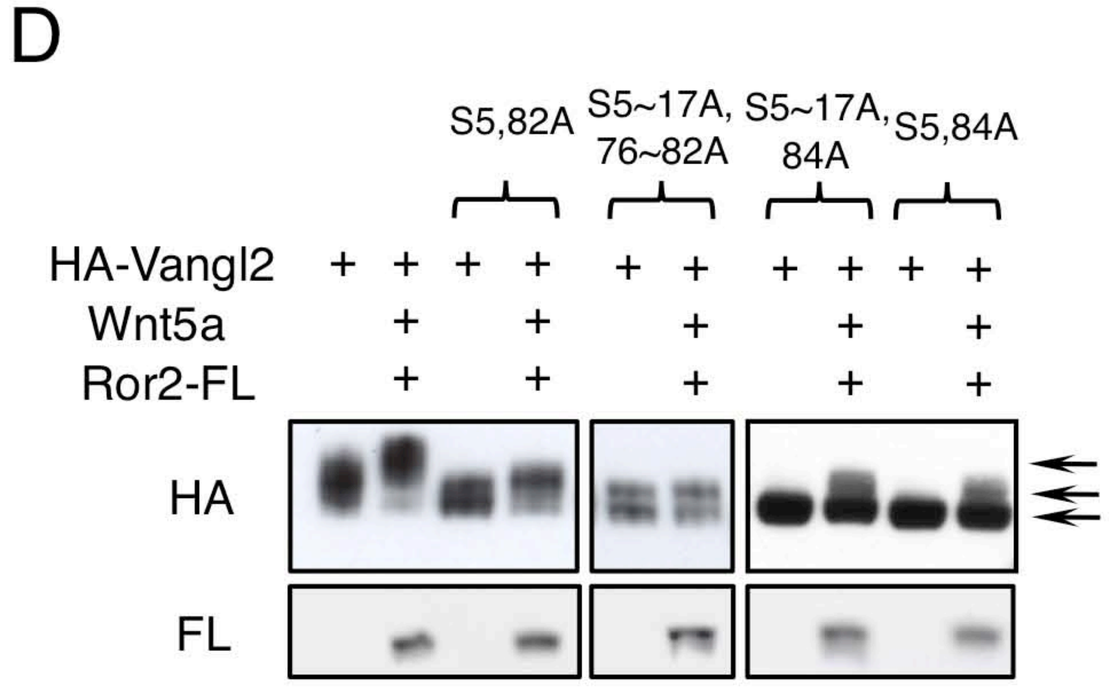
D
S5,82A
S5~17A, 76~82A
S5~17A, 84A
S5,84A
HA-Vangl2 + + + + + + + + + +
Wnt5a + + + + + +
Ror2-FL + + + + +
HA
FL

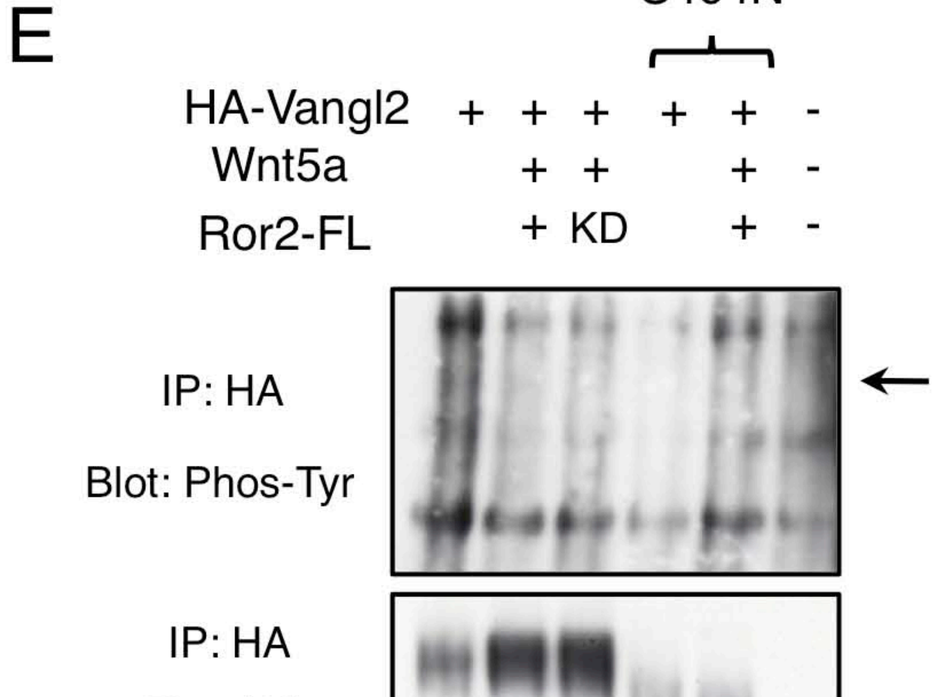
E
S464N
HA-Vangl2 + + + + + -
Wnt5a + + + -
Ror2-FL + KD + -
IP: HA
Blot: Phos-Tyr
IP: HA
Blot: HA

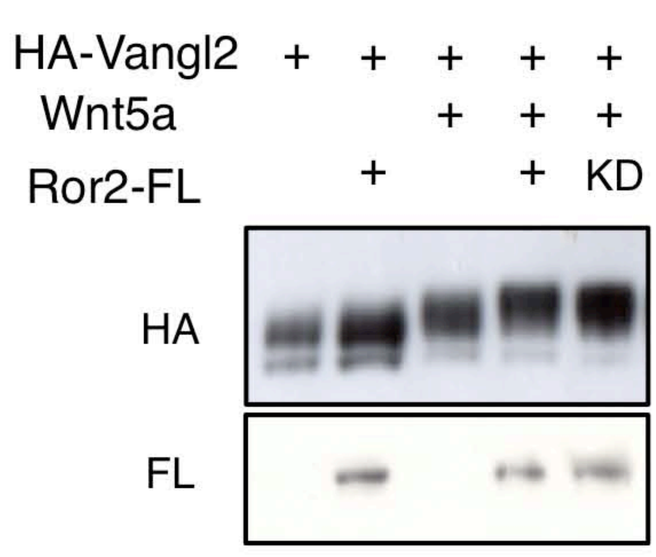
F
HA-Vangl2 + + + + +
Wnt5a + + + +
Ror2-FL + + KD
HA
FL

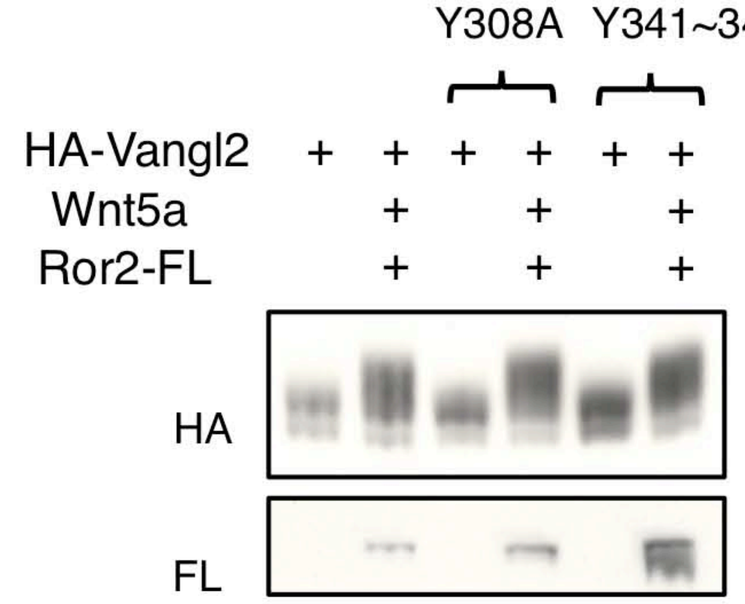
G
Y308A
Y341~343A
HA-Vangl2 + + + + + +
Wnt5a + + + + +
Ror2-FL + + +
HA
FL

Figure S6

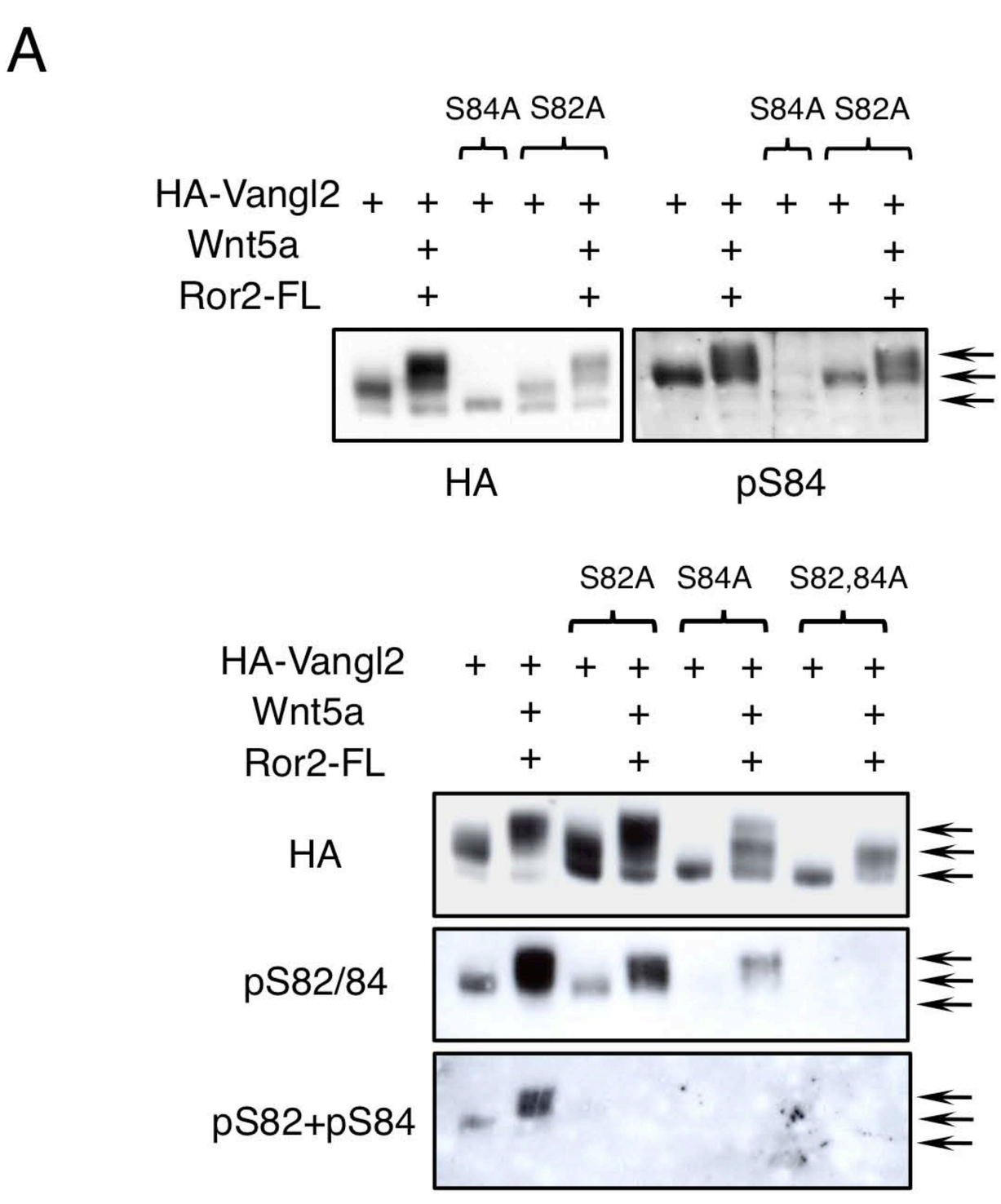
A
S84A S82A
S84A S82A
HA-Vangl2 + + + + + + + + + +
Wnt5a + + + +
Ror2-FL + + + +
HA
pS84
S82A S84A S82,84A
HA-Vangl2 + + + + + + + +
Wnt5a + + + +
Ror2-FL + + + +
HA
pS82/84
pS82+pS84

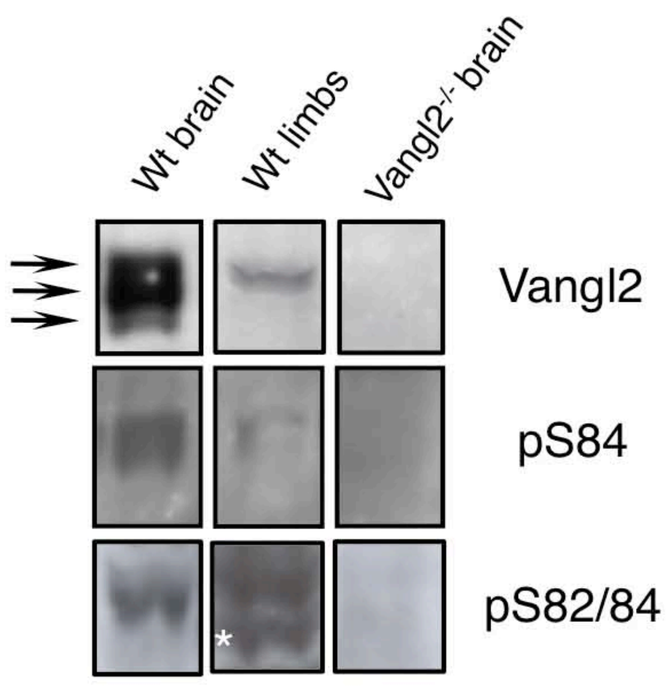
B
Wt brain
Wt limbs
Vangl2-/- brain
Vangl2
pS84
pS82/84
*

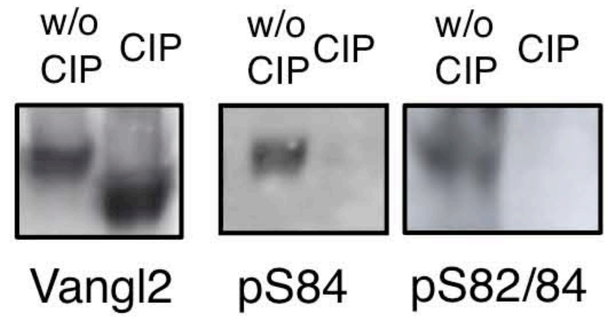
C
w/o CIP
CIP
w/o CIP
CIP
w/o CIP
CIP
Vangl2
pS84
pS82/84

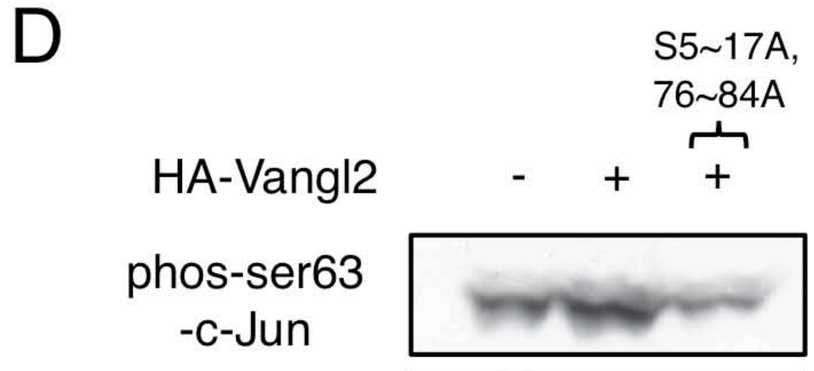
D
S5~17A, 76~84A
HA-Vangl2 - + +
phos-ser63 -c-Jun
c-Jun
GTP-Rho
Rho
HA

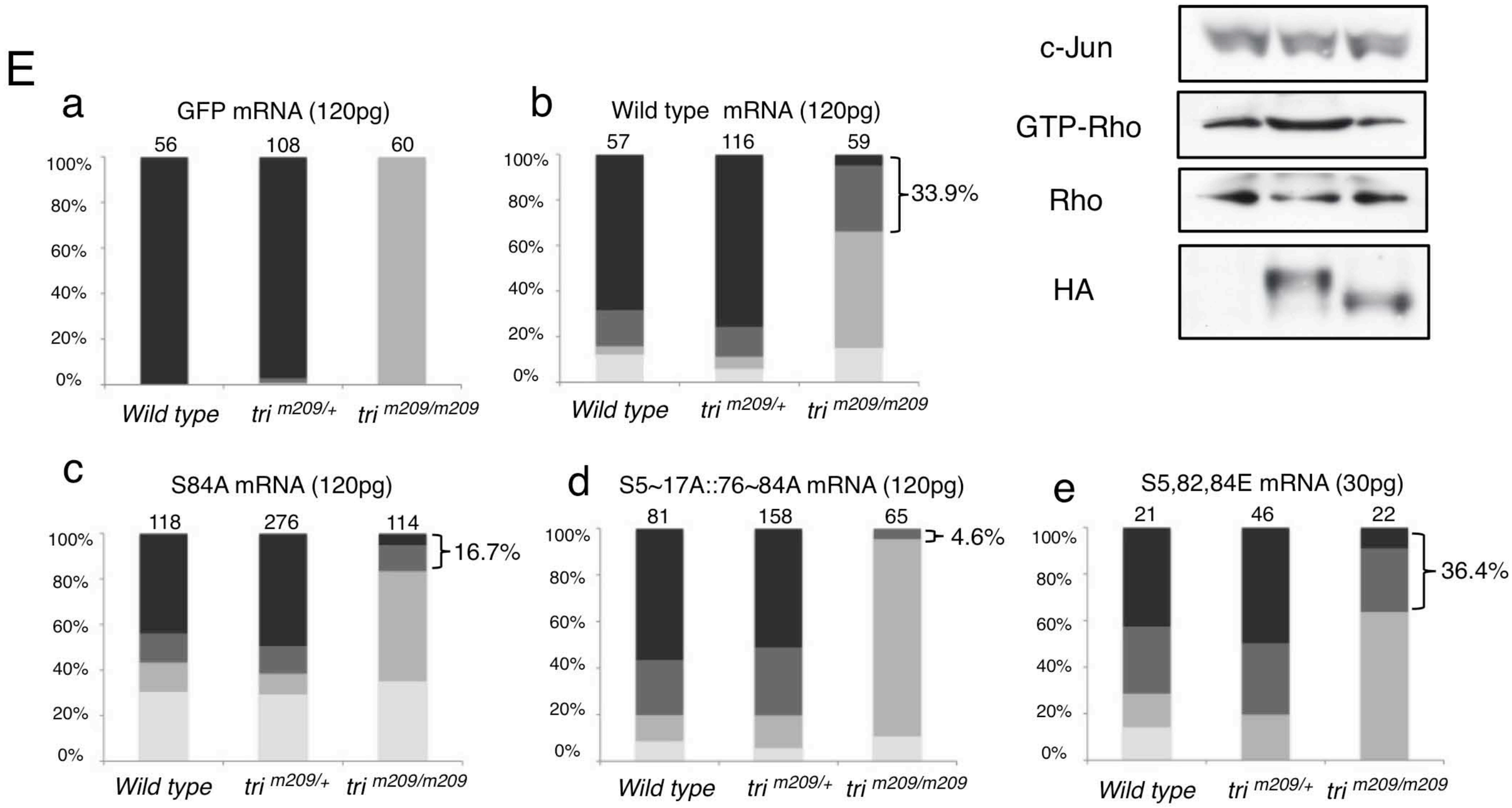
E
a
GFP mRNA (120pg)
56
108
60
100%
80%
60%
40%
20%
0%
Wild type
tri m209/+
tri m209/m209
b
Wild type mRNA (120pg)
57
116
59
33.9%
Wild type
tri m209/+
tri m209/m209
c
S84A mRNA (120pg)
118
276
114
16.7%
Wild type
tri m209/+
tri m209/m209
d
S5~17A::76~84A mRNA (120pg)
81
158
65
4.6%
Wild type
tri m209/+
tri m209/m209
e
S5,82,84E mRNA (30pg)
21
46
22
36.4%
Wild type
tri m209/+
tri m209/m209

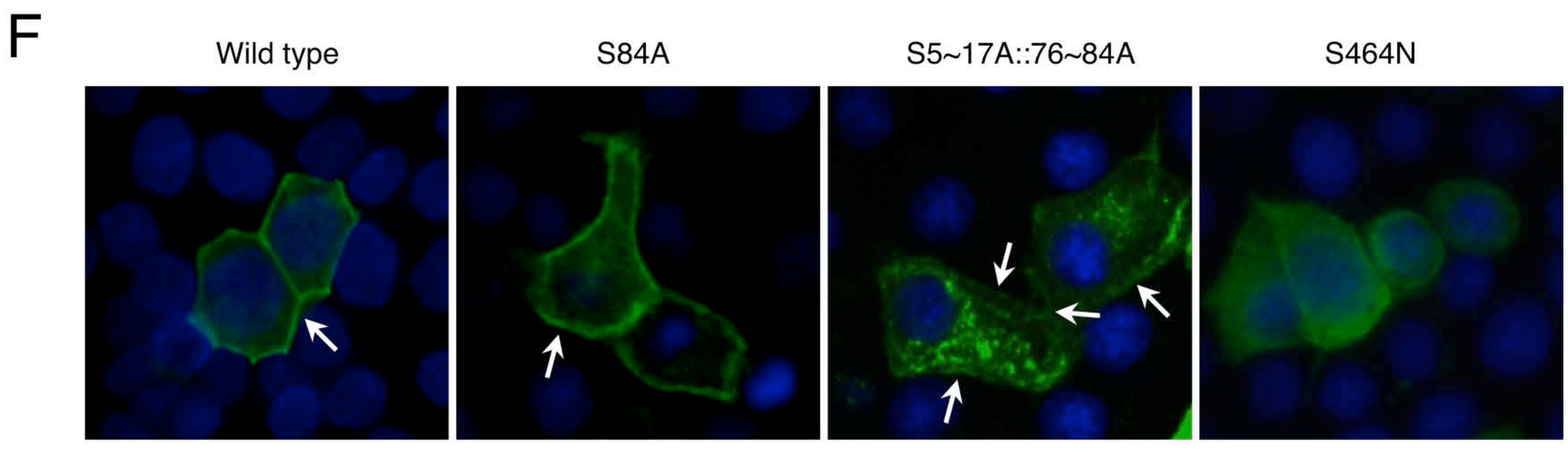
F
Wild type
S84A
S5~17A::76~84A
S464N

Figure S7

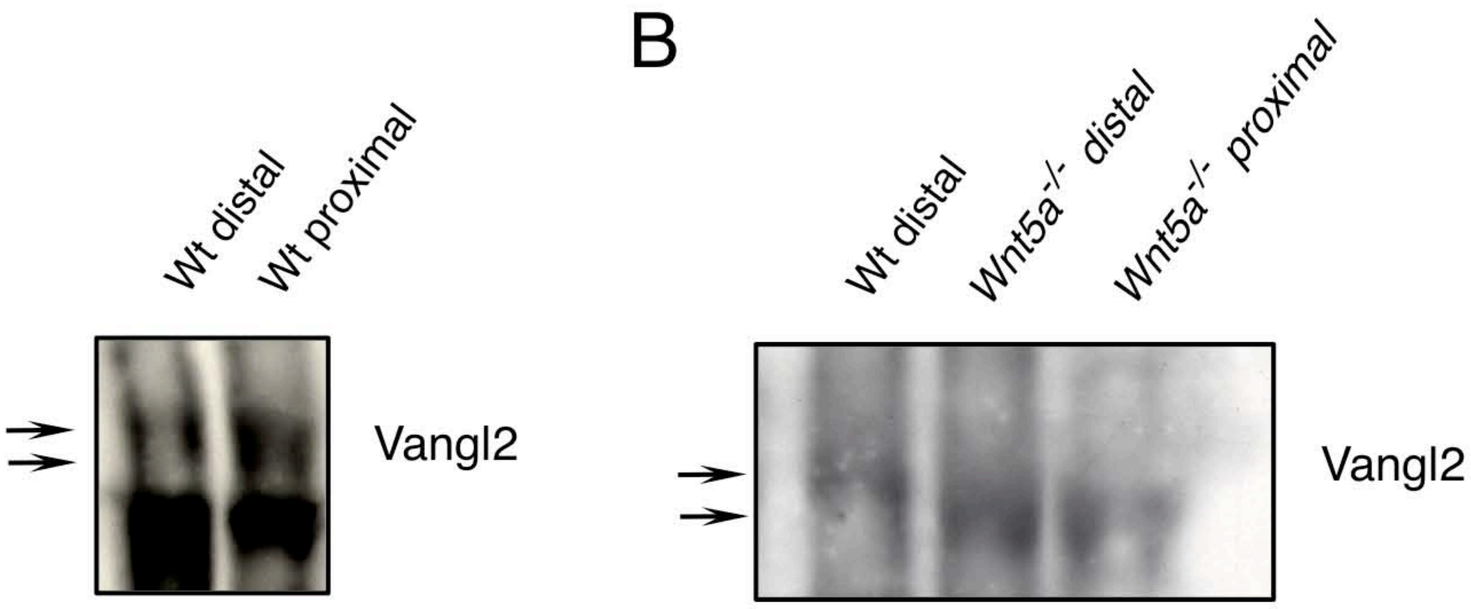
A
Wt distal
Wt proximal
Vangl2
B
Wt distal
Wnt5a-/- distal
Wnt5a-/- proximal
Vangl2
C
Wnt5a CEF
Wild type CEF
DAPI
Wnt5a
DAPI
Wnt5a
D
P
Wnt5a CEF (infected)
Wild type CEF (uninfected)
Wild type CEF
Wnt5a
Vangl2
Wnt5a Vangl2 DAPI

Supplemental Figure Legend

Figure S1, related to Figure 1. Expression of *Ror2* and *Vangl2* and their genetic interaction in mouse embryos. (A) *Ror2* expression was shown by X-gal staining of the $Ror2^{LacZ/+}$ embryos from E9.5 to E11.5. *Ror2* was strongly expressed in the neural tube (E9.5, red arrow), limb buds (E10.5, E11.5, white arrows) and craniofacial regions (E11.5, yellow arrows). *Ror2* expression became weak in the neural tube at E11.5. *Vangl2* expression was shown by whole mount *in situ* hybridization. Similar to *Ror2*, it's stronger in neural tube (red arrow), limb buds (white arrows) and craniofacial regions (yellow arrows). FL, forelimb. (B) Embryos at E15.5. The $Ror2^{-/-}$ embryo exhibited short limbs, tails and flat face (white arrows), similar to, but less severe than the $Wnt5a^{-/-}$ embryo. The $Wnt5a^{-/-}$; $Ror2^{-/-}$ embryo is indistinguishable from the $Wnt5a^{-/-}$ embryo. (C) Sections of E12.5 ulna and humerus were stained with β–catenin. Compared to wild type, chondrocyte shape and organization were similarly disrupted in the $Vangl2^{Lp/Lp}$, $Ror2^{-/-}$ and $Wnt5a^{-/-}$ mutants. (D) Chondrocytes shape and organization in Fig S1C were quantified by length-to-width ratio (two-tail *t*-test, all **p* value <0.01). Error bars are ± SD, n>60. (E) Phalloidin staining of E18.5 cochlea (upper panel, and schematic representations in lower panel). The $Ror2^{-/-}$; $Vangl2^{Lp/+}$ cochlea showed misorientation and disorganization of sensory hair cells and there were an additional row of and 180°-rotated hair cells (white arrows). The $Ror2^{+/-}$; $Vangl2^{Lp/+}$ cochlea had only mild stereociliary bundle orientation defect in OHC1 (black arrow). The $Ror2^{-/-}$ cochlea was largely normal. OHC: outer hair cells; IHC: inner hair cells. (F) Statistical analysis of hair cell orientation. Compared to $Ror2^{+/-}$; $Vangl2^{Lp/+}$, the $Ror2^{-/-}$; $Vangl2^{Lp/+}$ embryos have more OHC2, OHC3 and IHC affected (two-tail *t*-test, **p*=0.006). OHC: outer hair cells;

IHC: inner hair cells. (G) Removal of one copy of *Ror2* gene in the *Vangl*2 null background at E15.5 significantly delayed endochondral ossification (right panel, two-tail *t*-test). On the histological section, the cartilage was stained red by Safranin O whereas mineralized tissue (hypertrophic chondrocyte and osteoblast matrix) was stained black by the von Kossa method. Whereas the long bone of *Vangl2*$^{-/-}$ is slightly shorter than wild type (p>0.01) and *Ror2*$^{+/-}$ is normal, *Ror2*$^{+/-}$*; Vangl2*$^{-/-}$ long bone is significantly shortened (p<0.01). Error bars are ± SD, n=3.

Figure S2, related to Figure 2. *Ror2* and *Vangl2* mediate Wnt5a regulated non-canonical Wnt signaling. (A) X-gal staining of E13.5 embryos of the indicated genotypes. No ectopic X-gal staining as shown in Fig. 2B was observed in the distal digits of these embryos. (B) *Gdf5* expression detected by whole mount *in situ* hybridization. In the *Ror2*$^{-/-}$; *Vangl2*$^{-/-}$ mutant limb, there was no ectopic joint formation shown by lack of ectopic *Gdf5* expression in the distal limb. (C) Migratory of wild type and mutant mouse embryonic fibroblasts (MEFs) in response to Wnt treatment was measured in transwell chambers. Wnt5a-induced cell migration is abrogated in *Ror2*$^{-/-}$ and *Ror2*$^{-/-}$; *Vangl2*$^{-/-}$ MEFs. Statistic analysis of the results was shown (one-tail *t*-test). Error bars are ± SD, n=3. (D) The levels of total (lower panel) or phosphorylated (upper panel) forms of c-Jun, respectively, were determined by immunoblotting. The ability of Wnt3a or Wnt5a to induce c-Jun phosphorylation in *Ror2*$^{-/-}$; *Vangl2*$^{-/-}$ MEFs was reduced compared to the wild type MEFs. Quantified results by densitometer were shown in the lower panel. Error bars are ± SD, n=3. (E) The Wnt3a and Wnt5a induced GTP-bound, activated Rho was reduced in the *Ror2*$^{-/-}$; *Vangl2*$^{-/-}$ MEFs. Quantified results by

densitometer were shown in the lower panel. Error bars are ± SD, n=3.

Figure S3, related to Figure 3. Vangl2 localization and Wnt-induced Ror2-Vangl2 complex formation. (A) The developing cartilage was marked by Sox9 protein expression (red) in the limb bud of E12.5 embryo. The boxed region is shown in higher magnification on the right and Vangl2 protein localization (green) was shown (projected Z-stack). DAPI (blue) stains the nucleus. Vangl2 asymmetrical localization was only observed in the Sox9-positive chondrocytes (white arrows), not in the mesenchymal cells (yellow arrows). D, distal; P, proximal. (B) Vangl2 proteins are asymmetrically localized to proximal side of the cell in E12.5 distal limb. Arrowheads point to the Vangl2 proteins (green) localized to the proximal membrane of upper cells, and arrows indicate the membrane of an adjacent proximal cell. Cell membrane was marked by β–catenin staining (red). (C) Vangl2 proteins (green, arrows) are not colocalized with cilium (red, arrowheads) in E12.5 distal limb. (D) Co-immunoprecipitation of Ror2 and Vangl2 from the E12.5 limb bud. Binding of Ror2 and Vangl2 is reduced in *Wnt5a*$^{-/-}$ mutant. (E) Co-immunoprecipitation of Ror2 and Vangl2 in HEK293T cells. Overexpression of mouse cDNA constructs of several *Wnt*s strongly increased their interaction.

Figure S4, related to Figure 4. PCP in the limb cartilage. (A) The cartilage of the ulna region of E12.5 embryos was marked by Sox9 protein expression. The selected regions (box) are enlarged and shown with Vangl2 (green) and β-catenin (red) staining (projected Z-stacks). Vangl2 is asymmetrically localized in wild type chondrocytes (arrows). Such asymmetrical localization is completely lost in the *Wnt5a*$^{-/-}$ and *Ror2*$^{-/-}$ mutant limbs. (B)

Wnt5a *in situ* hybridization on E11.5 limb bud section indicated a gradient of Wnt5a expression from distal to proximal limb. (C) The E15.5 humerus was sectioned and stained by Safranin O. Proliferating chondrocytes are bright red after staining. Hypertrophic chondrocytes are enlarged cells that are lightly stained by Safranin O. All of the *Vangl2*$^{Lp/Lp}$, *Ror2*$^{-/-}$ and *Wnt5a*$^{-/-}$ mutant embryos showed similarly shortened and broadened cartilage and delayed chondrocytes hypertrophy. The length of humerus was quantified (two-tail *t*-test, all **p* values<0.01). Error bars are ± SD, n=3.

Figure S5, related to Figure 5. Regulation of Vangl2 phosphorylation. (A) Wnt5a has the strongest effect on inducing Vangl2 phosphorylation. The hyperphosphorylated (upper arrow) and hypophosphorylated (lower arrow) Vangl2 induced by different Wnts were quantified by densitometer. The ratio of hyperphosphorylated to hypophosphorylated Vangl2 were calculated and shown in the right column. Error bars are ± SD, n=3. (B) The hyperphosphorylated Vangl2 induced by 500 ng/ml recombinant Wnt5a proteins was observed by 1 hour after treatment in CHO cells. (C) Alignment of N-terminus of Vangl1 and Vangl2 protein sequences across multiple species. The identical amino acid residues among all species are indicated by asterisks. ":" indicates conserved substitutions and "." indicates semi-conserved substitutions. The Cluster I and II phosphorylation sites are highly conserved and showed in red color. Founder sites S5,82 and 84 are shown in bold. S84 is also underlined. (D) Mutating two founder sites of S5,82 or S5,84 is not able to abolish Wnt5a-induced phosphorylation in CHO cells. (E) Extracts of CHO cells expressing *Vangl2* were immunoprecipitated with HA antibody and subjected to immunoblotting with phosphotyrosine antibody (4G10 Platinum, upper

panel) and HA antibody. Lower panel shows total Vangl2. No obvious tyrosine phosphorylation was detected even with Wnt5a treatment. The arrow points to the size of Vangl2 proteins. (F) The Kinase-dead Ror2 (Ror2-KD) still retained the ability to enhance Wnt5a-induced Vangl2 phosphorylation in CHO cells. (G) Tyrosine to alanine mutations on highly conserved Y308 or Y341~343 had no effect on Vangl2 phosphorylation in CHO cells.

Figure S6, related to Figure 6. Characterization of phospho-Vangl2 antibodies and downstream signaling of Vangl2. (A) Phospho-specific Vangl2 antibodies recognize only correspondingly phosphorylated Vangl2 expressed in CHO cells. The pS84 and pS82/84 antibodies detected both hyper- and hypo-phosphorylated Vangl2 in CHO cells, whereas antibodies against both pS84 and pS82 (pS82+pS84 Ab) detected more highly phosphorylated forms. (B) Vangl2 is phosphorylated extensively in the brain and limb. * indicates a non-specific band in the limb. (C) Endogenous Vangl2 phosphorylation in the brain can be abolished by CIP. (D) In HEK293T cells, compared to wild type Vangl2, all-phospho-mutant Vangl2 failed to induce c-Jun phosphorylation and GTP-bound, activated Rho. (E) 120pg GFP mRNA has no effect on zebrafish embryos (a). Overdosed wild type (b, 120pg), S84A (c, 120pg) or S5,82,84E (e, 30pg) Vangl2 mRNA resulted in lower rescuing efficiency compared to lower dose injection (60pg or 20pg, Fig 6G). 120pg S5~17A::S76~84A Vangl2 mRNA still can not significantly rescue *tri*$^{m209/m209}$ embryos (d). The numbers of injected zebrafish embryos with the indicated genotypes are indicated above the bars. (F) Membrane localization of wild type and mutant Vangl2 protein in MDCK cells. The wild type and S84A Vangl2 localize on the membrane

(arrow). Although the membrane localization of S5~17A::S76~84A Vangl2 is much reduced, a substantial fraction of S5~17A::S76~84A Vangl2 proteins still reach to the membrane (arrows). However, the S464N Vangl2 proteins never reach to the membrane.

Figure S7, related to Figure 7. (A) The E11.5 mouse frontonasal tissues were separated into a distal part that expresses high levels of *Wnt5a* and a proximal part that expresses lower levels of *Wnt5a*. After immunoblotting with Vangl2 antibody, the distal part showed hyperphosphorylated Vangl2 (upper arrow), whereas the proximal part had more hypophosphorylated Vangl2 (lower arrow). (B) The phosphorylation levels of Vangl2 in distal or proximal part of E11.5 *Wnt5a*$^{-/-}$ limbs are similar, but reduced compared the wild type distal limb. (C) Wild type or Wnt5a-expressing (infected by RCAS-Wnt5a) chicken embryonic fibroblast (CEF) cell pellets were grafted into limbs of chicken embryos. After three days incubation, the chicken limbs were analyzed by immunofluorescence with Vangl2 (green) and virus specific (red) antibodies (projected Z-stack). The arrow indicates the grafted Wnt5a cell pellet. The boxed areas were shown in higher magnification in the lower panels. Vangl2 protein (arrowhead) was proximally localized in wild type or uninfected chicken limb cells, but its localization was randomized in Wnt5a-infected chicken limbs. D, distal; P, proximal.

Extended Experimental Procedures

Antibodies. Anti-Flag (M2, Sigma), anti-Flag (polyclonal, Sigma), anti-HA (3F10, Roche), anti-Myc (9E10, Santa Cruz), anti-Sox9 (H-90, Santa Cruz), anti-Wnt5a (R&D systems), anti-virus (AMV-3C2, hybridoma bank), anti-actin (AC-15, Sigma), anti-β-

catenin (BD Transduction Lab), anti-acetylated tubulin (Sigma), anti-phosphotyrosine (4G10 Platinum, Millipore), anti-c-Jun (Cell Signaling), anti-phospho-ser63-c-Jun (Cell signaling), anti-Vangl2 (N13, Santa Cruz), anti-Vangl2 (gift of Dr. Kelly)(Montcouquiol et al., 2006) and anti-Ror2 (gifts of Dr. Nusse)(Mikels et al., 2009) antibodies were used in Western blots, Immunoprecipitation, or immunofluorescence.

X-Gal staining. Embryos were fixed in fixative (0.5% formaldehyde, 0.1% glutaraldehyde, 2mM $MgCl_2$, 5mM EGTA, 0.02% NP-40) for 10 minutes. Staining on embryos or sectioned tissues was performed in staining solution (5mM $K_3Fe(CN)_6$, 5mM $K_4Fe(CN)_6$, 2mM $MgCl_2$, 0.01% NaDeoxycholate, 0.02% NP-40) for 4 hrs at 37°C, then overnight at room temperature before post-fix with 4% PFA.

Skeletal preparation. E17.5 fetuses mice were eviscerated, fixed overnight in 100% ethanol, and then transferred 100% acetone, followed by staining with Alizarin Red S (bone) and Alcian Blue (cartilage). Embryos were cleared by 1% KOH and stored and photographed in 80% glycerol.

Histological analysis. Embryos were fixed in 4% PFA overnight at 4°C, dehydrated with ethanol, and embedded in paraffin wax. Sections were stained according to the standard von Kossa staining and Safranin O staining procedures.

***In situ* hybridization.** *In situ* hybridization on embryos using digoxigenin-labelled riboprobes were performed according to standard protocols.

Cochleae analysis. Cochleae were dissected from E18.5 mice and fixed in 4% PFA overnight at 4°C. The entire cochlea was subjected to whole-mount staining with Phalloidin-Rod (1:200).

Cell migration assays. Transwell chamber (8um, Costar) was precoated with 0.1% gelatin for 2h at 37°C. Serum-starved MEFs (10^4 cells) suspended in 100ul DMEM containing 0.5% FCS was loaded into the upper well. The lower well was filled with 500ul 0.5% FCS-contained Control medium, Wnt3a conditioned medium or Wnt5a conditioned medium**.** The membrane was fixed in 4% PFA after 4 hours incubation. The filter was stained with crystal violet in 2% ethanol then rinsed in water. The upper side of the filter was cleaned with a cotton swab. Count the number of cells that migrated across the filters under microscope. Three identical replicates were performed for each migration condition.

Phospho-c-Jun and Rho activation assay. Wild type and *Ror2*$^{-/-}$; *Vangl2*$^{-/-}$ MEFs were seeded on fibronectin precoated dishes and starved overnight in DMEM containing 0.2% BSA and treated with 0.1%BSA, 100ng/ml Wnt3a (R & D Systems) in 0.1%BSA or 200ng/ml Wnt5a (R & D Systems) in 0.1%BSA for 3 hours prior to collecting lysates for immunoblotting. Rho activation assay was performed by using Rho Activation Assay Kit (Millipore) and following manufacture's protocol.

Zebrafish genotyping. Clipped zebra fishes were lysed in the buffer (50mM KCl, 10mM pH8.0 Tris, 0.45% NP40, 0.45% Tween20, 2mM $MgCl_2$) containing Proteinase K (250ug/ml). Lysates were heated at 95°C for 10 minutes before they were used for genotyping. Wild type allele was genotyped with: Stbm wtF (GTGTGTCTGCCTGTGTCTTACT) and Stbm R (GATAAACTCCTCCCCCAGGT); The *tri*^{m209} allele was genotyped with: Stbm mtF (GTGTGTCTGCCTGTGTCTTACA) and Stbm R.

Chicken embryonic fibroblasts grafts. Chicken embryonic fibroblasts (CEF) were trypsinized and resuspended in DMEM with 10% fetal calf serum and 5% chicken serum (around $2x10^7$/ml). A 20µl drop of resuspended cells was placed in a 35 mm Petri dish which was flipped upside down to form a hanging drop and then incubated for about 2 hours at 37°C. The cell aggregates that formed were cut into small pieces and grafted to chick limb buds.

References:

Mikels, A., Minami, Y., and Nusse, R. (2009). Ror2 receptor requires tyrosine kinase activity to mediate Wnt5A signaling. J Biol Chem *284*, 30167-30176.

Montcouquiol, M., Sans, N., Huss, D., Kach, J., Dickman, J.D., Forge, A., Rachel, R.A., Copeland, N.G., Jenkins, N.A., Bogani, D., *et al.* (2006). Asymmetric localization of Vangl2 and Fz3 indicate novel mechanisms for planar cell polarity in mammals. J Neurosci *26*, 5265-5275.